A geometallurgical study of the quartz-dominant ore varieties in a polymetallic base metal sulphide deposit, Northern Cape, South Africa

By: Graeme B Stroebel

Thesis presented in fulfilment of the requirements for the degree of Master of Earth Sciences, Stellenbosch University

Supervisors:

Associate Professor Jodie Miller (Stellenbosch University)

Associate Professor Megan Becker (University of Cape Town)

Associate Professor Kirsten Corin (University of Cape Town)

March 2020

Plagiarism Declaration

I am aware that plagiarism is the taking and using of other's work under the false pretence of it being my own. This thesis is my own work, if work that is not my own is used it is appropriately cited and referenced. Under no circumstances will I provide this thesis to someone else for the use of copying/fraudulent activities.

March 2020

Abstract

Geologically complex deposits require integrated approaches to characterisation, extraction and processing of ores in order to maximise the yield of the deposit. In this study, a complex polymetallic (Cu-Pb-Zn-Ag) base metal sulphide deposit was examined to evaluate whether the different ore bodies should be grouped into geometallurgical domains. Geometallurgy is the practice of incorporating the entire value chain, and in this case, means the incorporation of geological knowledge of a deposit with metallurgical/process mineralogical knowledge to create a predictive, all-encompassing, model of a deposit. This idea was investigated using a Cu-Pb-Zn deposit in the Northern Cape of South Africa. The deposit consists of three ore bodies, namely: the Upper Ore Body (UOB), the Garnet Quartzite Ore Body (GQOB) and the Lower Ore Body (LOB). The UOB consists of magnetite-dominated ores and the other two ore bodies are quartz-dominant ores. The two quartz-dominant ore bodies consist of three different ore types: (1) garnet quartzite (GQOB), (2) mineralised schist (LOB) and (3) sulphidic quartzite (LOB) (abbreviated as ores G, H and I respectively). In this study, an in-depth investigation into the feed mineralogy/morphology, minerals processing responses and flotation concentrate mineralogy/morphology was conducted to test the legitimacy of creating one quartz-dominant geometallurgical domain.

Mineralogical analysis of the feed was performed using QEMSCAN on samples milled to achieve a P80 of 65% passing 75 µm. Mineralogical analysis of the feed showed that the three ores were not as similar as originally proposed. Ore G had a unique feed mineralogy compared to ores H and I (which were similar to each other). Ore G consists of high (5.3 wt. %) amounts of chalcopyrite compared to that of ores H and I (1.1 wt. % and 1 wt. % respectively). In contrast ores, H and I consist of far higher (9.9 wt. % and 10.1 wt. % respectively) modal amounts of galena compared to the low amounts found in ore G (0.7 wt. %). Together with the differences in modal abundances of economic sulphides (ES) in the three ores, the two ore bodies had distinct sulphide gangue (SG) and non-sulphide gangue (NSG) populations. The NSG component of the three ores was, as expected, dominated by quartz, however, ore G has high amounts of garnet (10.2 wt. %) and magnetite (23 wt. %), whereas ores H and I has high amounts of mica (8.5 wt. % and 12.8 wt. %, respectively) and barite (8.7 wt. % in ore I). The mineral liberations and associations of ore G is also unique from ores H and I.

The results from the flotation experiments showed that, despite the unique feed mineralogy of each ore type, similar total solids vs water recoveries were obtained for each ore type. Further investigation into the flotation performance of the three ores was done by analysing the flotation concentrates using ICP-OES to create elemental grade vs. recovery and metal mass vs water recovery profiles. Through the analysis of these results, it was determined that the ores again showed a similar grouping to the feed mineralogy (GQOB ores distinct from LOB ores).

The analyses of the flotation concentrate showed that the target elements in the quartz-dominant ores (Cu and Pb) were being recovered as expected (in chalcopyrite and galena, respectively). The high iron recovery in the flotation concentrate (in particular of ore G) was a result of true flotation concentration of pyrite. This concentrate analysis once again showed that the three quartz-dominant ores were not as similar as originally thought. Ore G had a far higher pyrite content (56.7 wt. %) than ores H and I (29.8 wt. % and 20.7 wt. %, respectively) which were similar. As expected, ore G had a high chalcopyrite content (30.7 wt. %) in the concentrate, whereas ores H and I had a high galena content (57.4 wt. % and 67.3 wt. %) in the concentrate.

Based on the above information, it is proposed to make two geometallurgical domains from the three quartz-dominant ores, one made up solely of ore G and the other made up of the combination of ores H and I. Implementation of geometallurgical domaining of this Cu-Pb-Zn deposit would require further analysis of the feasibility of mining and processing ores in such a way to preserve the ore domaining throughout the mining chain. On existing mine sites this would likely prove challenging but the results of this study suggest that such an approach could improve the financial return on the mining activities.

In the case of this deposit, the ore domaining proposed for the quartz-dominant ores needs to take into consideration the UOB which is magnetite-dominant. Should the difference between the ores of the UOB and the quartz-dominant ores be more significant than the difference between the two proposed quartz-dominant domains, then the subdivision of the quartz-dominant ores might not make economic sense. Nevertheless, this study proposes that the quartz-dominant ores should be split into two domains aimed at grouping together ore types that exhibit similar processing responses.

Acknowledgements

I would like to say thank you to the entire CMR staff at UCT, who all helped make a foreign discipline and university a very enjoyable experience. Namely: Monde Bekaphi, Kenneth Maseko, Refilwe Moalosi (for all the help/laughter in the labs, It made the world of difference). Shireen, Lorraine, Gaynor and Keshree – for all the help with the analytical work and admin surrounding the project.

I would also like to thank the staff at the Dept. of Earth Sciences (Stellenbosch), in particular the CAF staff, for all the help with the analytical work and any other day-to-day admin that is often taken for granted.

I would like to give a vote of thanks to all my peers, friends and family - whether the input was direct or indirect, it meant and means a lot (special S/O to Ta-Roz Walker). A separate thanks to Henry, for all the mineralogical and contextual help (and all the ore).

To my three supervisors, you all have very different styles of supervision and sometimes opposing points of view, I have learnt a great deal and respect all of you for the help and guidance that you have given me - thank you for all that you've taught me, Profs.

I would like to give a vote of thanks to Black Mountain Mining (Pty). Ltd., for the funding that made this project possible.

Lastly, I would like to say thank you to Unai Emery, who consistently reminded me that no matter how bad it was going with my MSc, it could always be worse.

In all matters of opinion, our adversaries are insane – Oscar Wilde

Table of Contents

List of Figures

List of Tables

Chapter 1: Introduction

1.1 INTRODUCTION

The ready availability of mineral resource deposits that characterised much of the early 20th century is on a natural decline (Klinglmair et al., 2014), largely due to the finite nature of mineral resources, and the increasing complexity of ore deposits found at present compared to deposits found in the past. The modern minerals industry is cost-profit driven which in turn drives demand for the most cost-effective method of mineral extraction, the net result being that mineralogically simple deposits are mined out faster than mineralogically complex deposits (Calvo et al., 2016; Tilton, 2003). This leaves the mining industry increasingly dependent on geologically and hence mineralogically, complex deposits (Lishchuk et al., 2020).

With competition and pressure from investors, complex deposits are expected to be extracted at similar or lower costs than earlier simple deposits. A modern answer to this issue is the development of the idea of geometallurgy, which incorporates the whole value chain, from exploration to minerals processing and everything in-between (Lund and Lamberg, 2014). In effect, geometallurgy links commonly unlinked practices in a mining operation. Historically, different sectors of the mining operation (i.e. geological operation, minerals processesing operation, economic management operation, mine logistics operations, etc.) did not “communicate” with a high enough level of understanding. Geometallurgy aims to create one common “language”, and a broad level of understanding, throughout the entire mining operation to optimise the entire mining circuit (Boisvert et al., 2013; Coward et al., 2009; Lishchuk et al., 2020).

Modern industrial and technological industries have created a high demand for base metals, but these industries are dynamic such that the demand for certain metal resources changes over time. A more recent industry-driven pressure/demand cycle is the migration towards highly electronic biased operating systems, such as the development of electric engines. These shifts are most vividly seen in the emerging markets (Elshkaki et al., 2016). As an example, the modern electric engine requires, in some cases, more than double the amount of Cu when compared to the internal combustion engine. Hence, the transition into the fourth industrial revolution will generate ongoing demand for valuable metals such as copper (Fig. 1), platinum, lithium, and nickel, etc. (Calvo et al., 2016; Gaines, 2014).

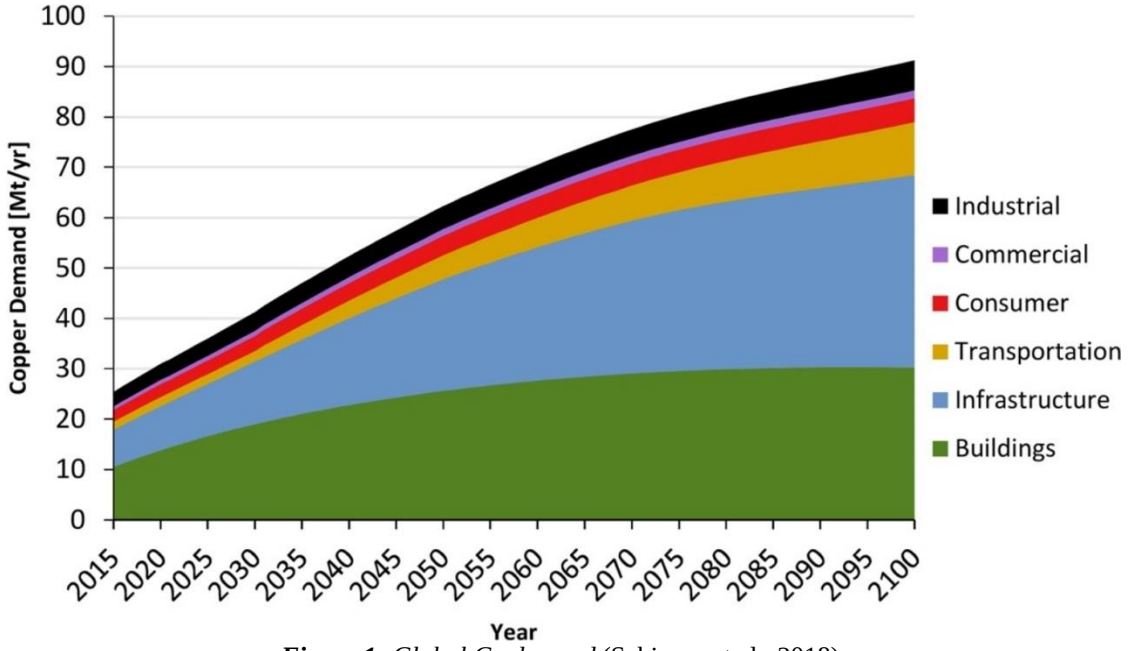

Figure 1: *Global Cu demand* (Schipper et al., 2018).

In response to this demand, the mining industry has sought to develop better and more efficient ways in which to extract various metals and this is where geometallurgical approaches take centre stage. However, before a geometallurgical mining approach fora mine can be introduced, it is necessary to obtain correct mineral, structural, ore-domain and ore-body classifications. This is done by the implementation of accurate and representative sampling campaigns, and incorporating base level geological knowledge of mineralogy and structure with secondary knowledge of minerals processing and minerals beneficiation (Lund and Lamberg, 2014).

The final step to incorporating this holistic approach to mining practice is the incorporation of mining economics. The combination of all three skillsets is then used to create a fully functioning block model of a mine that is able to relay real-time, processed, big data to the concerned party (plant engineers, grade control geologist, etc), in order to optimise current operations. The ability to forecast would also be crucial to mining management, allowing mining houses to give relatively accurate predictions to investors, with the incorporation of economic/metal price fluctuations.

Black Mountain Mining, a subsidiary of Vedanta Resources, based in Aggeneys, Northern Cape, is currently mining a polymetallic base metal sulphide deposit. The valuable elements targeted at this operation are: Cu, Pb, Zn and minor silver. The Aggeneys-Gamsberg Ore district (A-GOD) has undergone several stages of deformation, as well as several stages of mineralisation, making the mining and processing of this ore body intrinsically complicated.

Previous work done on this deposit (Gordon et al., 2018) aimed to create baseline geometallurgical domains based solely on the mineralogy of the different ore types. In this work, it was proposed that the quartz-dominant ores be grouped based on their comparable mineralogy. This study aims to investigate the feasibility of creating one unified geometallurgical domain for the three quartz-dominant ore types of the Garnet Quartzite Ore Body (GQOB) and Lower Ore Body (LOB). A mineralogical investigation into the feed morphology will be conducted, followed by flotation test work, to measure the mineral processing responses of the ores. Finally, the flotation concentrate will be

characterised mineralogically to evaluate the role of feed mineralogy and texture on the production of the concentrate. The combination of these three characterisation stages, feed characterisation, flotation response characterisation and concentrate characterisation, will be used to evaluate whether the creation of a single or multiple quartz-dominant geometallurgical domains is valid.

1.1.1 Project rationale

The most fundamental aspect of process mineralogy is trying to achieve a grade and recovery as close to the theoretical grade-recovery curve as possible. The theoretical curve is attained if the exact ore (as analysed to generate the theoretical curve) is passing through the circuit (the circuit must also be achieving complete recoveries), void of unexpected impurities (Chauhan et al., 2013; Cropp et al., 2013). The mining plant in question has achieved erratic economic metal grades/recoveries in the past. To understand these processing issues and possibly eradicate such inconsistencies, geometallurgical investigations need to be made on each of the nine individual ore types found in this deposit. Geometallurgical domains are used to manage risk/unexpected processing outcomes by grouping ores together that exhibit similar processing responses.

1.1.2 Project aims and objectives

The central goal of this project is to determine the mineralogical, textural and processing characteristics of the quartz-dominant ore types at Black Mountain Mining and to evaluate the influence of varying mineralogical characteristics on the beneficiation process. The final objective is to propose whether geometallurgical domains should exist. To evaluate this, the following key objectives have been identified.

Objective One: To characterise the mineralogy and texture of the LOB and GQOB ore types.

- **1.1** What is the full mineralogy of the LOB and GQ ores both in terms of ore minerals and gangue minerals present?
- **1.2** What is the textural variability of the economic sulphide minerals?
- **1.3** How does the grain-size distribution and mineral liberation vary between the three quartz-dominant ores?
- **1.4** What beneficiation-orientated forecasting can be made through the analysis of mineralogical characteristics?

Objective Two: To characterise the mineral processing performance of the LOB and GQOB ore types.

- **2.1** Do the quartz-dominant ores behave differently during flotation and if so, how, particularly with respect to solids vs water recovery?
- **2.2** Does the variation in feed mineralogy influence the mechanism of mineral recovery (i.e. entrainment, true flotation, recovery by association)?
- **2.3** Do the mineral processing outcomes speak to the creation of one quartz-dominant domain?

Objective Three: To characterise the mineralogy of the bulk flotation concentrate C_1.

- **3.1** How does the bulk mineralogy of the flotation concentrate C_1 vary between quartz-dominant ore types?
- **3.2** Can variances in metal mass pull vs water recovery between ore types be explained by the mineralogy of the flotation concentrate C_1?
- **3.3** How does the quantitative textural information of economic sulphide minerals vary between quartz-dominant ore types (liberation, association, etc.)?
- **3.4** Were deleterious minerals recovered, and if so, how can this be avoided?

Objective Four: To assess the possible implementation and relevance of creating a geometallurgical domain for the quartz-dominant ores.

- **4.1** Can the quartz-dominant ores be interpreted as a single mineralogical suite through a combination of mineralogical characteristics?
- **4.2** Do certain processing results relate to mineralogy (i.e. milling time – ore hardness, mineral density – flotation speed, etc.), and would it be beneficial to group ore types for optimal processing performance?
- **4.3** Taking a holistic approach to geometallurgical domain generation at this deposit, should the quartz-dominant ores be grouped into one domain?

1.1.3 Organisation and structure of thesis

This thesis will be presented as a combination of three sections supported by an overarching introduction (Chapter 1) and methods (Chapter 2) chapter as well as a conclusions and recommendations chapter (Chapter 6). The three sections are: Chapter 3: “Mineralogical and feed classification of the GQ Orebody (GQOB) and the Lower Orebody (LOB) (quartz-dominant ore horizons)” – where both the textural characteristics and the bulk feed mineralogy (and related topics) will be investigated; Chapter 4: “Minerals processing characterisation of the quartz-dominant ore varieties” – where the results from bulk flotation experiments will be interpreted; and Chapter 5: “Mineralogical characterisation of flotation concentrates of the quartz-dominant ore horizons” – where the mineralogy (and related topics) of the flotation concentrate C_1 from the previous chapter (Chapter 5) will be discussed.

1.2 BROKEN HILL-TYPE DEPOSITS

The Broken Hill-Type (BHT) deposit style finds its name from the type deposit, in Broken Hill, New South Wales, Australia (Groves et al., 2008). This deposit type has somewhat characteristic sedimentary exhalative (SEDEX) features, with differences being the experienced metamorphism and related remobilisation (Höy, 2001), as well as certain geochemical and petrological signatures (Roache, 2004). It is common to have both volcanogenic massive sulphide (VMS) and SEDEX features with alteration and loss of original formation structure, creating a new group of deposit styles with a said Broken Hill-Type affinity, with the geometry of said deposit being integral for the

classification of a BHT deposit (Beeson, 1990). The argument of pre-existing vs post-metamorphic geometry as well as shear zones (and their related brines) being the classification cornerstone to this deposit style is discussed in detail in literature (Gustafson et al., 1950; Rothery, 2001). Figure 2a shows the typical formation of a VMS deposit, where a feeder vent is found on the seafloor and in the correct environment (REDOX, temperature, etc.) the hydrothermal fluids of this vent precipitates out metals in the surrounding strata (Piercey, 2015). SEDEX deposit types differ from VMS deposit types by the condition under which metals precipitate out of solution, and also the proximity to the feeder vent (although two types of SEDEX deposits are found, vent proximal and vent distal) (Fig. 2b). The other major difference between the two deposit types is the nature of the ore/groundmass. VMS deposits are massive sulphide hosted whereas SEDEX are sulphide deposits hosted in sedimentary beds (Sangster, 2018; Valdes-Nodarse, 1998). SEDEX brines (which transport and concentrate the metals) are common, and are considered to be related to the basal brines found in the enrichment of Mississippi Valley-Type (MVT) deposits (Sangster, 2018).

Walters and Bailey (1998) describe BHT deposits by a set criterion of elemental and mineralogical characteristics, making the exact classification more stringent. Some significant features of a BHT deposit can be summarised by the following characteristics: close association with exhalative marker units, base metal manifestations, periodic association with magnetite and metamorphism associated alteration (Höy, 2001).

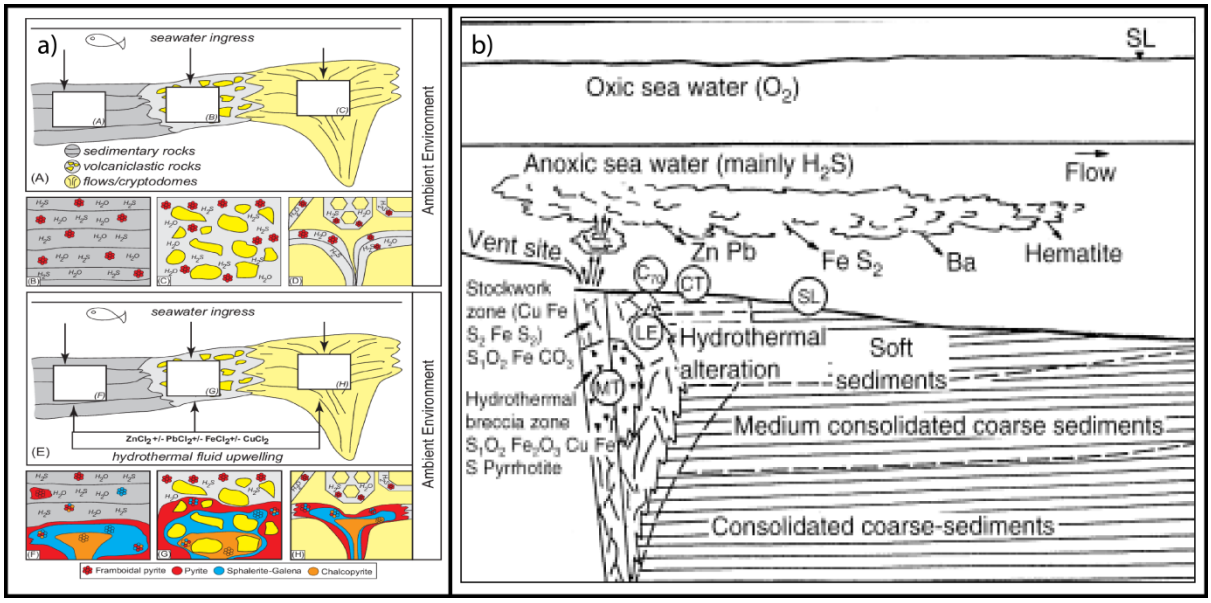

Figure 2: *(a) VMS* (Piercey, 2015) *vs (b) SEDEX* (Valdes-Nodarse, 1998) *deposit styles Note the differences between the massive nature of the VMS deposit style and the stratiform-stratabound nature of the SEDEX deposit style. (a) Moving from top to bottom shows the mineralisation style of a VMS deposit, and the differences in mineralisation between vent distal and vent proximal. (b) The abbreviations (MT, LE, CT, SL and C_{70}) bare no importance to the deposit style in this figure.*

The stratiform and stratabound beds of the ore bodies in the A-GOD district are widely regarded as a type location of a world-class BHT deposit (Colliston and Schoch, 2003; Höy, 2001; McClung and Viljoen, 2011; McClung et al., 2007).

Table 1: *Examples of BHT-deposits around the world characterised by their Cu-Pb-Zn grades.*

Deposit Name	Location	Cu grade	Pb grade	Zn grade	Citation
Broken Hill**	New South Wales Australia	-	5.6%	8.5%	(Morland and Webster, 1998)
A-GOD	Northern Cape, South Africa	0.21%	1.43%	3.6%	(McClung et al., 2007)
Cannington	Northwest Queensland, Australia	-	11.6%	4.4%	(Walters and Bailey, 1998)
Pegmont	Mt Isa, Australia	-	8%	4%	(Beeson, 1990)
Boquira	Bahia, Brazil	-	9%	2%	(Beeson, 1990)
Menninie Dam*	South Australia, Australia	-	3.2%	4%	(Oleynik, 2005)
Zinkgruvan*	South-Central Sweden	1.8%	2.9%	7.2%	(Richardson et al., 2017)

*Notes: **Type location, *higher Zn grade than Pb grade*

A-GOD is the location of four BHT deposits, all in close proximity to the town of Aggeneys, Northern Cape. These deposits are namely: Gamsberg, Black Mountain, Broken Hill-Broken Hill Deeps and Big Syncline, with an estimated combined tonnage of 439 million tonnes (Stalder and Rozendaal, 2004; McClung et al., 2007; McClung and Viljoen, 2011).

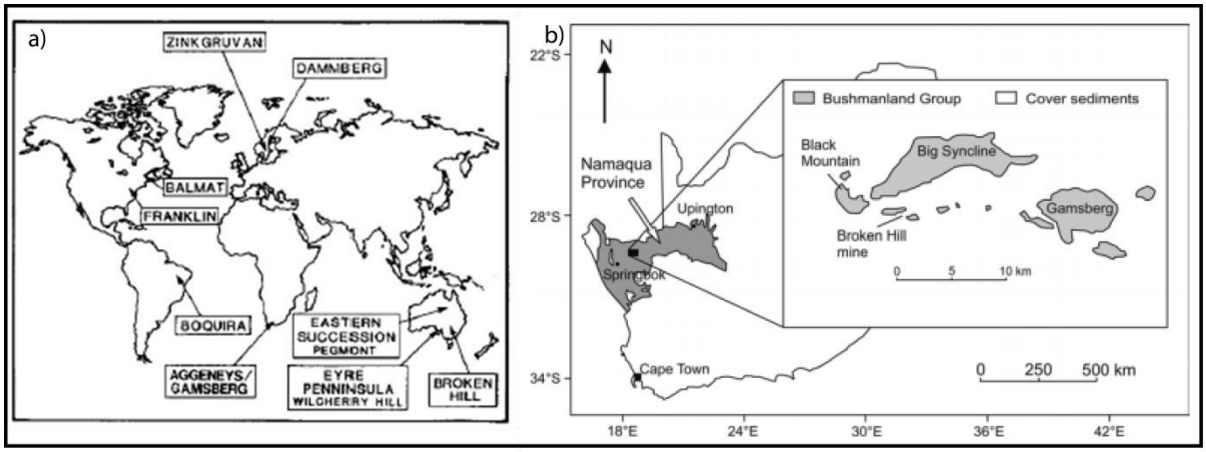

Figure 3: *(a) Examples of BHT deposit locations around the world* (Beeson, 1990)*; (b) the A-GOD deposit layout* (Stalder and Rozendaal, 2004).

1.3 GEOLOGICAL SETTING

Polymetallic base metal sulphide mineralisation is prevalent to the east of Springbok in the Northern Cape and is associated with the Namaqua sector of the Namaqua-Natal Metamorphic Belt (NNMB). The NNMB is an arcuate belt of largely metamorphic rocks of a varying grade but also encompassing pre-metamorphic magmatic rock assemblages spanning the period 1.9 to 1.0 Ga (Colliston and Schoch, 2000; Cornell et al., 2006; Macey et al., 2018, 2017; Tankard et al., 1982). The belt runs from southern Namibia through to the KwaZulu-Natal province of South Africa. This metamorphic province has been extensively studied; due to this a wide variety of nomenclature is used in academia for its descriptions (i.e. Subprovince vs Subgroup) (Macey et al., 2018). For the purpose of this study the

nomenclature of Cornell et al. (2006) will be followed. The Namaqua Sector of the NNMB is made up of five distinct Subprovinces, these being from west to east the Richtersveld, Bushmanland (extending and wrapping around the southern portion of the Namaqua Province), Kakamas, Areachap and Kaaien Subprovince (Fig. 4) (Cornell et al., 2006). Polymetallic base metal sulphide mineralisation is associated with the Bushmanland Subprovince. The Namaqua Sector underwent metamorphism, with a maximum temperature of approximately 680 ^{o}C and pressure of ≈3.5 kb (Bailie and Reid, 2005; Lipson, 1980; McClung et al., 2007; Ryan et al., 1986). The early geological evolution of the province has been depicted as the closing of a retro-arc environment onto the Kaapvaal Craton. This was then followed by collision and related crustal thickening (Cornell et al., 2006; Tankard et al., 1982). More recent studies have reinterpreted the geological history as representative of early closing of a two-arc model (Sperrgebiet and Richtersveld Magmatic Arcs: (Macey et al., 2018, 2017; Thomas et al., 2016)) with reworking of the Sperrgebiet Arc into the Richtersveld Magmatic Arc (Macey et al., 2017), followed by compression-related Namaqua-Natal metamorphism.

1.3.1 Namaqua Sector Subprovinces

The area has a wide range of rock types that have experienced post-emplacement/post-deposition metamorphism. The range of rock types are attributed to the wide variety of tectono-magmatic/tectono-sedimentary settings that have encompassed this area, ranging from mid-ocean ridge mafics and plutonic felsics to Kheisian sediments, deriving from the Kheis Orogeny and its related sedimentation at ≈1.8Ga (Van Schijndel et al., 2019). The exact metamorphic history of the A-GOD is, however, complex. This is largely due to the four main deformation events and related metamorphic peaks (D_{1-4} and M_{1-4} respectively) with D_1/M_1 representing ages of 1850 Ma (Robb et al., 1999). The vast majority of all textures and assemblages that were created during D_1 and M_1 were subsequently overprinted and largely removed by D_2 and the related (but not necessarily coeval) metamorphic peak. The progression between D_2 and D_3 is said to be the period of time that is responsible for peak metamorphic conditions. These conditions were that of upper amphibolite facies, 2.8-4.5 kb and 630-670 ^{o}C, and lower granulite facies, 4.5-6 kb and 750-870 ^{o}C (Bailie and Reid, 2005; Cornell et al., 2006; Macey et al., 2018; Ryan et al., 1986).

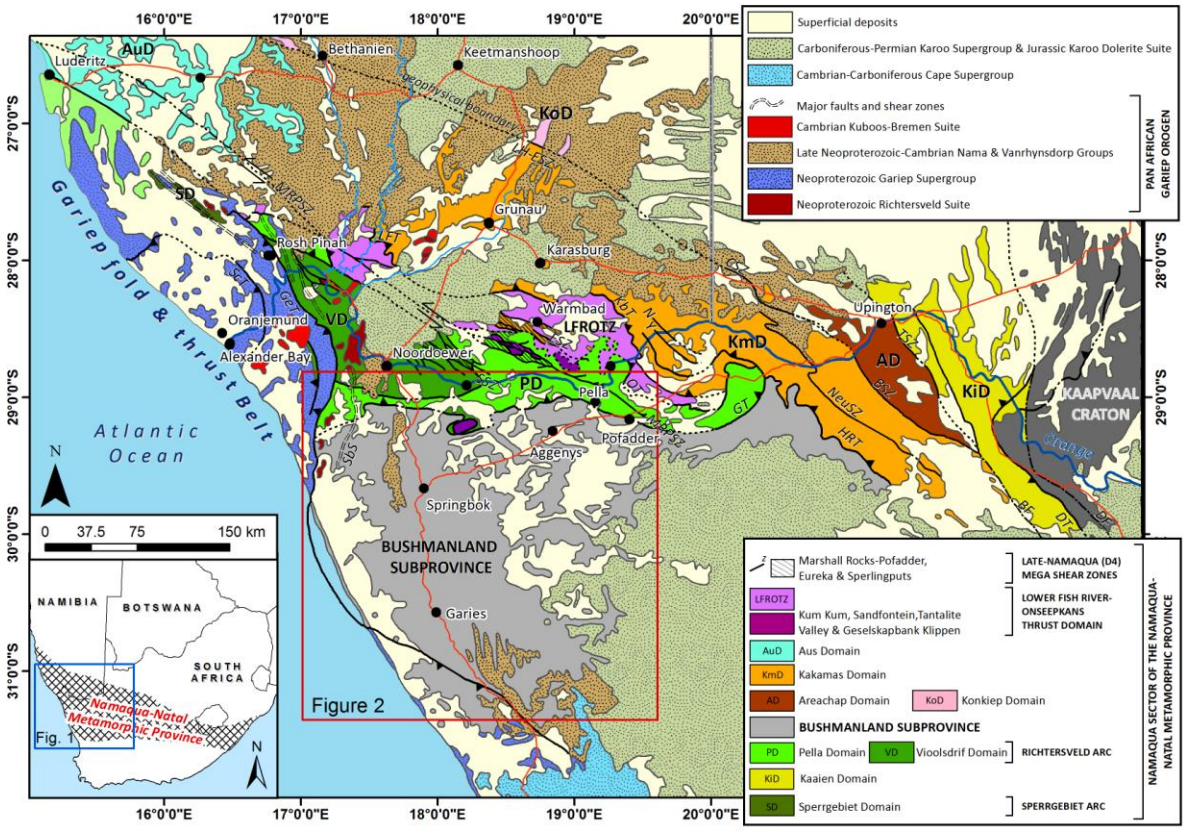

Figure 4: *Namaqua Sector of the NNMB* (Macey et al., 2018).

The second metamorphic event is thus interpreted as an event spanning over close to 200 million years (from ≈1.2 Ga until ≈1 Ga). Further studies have found that the second metamorphic event can be subdivided into two different events, M_{2a} and M_{2b} (Cornell et al., 2006; Raith et al., 2003). Common structures, related to the deformation event, found in the Bushmanland area are ENE to NE trending upright, tight, sheath/periclinal folds and related nappe structures, both are common in compressional tectonic regimes (Namaqua-Natal orogeny). Also common in this region is ESE trending shear zones (Colliston and Schoch, 2006, 2003, 2000). The majority of the structures in the area that were created during the first two deformation events were slightly superimposed by the latter two deformation events, with particular structural confidence in the widespread second deformation event (D_2) (Cornell et al., 2006; Tankard et al., 1982).

The Bushmanland Subprovince, more specifically the area surrounding Aggeneys, consists of metasediments with a believed Kheis Orogeny origin, with both meta-felsics and meta- tholeiitic igneous rocks from an intrusive (1.2 Ga collision) and rift (1.6 Ga extension) related origin, respectively (Colliston and Schoch, 2003). These sediments are said to have eroded during a back-arc rifting stage and were deposited into an ocean environment related to the then retro-arc foreland basin. This was the source for the thermal base-metal rich brines needed to create the then initial low-grade sedimentary exhalative base metal deposit (Crockford et al., 2019) . The main sedimentary units in the area exhibit an upward coarsening from hemi-plegics to fluvial arkose sediments, typical of a basin closing/filling. These sediments now take the form of a range of gneisses, meta-arkoses

and metaconglomerates (Colliston et al., 1991; Raith et al., 2003; Reid et al., 1987; Rozendaal et al., 2017; Tankard et al., 1982).

1.3.2 Bushmanland Subprovince

The Bushmanland Subprovince is largely made up of metavolcanics and metasediments, and is bounded by the Groothoek Thrust to the north and the Hartbees River Thrust to the east, while the younger Karoo Supergroup defines a pseudo boundary to the south (Rozendaal et al., 2017). This large age range of units in the province (2100Ma – 1020Ma) is due to the series of several tectonic events which led to the initial formation as well as the reworking and latter formation of units in the area that spanned over 1000 million years (McClung et al., 2007; Raith et al., 2003; Ryan et al., 1986). Rozendaal, Rudnick and Heyn (2017) defined 3 main terranes in the Bushmanland Subprovince, namely: the Okiep, the Garies and the Aggeneys Terranes, in the west, south and east respectively.

1.3.2.1 Okiep Terrane

The Okiep Terrane is located around the town of Springbok and the main rock types are meta-volcanosedimentary units combined with granitoids. Originally the Okiep Terrane was not part of the Bushmanland Subprovince, but after further studies, it has become a subsidiary of the larger Subprovince (Raith et al., 2003). The main economic interest in the region is Cu-related mafic dykes and pipes (Rozendaal et al., 2017). The different subgroups in the area have two main origins, pre- and syn-Namaqua orogeny. The age of the metasediments of the Khurisberg subgroup relate to the Orange River Orogeny (±2 Ga) and the younger plutonic granitoids of the Spektakel Suite are related to the Namaqua-Natal Orogeny (±1.1 Ga) (Colliston and Schoch, 2006). Raith et al (2003) proposed that the intrusives of the Spektakel Suite could even be post-Namaqua Orogeny; this description is defended by the minimal deformation exhibited in this suite (Macey et al., 2018).

1.3.2.2 Garies Terrane

The Garies Terrane has a well-preserved deformation history; this history is however not one of a protolith reworking nature, but more of a protolith preservation nature (Eglington, 2006). The terrane wraps around the southern portion of the Bushmanland Subprovince. This terrane is bound on its eastern margin by the Hartibees River Thrust, and it too has large base metal sulphide deposits. This terrane has common accruing mafic intrusives, with said intrusives being the host for the vast majority of the base-metal sulphide deposits in the region (Rozendaal et al., 2017).

1.3.2.3 Aggeneys Terrane

This is the main ore province of the Bushmanland Subprovince, with four major deposits in proximity to the town of Aggeneys, namely: Gamsberg, Swartberg, Deeps (with deeps being an extension of the western Swartberg) and Big Syncline (Cornell et al., 2009). The supracrustal succession of theAggeneys Terrane in the Bushmanland Subprovince is divided into six formations, namely: Koeris, Hotson, T'hammaberg, Skelmpoort, Witputs and Wortel (Praekelt and Schoch, 1997). A brief

description of each formation will be explained with a majority of the focus on the ore-rich Hotson Formation.

1.3.3 Aggeneys Terrane stratigraphy

1.3.3.1 Koeris Formation

The Koeris Formation represents the final stages of sedimentation in a lake environment, moving from shallow marine fines at the basal contact with the Hotson Formation to larger fluvial sediments at the upper limits of the formation (Praekelt et al., 1997). The age constraints are erratic and commonly defined by the intrusives in the formation; these ages are however poorly constrained, and similar to the metasediments in this Formation, this result in inconclusive age ranges (Cornell et al., 2006). The Koeris Formation has a maximum defined thickness in the Gamsberg area of ±600m (Cornell et al., 2006). The main constituents of the formation are felsic meta-lavas and the sediments of their reworking, such as: amphibolite, meta-arkose (sedimentary gneiss), quartzite and metaconglomerates ranging from matrix to clast dominated (Colliston et al., 1989, 1991; Praekelt et al., 1997; Reid et al., 1987; Rozendaal et al., 2017).

1.3.3.2 Hotson Formation

The Hotson Formation has been the most extensively investigated formation in the area due to its valuable inlying base-metal sulphide deposits (around the Aggeneys area). Similar to the Koeris Formation the Hotson Formation is defined by gradual upward coarsening of sediments (Praekelt et al., 1997). The intermediate-depth marine environment of a terminating retro-arc foreland basin is the type location in South Africa of the Broken Hill Type ore formation (Roache, 2004). The presence of low concentration base metals in the aqueous marine environment, that were further upgraded post-deposition due to metamorphism, is the precursor to the Aggeneys ore district (Cornell et al., 2006; Robb, 2005). The variable thickness of this formation is well documented, with upper limits of thickness found in the western portion of the formation (500m) (Cornell et al., 2006) The main rock units include: sedimentary schists (increasing in occurrence in the upper portions of the formations), gneisses and quartzites. The first occurrence of the banded iron formation, of the Bushmanland Subprovince, appears in the upper portion of this formation. The most economically significant portion of the formation is the Gams ore member; this is found in the upper ±200m of the formation (Colliston et al., 1989; Cornell et al., 2009; Praekelt et al., 1997).

1.3.3.3 T'hammaberg, Skelmpoort, Witputs and Wortel Formations

The T'hammaberg Formation does not exceed 300m in thickness, with the largest constituent of the formation being made up of metasedimentary schists and sporadic intermittent graphite (Colliston et al., 1989; Cornell et al., 2009, 2006). The thinner Skelmpoort Formation (<60m) comprises basal dark quartzites progressing upward into more graphite-bearing schistose type deepwater metasediments (Cornell et al., 2006). The Witputs and Wortel Formations share a variety of similarities in rock types; the combined thickness of the two formations is over 1100m.

1.3.3.4 Gams Ore Member

The upper portions of the Hotson Formation, namely: the Gams ore member, is said to have been deposited during stages of fluctuating water levels (Praekelt et al., 1997). According to Praekelt et al. (1997), the source of the sulphides (ranging in abundance and concentration) is from fumarolic activity. This is consistent with the deposit type classification, however, the absence of a proximal vent site in the area is still cause for much debate. A large majority of the ore horizons are made up of mineralised schists, massive sulphides and banded iron formations, this laminated package has a high sulphur content (Praekelt et al., 1997, 1983; Rozendaal et al., 2017).

1.3.4 Structure

The Aggeneys region is dominated by sheath folds combined with fold nappes; this is largely due to the deformation related to the Namaqua-Natal metamorphism event, and its predecessors the Kheis/Orange River Orogeny (Rozendaal et al., 2017). The majority of the geology in the region comprises of metasediments with a gneissic basal unit (this has not been confirmed as the basement as of yet) (Colliston and Schoch, 2003). The fold nappes and sheath folds both preserve and uplift the districts of valuable base metal sulphide ore and intuitively are the main regions under exploitation and exploration. The fold hinges have an average orientation subparallel to the direction of extension, which logically should be perpendicular to the north-eastern direction of shortening, this region has however undergone shearing and related rotation, resulting in fold hinges being in the northeastern direction of shortening (Colliston et al., 1991; Colliston and Schoch, 2003). Some authors go as far as saying that this possible shearing/thrusting (e.g. Pofadder shear) could be the origin of the deformation structures, such as the Gamsberg sheath fold.

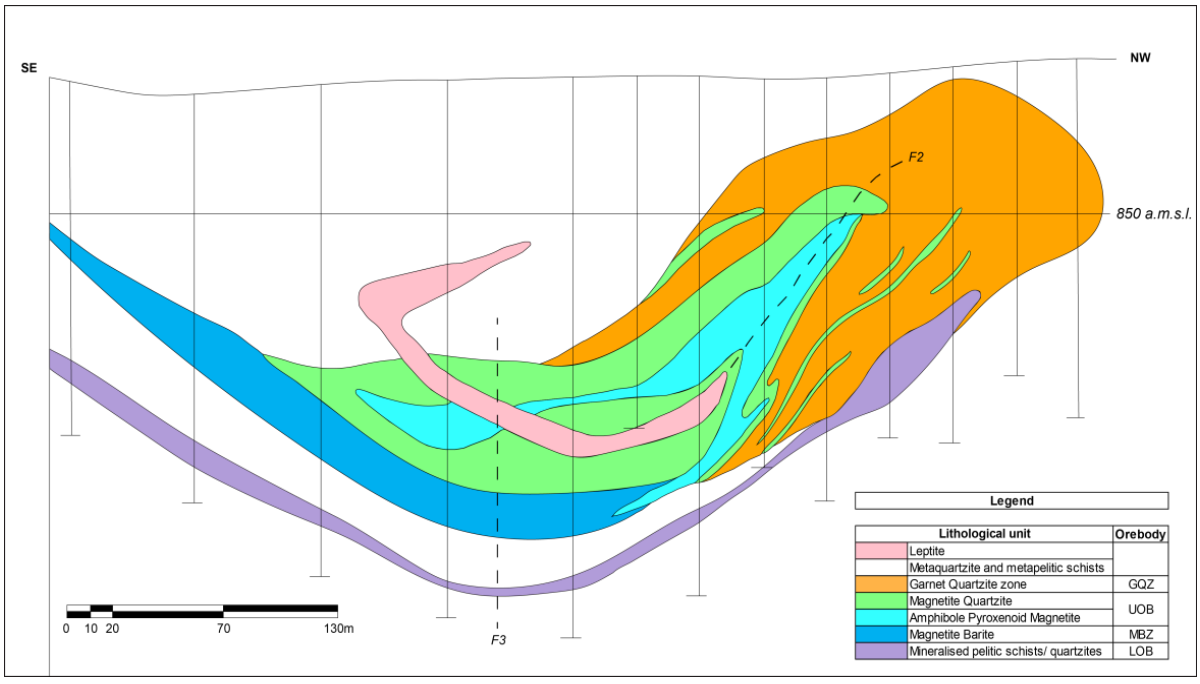

Figure 5: *Cross-section of the deposit depicting the reworked and complex structural nature of the base metal deposits in the region. Redrafted image of deposit cross-section derived from Ryan et al. (1986).*

1.4 MINERALS PROCESSING

Minerals processing is the physical act of separating target minerals from gangue. This is done through methods such as: milling/grinding, flotation (or other forms of separation such as magnetic separation) (Beers et al., 2008; Boger, 2000; Chandra and Gerson, 2009). The minerals processing sphere starts after mining/extraction and ends before the metallurgical stages of extraction. This practice is a fundamental cornerstone in the mining industry (Lishchuk et al., 2020).

1.4.1 Particle Size Distribution (PSD) and Milling

PSD is one of the most fundamental, and simplistic, characterisation techniques for soils/ores. PSD is defined by the weight percent of a sample that is defined by a certain size fraction (Eshel et al., 2004). The accurate identification of the run-of-mine (ROM) PSD is a crucial parameter, which needs to be understood, for a correct and consistent grind. The importance of PSD and milling in the beneficiation circuit is due to the hugely expensive nature of grinding/milling (Wei and Craig, 2009). The main role of milling and grinding in the minerals processing circuit is size reduction. Size reduction is a crucial step that goes hand-in-hand with valuable mineral liberation from gangue phases, which is imperative for downstream valuable mineral concentration. The study of milling and grinding is an in-depth field that analyses the roles of an ore's hardness and the interlocking capability of minerals and their interaction with the milling medium over time (Chenje et al., 2004).

1.4.2 Bulk flotation

Mineral separation via flotation is used extensively for concentration of economic minerals from base metal deposits across the world. The core principle of flotation is being able to induce hydrophobicity on target minerals and extract the target minerals from a slurry by running air/gas through the slurry thereby colliding the target minerals and bubbles. These minerals have specific optimal angles of collision and optimal interaction times that increase the joining capabilities to the bubbles; thereafter the minerals are floated to the surface in a bubble-ore composite, allowing for easy separation (Albijanic et al., 2011; Chandra and Gerson, 2009; Chipfunhu et al., 2019). The name for the additives that induce said hydrophobicity is "collectors". A common collector group used in sulphide ores is the xanthate group (Wiese et al., 2005). Collectors are often used together with a co-collector/secondary collector; in the case of this study, the co-collector is "Senkol 700". The main collector (sodium ethyl xanthate, SEX) has been commonly used with high efficacy in the recent past, however the addition of the co-collector "Senkol 700" has added benefit. Mainza. et al (1999) found that Senkol 700 exhibited fast flotation kinetics for the flotation of Cu and Co in a Cu-sulphide ore. It was also found that Senkol 700 and SEX showed comparable Cu grade recoveries. Certain elements do not respond well to xanthate collectors, an example of such a is Zn. The Zn-xanthate connection is unstable and readily decouples. To overcome such challenges another reagent must be added to the suite, termed "activators" (Chandra and Gerson, 2009). The addition of an activator, in this sense, increases the difference in wettability (hydrophilicity) of a target mineral (Zn-sulphide in this case) and gangue, resulting in the increased recovery of these target minerals. An example of a common activator in valuable element-sulphide flotation cells is Cu sulphate ($CuSO_4$) (Cao et al., 2009).

Separation by flotation is not without its limitations. One limitation to this method of mineral separation/concentration is the unwanted recovery of fine and ultrafine gangue minerals in the flotation froth (Gong et al., 2010). One common technique used to suppress this unwanted gangue recovery is the addition of depressants into the slurry. These depressants target certain gangue minerals and increase their hydrophilic potential (Bulatovic, 1999). Another common problem area in flotation performance is the low concentration of ultra-fines in the concentrate. This can be attributed to a large bubble size that is too large in the flotation cell (Rodrigues and Rubio, 2007). These ultra-fine (<10 μm) particles are a common result of overgrinding in the initial stages of ore processing (Johnson, 2006; Mikhlin et al., 2016).

In bulk sulphide flotation it is common to float sulphide gangue (pyrite, pyrrhotite, which are slower floaters than other economic sulphides, such as chalcopyrite) (Wiese et al., 2007), thus decreasing the relative concentration of the economic sulphides in the flotation concentrate (Chandraprabha et al., 2004; López Valdivieso et al., 2004). The abovementioned activation of Cu is commonly associated with the unwanted flotation of pyrite (Mehrabani et al., 2010). The conventional method of depressing pyrite in a flotation cell is, but not limited to, the addition of an inorganic chemical depressant, most commonly cyanides (Mehrabani et al., 2010). The environmental repercussions of including cyanides in the processing circuit make this method of sulphide gangue depression unattractive, thus an enviro-economically feasible method of sulphide gangue depression is the logical direction followed to eliminate this issue (Rath et al., 2000).

Pyrite is the most abundant metal-sulphide mineral in the quartz-dominant ore horizons in this study, and the world. A less common practice used for pyrite suppression, due to the environmental repercussions, is the addition of sodium cyanide to the flotation cell (Amini et al., 2009). One technique of pyrite suppression/depression in the flotation cell is through the addition of polysaccharides (e.g. guar gum). The effectiveness of pyrite suppression through the addition of guar gum (and other polysaccharides) is discussed in the studies: Steenberg and Harris, 1984; Rath et al. 2000; Bicak et al., 2007; Mu et al. 2016 and Khoso et al., 2019. The use of bacterial culture as a suppressant/depressor is both an effective and enviro-economically friendly method of pyrite suppression in a xanthate present flotation environment (Mehrabani et al., 2010).

Chapter 2: Methodology

2.1 INTRODUCTION

Three ore types were received from the mining operation, on which a series of flotation experiments were conducted. This involved particle size reduction to generate a milling curve in order to prepare a P80 feed for bulk sulphide flotation experiments designed to create the most favourable conditions for the creation of geometallurgical domain proxies. Quantitative Evaluation of Materials by Scanning Electron Microscopy (QEMSCAN), Quantitative X-ray Diffraction (QXRD) and Inductively Coupled Plasma - Optical Emission Spectrometry (ICP-OES) were used to mineralogically characterise the feed for the flotation experiments as well as the concentrate derived from said flotation experiments. The entire processing and analysis chain used for the sample preparation, bulk sulphide experiments and feed and concentrate analysis of the three ore types is illustrated in Fig. 6.

2.2 SAMPLE SELECTION AND PREPARATION

2.2.1 Sample preparation

Samples were located on-site in the mining operation (underground), by underground geologists. The samples were initially reduced in size (until approximately 75 kg) underground (in individual ore types), and then extracted. The ±75 kg samples were labelled and put into steel drums and transported to the Centre for Minerals Research, Department of Chemical Engineering at the University of Cape Town. Individual ore types were separated and manually reduced in size, using a variety of sledgehammers (6, 10, 14 lbs), until made up of roughly fist-sized pieces. The fist-sized pieces were then small enough to be crushed using a jaw crusher. Samples were crushed using a TERMINATOR jaw crusher, with a jaw width set to 3 mm. The jaw crusher was cleaned between ore types by passing quartz through and then cleaning with high pressured air. After crushing, each ore type was split into approximately 1.3 kg aliquots, using a 10 ways rotary riffle splitter to avoid sampling bias. Each 1.3 kg aliquot was then placed into a zip lock bag and labelled. The riffle splitter was cleaned using pressurised air to avoid cross-contamination of fines between different ore types.

2.2.2 Sample codes

The three ore types that were used in this study came from the Garnet Quartzite Ore Body (GQ) and the Lower Ore Body (LOB). Throughout the mineralogical characterisation and processing test work however, the samples were referred to with simplified sample codes. The table below indicates the relationship between the different sample codes, ore type names and ore bodies of origin for each ore type.

Table 2: *Ore code table used for defining the shorthand names of quartz-dominant ores. Location of the ores in the deposit can be seen in Fig.5.*

Shorthand code	On-site name (abbreviation)	Ore body of origin
Ore G	Garnet Quartzite (GQ)	Garnet Quartzite Ore Body (GQOB)
Ore H	Mineralised Schist (MC)	Lower Ore Body (LOB)
Ore I	Sulphidic Quartzite (SQ)	Lower Ore Body (LOB)

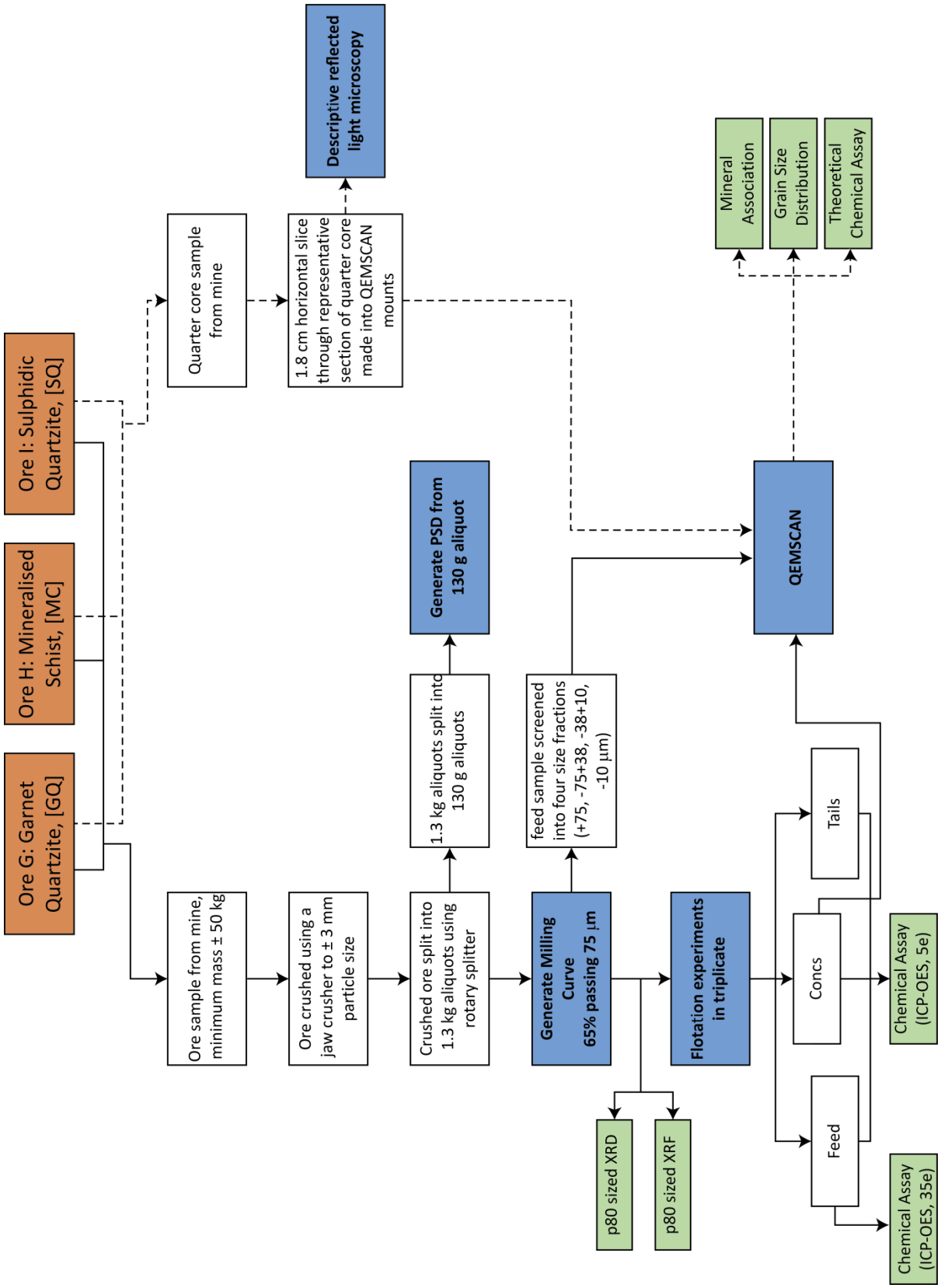

Figure 6: *Work flowsheet from start to finish of all processes. Brown boxes represent 1.3 kg aliquots at the start of the minerals processing experiments, blue boxes represent a process that generated data and green boxes represent that data.*

2.4 MINERALS PROCESSING

2.4.1 Milling curve

Each ore type was dry sieved for 20 mins using an Analysette 3 Pro with a time interval of 10s and a vibration amplitude of 1.8 mm. Sieve mesh spacings were 3.35; 2.8; 2; 1.4, 1; 0.85; 0.5; 0.425; 0.25; 0.15; and <0.15 mm. A milling curve was then created. If the particle size distribution (PSD) derived from the dry sieving was similar between similar ore types then comparable milling responses could be assumed (PSD results can be seen in Appendix A). The milling took place in a clean 10 L rod mill with the following rod configuration upon commencement: 6 (285 x 25 mm), 8 (285 x 20 mm) and 6 (285 x 15 mm). This configuration was from mill wall towards the centre (stacked upon one another). The rods were then cleaned to remove any previous ore and placed in a mill in the above-stated configuration. A 1.3 kg aliquot was added into the mill after loading of the rods along with 650 ml of premade plant water (described in Table 4) to yield a slurry of 67% solids. The run speed was then set to 94.1 rpm and the mill was firmly closed, simultaneously the mill and the stopwatch (to track milling time) were started.

To create a milling curve each ore type was milled for a variety of durations (14 and 20 mins). The whole milled sample was then removed and filtered (in a pressure filter on filter paper) to remove the fluid, and then dried overnight in an oven set to 80 °C. The sample was split down from 1.3 kg into 130 g aliquots using a rotary riffle splitter. The then dried and split sample was wet screened (in this case through a 75 µm screen) until no sample would pass. The passing, and non-passing, ore/water mixture was then filtered and dried overnight in an oven set to 80 °C (separately). The passing and non-passing ore was then separately weighed, and a percentage passing 75 µm was determined for a respective milling time. Once this procedure was repeated for each milling time, the data was plotted on a graph and a milling curve (and best fit milling curve equation) was generated. The milling process was then repeated for this specific time duration, to double-check the accuracy of the curve. This process was repeated for each ore type, due to the differences in hardness and particle interlocking characteristics of each ore type.

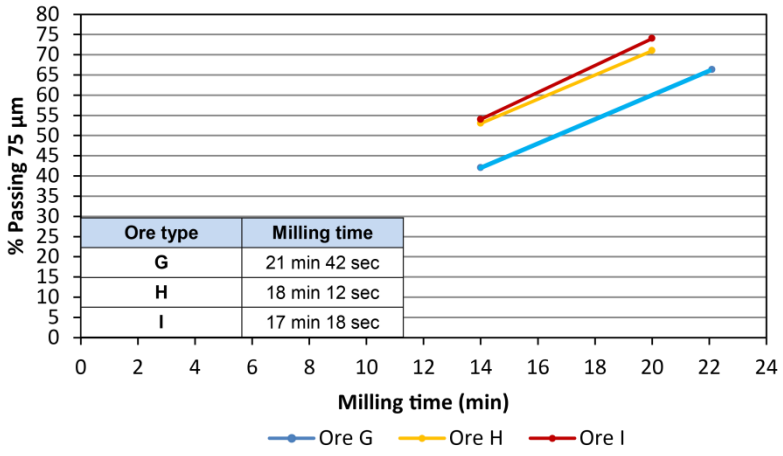

Figure 7: *Milling curve for the three quartz-dominant ores. The inset table shows the exact time necessary for a P80 grind of 65% sample passing 75 µm.*

2.4.2 Flotation Experiments

2.4.2.1 Plant water

Synthetic plant water was made for all flotation and milling experiments and stored in a sealed 40 L drum. Plant water is used to increase the preference of the reagent suite. The recipe used for this synthetic plant water is given in Table 3. The salt water mixture was stirred thoroughly until all the salt had dissolved, and periodically re-stirred to ensure that all the salts remained in solution and had not re-precipitated.

Table 3: *Plant water recipe with salt names and quantities (following the standard plant water recipe used at the Centre for Minerals Research, UCT)***.**

Salt Name	Concentration (PPM)
Magnesium Sulphate	615
Magnesium Nitrate	107
Calcium Nitrate	236
Calcium Chloride	147
Sodium Chloride	356
Sodium Carbonate	30

2.4.2.2 Flotation Setup

Firstly, the ore was extracted from the rod mill into a clean plastic bucket removing all ore using plant water. With certain ore types (Ore G) large pebbles (up to 5 mm) were found to lodge themselves in the corner between the mill wall and base. This resulted in the addition of a step during the extraction of the ore from the mill into the flotation cell, in the form of passing the ore through a 1 mm sieve. This was done to avoid the possible damage of the impeller in the flotation cell.

The cell used for the batch flotation experiments was a 3 L barker froth flotation cell. The air pressure was set to 7.5 L/min and the impeller speed was maintained to 1250 rpm. All floats were performed under the same conditions in the same cell. The sodium ethyl xanthate (SEX) was prepared at 1% (w/v) daily, with all reagents stored in a fridge when not used. Four concentrates were taken at time durations of: 2, 4, 6 and 8 mins. The top of the cell was scraped every 15 seconds and the entire float procedure (excluding conditioning times of reagents) lasted 20 minutes.

The ore was removed from the plastic bucket into the clean batch flotation cell, using only plant water. Plant water was added to the cell until the top of the pulp was at the required and marked level (3.75 L in this case). A 50 ml feed sample, using a 50 ml syringe, was taken from the slurry inside the cell. The collector (SEX @ 80 g/t) and co-collector (Senkol 700 @ 6 g/t) were then added to the slurry in the cell and allowed to condition for 2 minutes. After that, the frother (MIBC @ 25 g/t) was added to the slurry in the cell and allowed to condition for 1 minute. At this stage, the flotation procedure could start.

The air was turned on (7.5 L/min) and scrapes of the froth were made after 15 seconds, and every 15 seconds until the end of that specific float. Each concentrate (concentrate$_1$ (C_1) – concentrate$_4$ (C_4)) had different time durations, as follows: C_1 (2 mins); C_2 (4 mins); C_3 (6 mins); C_4 (8 mins). Thus, the entire duration of the concentrate collection lasted 20 minutes. The air was then turned off, and two 50 ml tails samples (using a 50 ml syringe) were taken out of the slurry in the cell. The cell was then emptied into a clean bucket and the whole remaining tails were filtered using a pressure filter.

Once the float procedure was finished each dish (including froth-pulp mixture) was weighed, each squeeze bottle (with remaining water) was also weighed. All concentrates, feed syringe and tails syringes were filtered and dried overnight in an oven set to 80 ^{o}C. The dried samples are then weighed. The individual samples are then bottled in sample bottles and labelled with respective float stage and ore type for chemical assay.

Initial flotation experiments were conducted with 12 g/t MIBC (frother dosage), and the same collector and co-collector dosage. The formation of “dead zones” on the lip of the flotation cell resulted in misrepresentative recovery results for the first two concentrates in the flotation procedure. The “dead zones” prohibited the natural overflow of concentrate froth as it entrapped the froth and sank it back into the pulp mixture. These “dead zones” were most prominent in the less volatile floating ores, and several attempted solutions were implemented. An increase in airflow, as well as an increase and decrease in impeller speed, were tested to try and rid the “dead zones” from the flotation experiments. The final solution reached was doubling the frother dosage, which increased the effervescent nature of the bubbles in the flotation cell and broke the dead zone, creating a consistent natural concentrate overflow during the initial stages of the flotation process, which is common and expected.

2.4.3 Screening for separation through four size fractions

Screening for mineralogy was done to four size fractions (+75, -75 +38, -38 +10 and -10 µm). Each ore type was milled to required P80, and dried overnight. The milled 1.3 kg aliquot was split 10 ways into 130 g aliquots. The 130 g aliquot was then wet screened through a 38 µm screen. All the sample that passed was filtered using a pressure filter and filter paper. The passing sample was placed in an oven to dry overnight. The sample caught by the screen was passed through a 75 µm screen, the passing and non-passing sample was filtered in a pressure filter and a benchtop Buchner vacuum flask respectively. The passing material represents the -75 +38 µm size fraction and the non-passing represents the +75 µm size fraction. Both samples were dried in an oven overnight. The sample that passed the 38 µm screen was placed in an ultrasonic bath with a 10 µm cloth at the bottom. A propeller is placed in the bath to keep the sediment in suspension. The 10 µm screening (through the cloth) was run for six hours, with the water being replaced every 2 hours. The water that is removed was filtered in a pressure filter (through filter paper) and dried in an oven overnight. The passing material represents the -10 µm size fraction. The sample that was caught in the 10 µm cloth was washed off the cloth, filtered using a pressure filter and dried overnight, this material represents the -38 +10 µm size fraction. The samples that had been dried overnight in the oven were removed from their respective filter papers and placed in zip-lock plastic bags.

2.5 ANALYSIS TECHNIQUES

The chemical and mineralogical analyses were conducted at three different facilities: Stellenbosch University (Central Analytical Facility), University of Cape Town (Department of geological sciences, Department of Chemical Engineering) and externally (Scientific Services CC).

2.5.1 Quantitative x-ray diffraction

Quantitative X-ray Diffraction (QXRD) of each ore type was performed on un-sized feed samples, these samples had been crushed and milled in accordance with section 2.4.1. The samples were analysed using a Bruker D8 Advance diffractometer with a LynxEye detector and CoKα radiation. Samples were scanned over a range of 5-90° 2θ with a step size of 0.02° and a counting time of 1 second per step. The QXRD generates mineral lists by analysing the crystallographic structure of each sample. Comparison of the analysed spectra of each sample with known peak positions and intensities of minerals allows the generation of a list of minerals present in the sample. EVA software was used to identify the minerals, TOPAS was used to quantify their abundances. The quantification was done using the Rietveld refinement method. QXRD has a lower detection limit of ±2% and minerals present in abundances less than this can therefore not be identified.

Correction techniques were applied to the QXRD analysis in order to avoid bias/over- under-estimation of minerals. These techniques all form part of the Rietveld refinement method (i.e. background corrections, preferred orientation corrections and Brindley microabsorption correction).

2.5.2 QEMSCAN

Samples were wet screened to required size fractions (section 2.3.4), dried and split (using a rotary splitter) into 1 g aliquots for QEMSCAN blocks (typically 3 x blocks per fraction). Milled graphite that is one size fraction smaller than the sample was added. The sample was mixed and screened through a sieve, one size bigger than the required sample. The ratio of sample to graphite is 2: 1. Graphite was added to minimise touching particles and also to help with electron conductivity. The mixed graphite and sample were carefully added with the desired mass of resin to form the mould. The sample moulds were placed into a Citovac vacuum chamber for 10 + 5 minutes (breaking the vacuum in between to release trapped air bubbles). Once the moulds had cured, a printed label was added and secured with further resin. Once completely cured the blocks were removed from the moulds for polishing. Polishing was done in a series of grinding and polishing steps until a 1 µm polish. After all of the polishing steps were complete and the samples had been rinsed of the polishing liquid they were placed in the ultrasonic bath for approximately 10 minutes. The quality of the final polish was checked using an optical microscope, ensuring that there were no plucked grains, large differences in relief, cracked / or grungy looking grains on the sample surface. The samples were carbon-coated using the Emitech carbon evaporator. The carbon coat is needed to diffuse electrons off the surface of the sample when they are in the QEMSCAN.

The operating conditions for the QEMSCAN analysis on the quarter core were unique to that of the feed and concentrate operating conditions. For the analysis of the quarter core, the QEMSCAN was

run at an accelerating voltage of 25 kV and a beam current of 10 nA using the field image analysis routine at a 1500 µm field size and a 15 µm pixel size. The operating conditions for the analysis of the feed and concentrate used the same accelerating voltage and beam current, the field image analysis routine was however changed, and unique for each size fraction analysed. The pixel sizes are 4 µm for the +75 fraction and 2 µm for all other fractions.

Each ore type had one or more epoxy mounts made, from both sections of quarter core (selected for their ore type representivity) and individual ore type feeds and concentrates (Fig. 8) (sized into four size fractions, described in Section 2.3.4). The quarter core epoxy mounts were used for reflected light microscopy. The vertical section technique was used in the setting of these QEMSCAN mounts, because of the sharp density difference between minerals found in the same ore type. The vertical section technique alleviates analysing bias (over-reporting heavy sulphide minerals and under-reporting lighter silicate minerals).

iDiscover was used to process the raw data generated from the QEMSCAN scans. A specific Species Identification Protocol (SIP) list was created in iDiscover for the quartz-dominant ores. The SIP list for the quartz-dominant ores consisted of 16 minerals, and one mineral named “other”. The “other” phase was used as a trap site for pixels that did not fit the criteria (signature) of any of the existing minerals. The “other” mineral does not exceed 1.85 wt. % in any of the samples. Trap phases were added to the main mineral phases (e.g. “chalcopyrite trap” – would fall under “chalcopyrite). This was done if one pixel within a well-established mineral displayed slightly unexpected values, which could be due to a few measurement inaccuracies (e.g. grain boundary of two minerals falling in the middle of the pixel or an uneven mineral surface, creating reflection artefacts). Post-processors were run on each sample in order to clean up the data before extraction. The pre-processors that were run included: size filter (>2 µm), boundary phase and touching particles. The mineral chemistry (probe data) was obtained from previous MSc work done on the deposit (Rudnick, 2016). This mineral chemistry (when appropriate) was used to give specific mineral formulas in the QEMSCAN, thus adding to the accuracy of the QEMSCAN analysis.

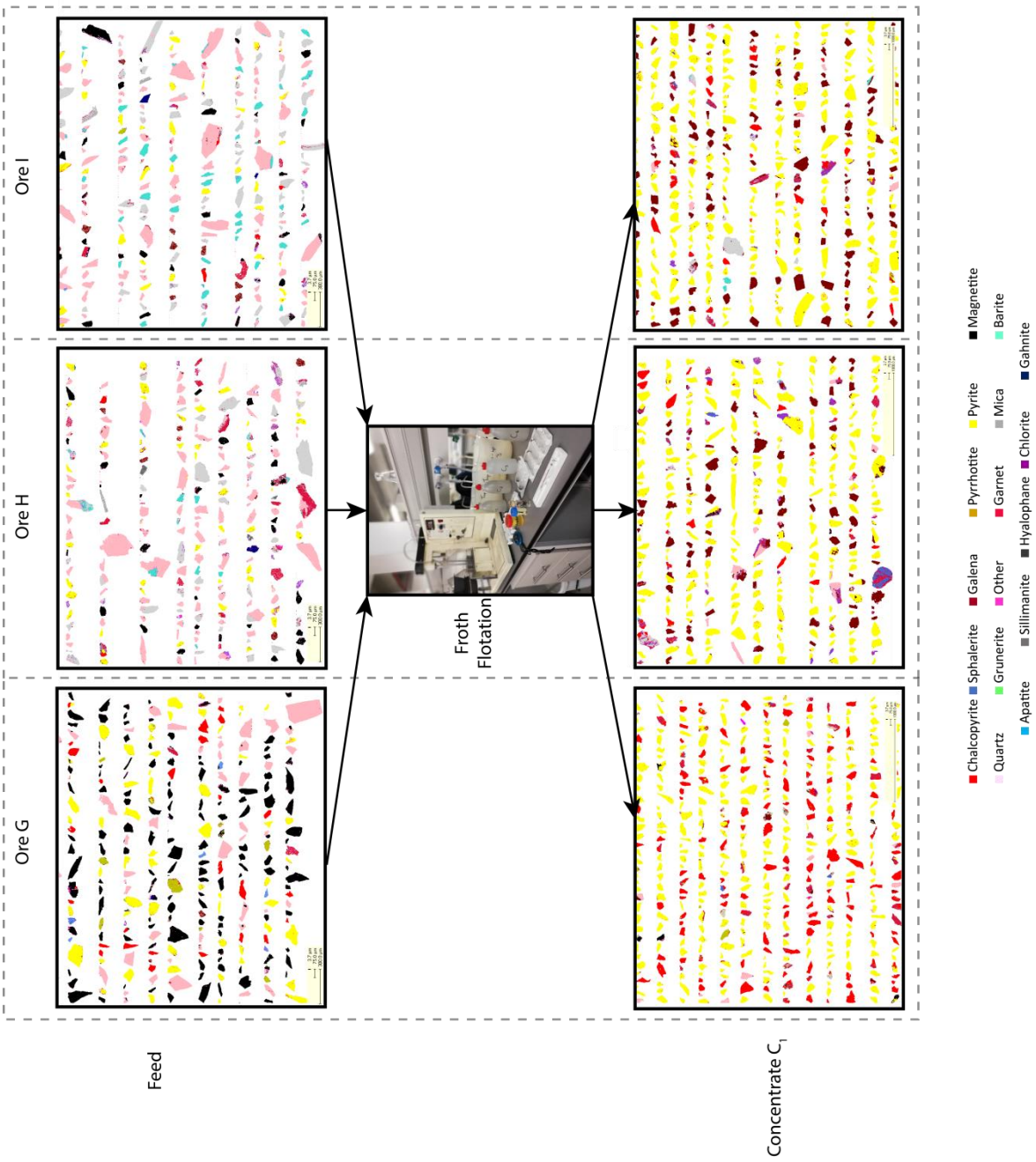

Figure 8: *False coloured feed (pre-flotation) and Concentrate C_1 (post-flotation) field scans of the three quartz-dominant ores using the QEMSCAN.*

2.5.3 X-ray fluorescence

The high sulphur nature of these samples leads to complications in determining certain elements using the X-ray Florescence (XRF) technique. Initially, samples were analysed at the Department of Geology (UCT), and then subsequently at the Central Analytical Facility (CAF) at Stellenbosch University. This was done in order to verify the results; the subsequent analysis at CAF took into special consideration the high sulphur nature of the crushed ore.

All ore types were submitted as un-sized feed samples. Major element oxides, as well as specific elemental concentration, were determined via XRF. High sulphur samples were analysed using

"Pellet Majors", and Zn-Cu-Nickel analysis was done on pressed pellets. A Panalytical Axios wavelength-dispersive XRF spectrometer with sample-changer (56 sample capacity) and a rhodium end-window X-ray tube was used for XRF. Trace element analysis of Zn-S-P was done using the pressed powder pellet method by XRF, Rh Tube. Base Metal analysis of Cu-Ni-Co-Fe-Pb was done using the pressed powder pellet method by XRF, Rh Tube, 3 kW.

Trace element, Sulfur, Phosphorous and base metal compositions were determined by XRF spectrometry on a PANalytical Axios Wavelength Dispersive spectrometer at the CAF, Stellenbosch University, South Africa. Unsized samples were crushed into a fine powder (in accordance with the procedure of section 2.4.1). Pressed powder pellets were prepared for XRF analysis using 8 g of the rock sample and a few drops of MOVIOL for binding. The spectrometer is fitted with a Rh tube and with the following analyzing crystals: LIF200, LIF220, LIF420, PE, and PX1. The instrument is fitted with a gas-flow proportional counter and a scintillation detector. The gas-flow proportional counter uses a 90% Argon, 10% Methane gas mixture. Matrix effects in the samples were corrected for by applying theoretical alpha factors and measured line overlap factors to the raw intensities measured with the SuperQ PANalytical software. The concentration of the control standards that were used in the calibration procedures for major element analyses fit the range of concentration of the samples. Amongst these standards were NIM-G (Granite from the Council for Mineral Technology, South Africa) and BE-N (Basalt from the International Working Group). A comparison of the measured and accepted major element compositions of the control standards used, as a reflection of the accuracy of the analytical technique, was presented with the data.

2.5.4 Inductively coupled plasma optical emission spectrometry (ICP-OES)

The analysis using ICP-OES was run at Scientific Services C.C. Initially a five-element (Cu, Pb, Zn, Fe and Mn) analysis was done on duplicate feed, concentrates and tails samples of each ore type. Subsequently, a 35 element analysis was done on feed samples from each ore type. To ensure the best resolution available, a Spectro Arcos ICP-OES was used for this analysis. This instrument is equipped with Charged-Coupled Device (CCD) detectors, the radial view limits the matrix effects.

2.6 DATA ANALYSIS AND COMPARISON

The generation and validation of a mineral list, as well as chemical data, was done by using more than one technique in order to cross-reference generated data. Chemical assays were generated through three techniques: XRF, ICP-OES and QEMSCAN. The QEMSCAN mineral list was validated by the mineral list generated by QXRD.

Chemical data accuracy and validation was done by converting all measurements to either elemental weight percentages or major element oxide concentrations (this was done by applying a conversion factor). The first and second rounds of QXRF, together with the ICP-OES results were compared to each other. A percentage error was given when comparing two different techniques, and if the ratio of one technique result over another was within this error range it was considered a good result. The same principle was applied to the mineral list, by using the QXRD and QEMSCAN data. The rationale behind having two rounds of QXRF analysis was because the initial results presented inaccuracies,

common in the QXRF analysis of high sulphur content samples. The second round of QXRF was focused on achieving more accurate sulphur concentrations, together with validating the other elemental concentrations in each ore type. The comparative results can be seen in below Figs. 9-11. The XRF vs QEMSCAN chemistry analysis excludes SO_3 due to its volatile nature and inconsistent analysis accuracy.

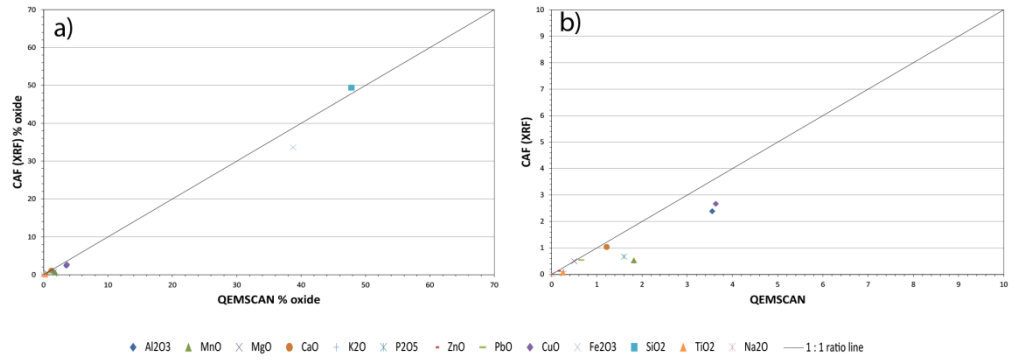

Figure 9: *Ore G major element oxides of XRF vs QEMSCAN. (a) Total major element oxides (excluding SO_3); (b) zoomed-in section, removing iron-oxide and silica-oxide.*

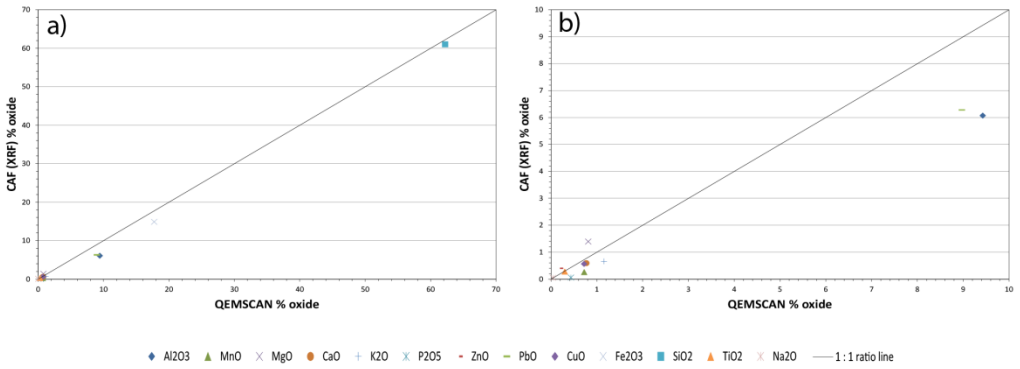

Figure 10: *Ore H major element oxides of XRF vs QEMSCAN. (a) Total major element oxides (excluding SO_3); (b) zoomed-in section, removing iron-oxide and silica-oxide.*

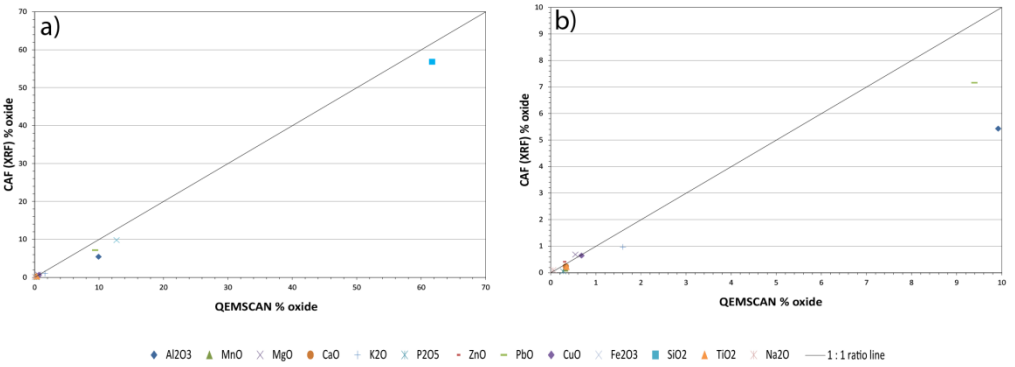

Figure 11: *Ore I major element oxides of XRF vs QEMSCAN. (a) Total major element oxides (excluding SO_3); (b) zoomed-in section, removing iron-oxide and silica-oxide.*

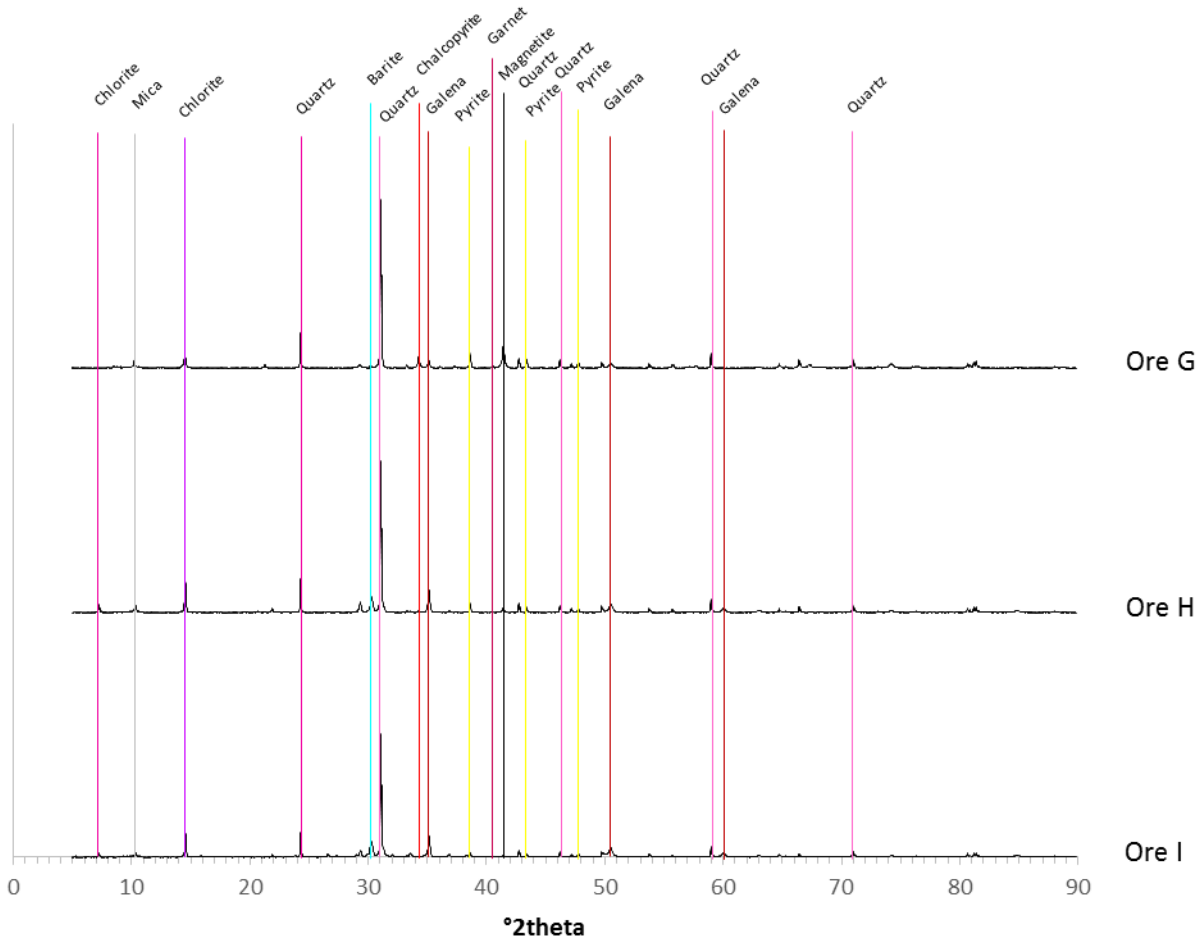

Figure 12: *XRD diffractograms showing proposed initial mineral list for Ore G, H and I.*

Chapter 3: Characterisation of Feed Ores

3.1 INTRODUCTION

The two valuable historical advances in the study of minerals processing were (1) the newfound understanding of the synergy between mineralogical understanding and minerals processing in the early eighties and (2) the development of automated mineralogical analysis techniques (Lotter et al., 2011). The fundamental knowledge base that underpins any mining operation is the implementation of an accurate and representative sampling campaign, together with detailed characterisation of the mineralogy and mineralogical textures of the valuable and non-valuable minerals in the ore (Hope et al., 2001; Lamberg et al., 2013; Olubambi et al., 2008). With significant advances in ore beneficiation techniques becoming less frequent, the detailed characterisation of an ore's minerals in terms of their morphology, chemistry and association with other minerals in the deposit is becoming of paramount importance (Cook, 2000). The in-depth study of ores helps explain and forecast most processing performances experienced by a mines' processing plant (Cropp and Goodall, 2005; Pinto and Gaspar, 1991; Xiao and Laplante, 2004). The importance of a detailed mineralogical understand of an ore deposit is also beneficial in generating exploration targets, and provide a comprehensive framework to predict mineralogy and related processing effects/performances (Olubambi et al., 2008; Sant'Agostino et al., 2001).

With modern advances in automated mineralogy, the once tedious process of keeping a consistently up-to-date mineralogical understanding is no longer as time-consuming (Bradshaw, 2014; Gu et al., 2014; Hope et al., 2001). These automated approaches to mineralogy (i.e. Quantitative Evaluation of Minerals by Scanning Electron Microscopy (QEMSCAN) or Mineral Liberation Analyser (MLA)) come with their drawbacks, although some drawbacks are similarly experienced in the analogue versions (I.e. reflected light microscopy) of these automated mineralogy techniques. The most fundamental issues are the representativity of the sampling campaign, and the sample analysed as well as diligence placed on sample preparation. However, sample representativity issues are somewhat overcome by the number of samples that can be analysed using automated techniques. The representativity of the sampling campaign and the diligence placed on sample preparation are however still critical to achieving good results (Goodall and Scales, 2007). Using automated mineralogy techniques, such as QEMSCAN, has other drawbacks such as the operator needing to be trained in the specific software. QEMSCAN can also underestimate grainsizes if the analysed sample

is not big enough. QEMSCAN is also prone to a fundamental bias when two minerals have opposing stereological dimensional properties (higher dimensional properties with lower-dimensional properties) (Spencer and Sutherland, 2000). Also, the generation of a specific species identification protocol (SIP) list for each deposit is unique, and requires a lot of time and chemical knowledge (of the minerals in that deposit specifically) in order for QEMSCAN analysis to be accurate (Pascoe et al., 2007).

Through the incorporation of automated mineralogy, this section will aim to create initial recommendations on the similarity/dissimilarity of quartz-dominant ore types. By analysing the makeup of individual ore types initial interpretations will be made, and potential minerals processing performances will be hypothesised for the individual quartz-dominant ore types. The potential grouping of quartz-dominant ores will be inferred; these insights will be based solely off mineralogical and textural information of the ore types and feed mineralogy/morphology.

3.2 METHODS

Selected quarter core was cast into epoxy mounts for QEMSCAN analysis, this was done based on the representativity of that section to its respective ore type. Reflected light microscopy descriptions were made (Section 3.3) on the same mounts as the QEMSCAN quarter core analysis. Bulk feed samples were split into four size fractions (+75, -75 +38, -38 +10 and -10 µm), by the process described in Section 2.3.3. These feed samples were then run through QEMSCAN and relative quantitative statistics were generated (process described in Section 2.4.2). Bulk mineralogy verification generated for the unsized feed was done by QXRD analysis (Section 2.4.1), this was done to validate the QEMSCAN analysis (Figs. 9-11).

3.3 ORE PETROGRAPHY

Ore mineralogy descriptions are made off false coloured QEMSCAN scans and ore textural descriptions are made off reflected light microscopy images of drill core sections of each ore type.

3.3.1 Ore G (HG_017)

This QEMSCAN section has areas of mica (muscovite and biotite; grouped for simplicity) foliation (bottom right), migrating into sections void of foliation (middle to top left). This mica, defining a foliation, is however minor in concentration (Fig. 13a). The chlorite does not follow the same foliation as the mica and is found as larger grains. The main groundmass is made up of quartz, magnetite and garnet (in order of decreasing concentration). Large subhedral grains of chalcopyrite are distributed across the sample, in some cases with locked non-economic sulphides (pyrite, pyrrhotite). Fibrous sillimanite grains show an association with the mica minerals (labelled as “mica” in the key). Relict large grains of garnet show poor re-equilibration, and are now found in the form of lobate, globular and disseminated smaller grains (Fig. 13a).

Figure 13b shows evidence of disseminated chalcopyrite grains closely associated with magnetite, pyrite and the quartzitic groundmass. Figure 13c similarly shows chalcopyrite association with

magnetite and quartz, both are photographs from the same sample in different locations on the sample, showing a wide variety of chalcopyrite grain sizes. The bottom image has distinctly larger overall grainsize, cleaner grain boundaries and overall subhedral grain shapes. The chalcopyrite grains show similar magnetite and quartz association (Fig. 13a and 13b). All chalcopyrite grains show alteration (possibly oxidation based alteration), commonly found in ores that undergo several stages of fluid migration/mineral dissolution. All chalcopyrite grains exhibit lobate grain boundaries and a low degree of grain "bending". The bottom image has a large chalcopyrite grain with locked magnetite and pyrite grains.

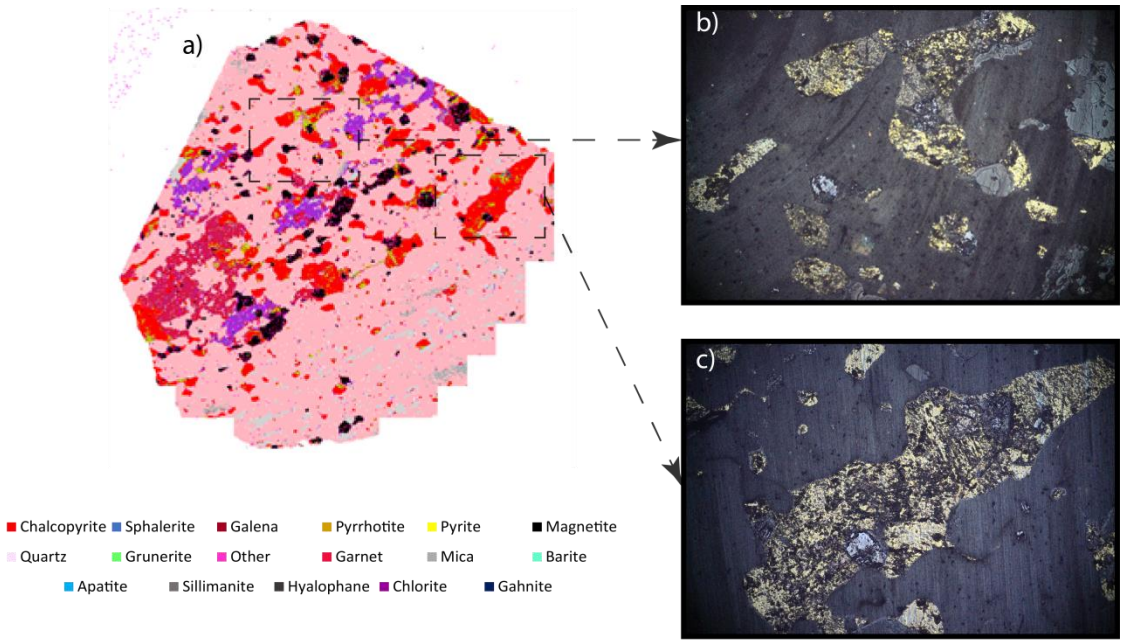

Figure 13: *(a) QEMSCAN false coloured image of ore G quarter core and two (b) and (c) reflected light photomicrographs taken off the same block (field of view of photomicrograph= 5mm). Due to the varying hardness of the minerals in the same ore, smooth polishing of the blocks fit for optical microscopy proved difficult.*

3.3.2 Ore H (HG_65)

A well-defined foliation is formed by elongate mica grains, and closely (and foliation following) related barite grains (Fig. 14a). The groundmass is made up of quartz with varying grainsize (<1 mm – 3 mm). Massive galena is found in the top right of this sample and appears to be void of foliation (Fig. 14a). A large locked, euhedral to subhedral, pyrite grain is found in galena, with galena inclusions respective found inside the locked pyrite (Fig. 14b). Fibrous and elongated sillimanite grains are found in the mica, with a minor prominence of an elongation direction subparallel to the mica (Fig. 14c). The foliation seems to wrap around the massive Pb sulphide, this may be due to galena replacement of a relict grain. Minor magnetite is scattered across the sample, with a slight association with galena. A

slight intensification of foliation is found moving through from the northeast to the south-west of the sample.

The mica's lamellae are curved around harder quartz, barite and magnetite (Fig. 14c). Figure 14a shows large-grained galena and pyrite, the galena has characteristic triangular pitting. The galena in Fig. 14c is also associated with barite, with galena being locked by barite in some cases. The bottom displays small-grained and disseminated galena and sphalerite associated with a wide variety of minerals (pyrite, magnetite, mica, quartz and barite). Supposed bending of the lamellae in the phyllosilicate minerals points towards the schistose/metamorphic nature of this ore. Poor re-equilibration can be determined by lack of triple junctions and anhedral mineral shapes

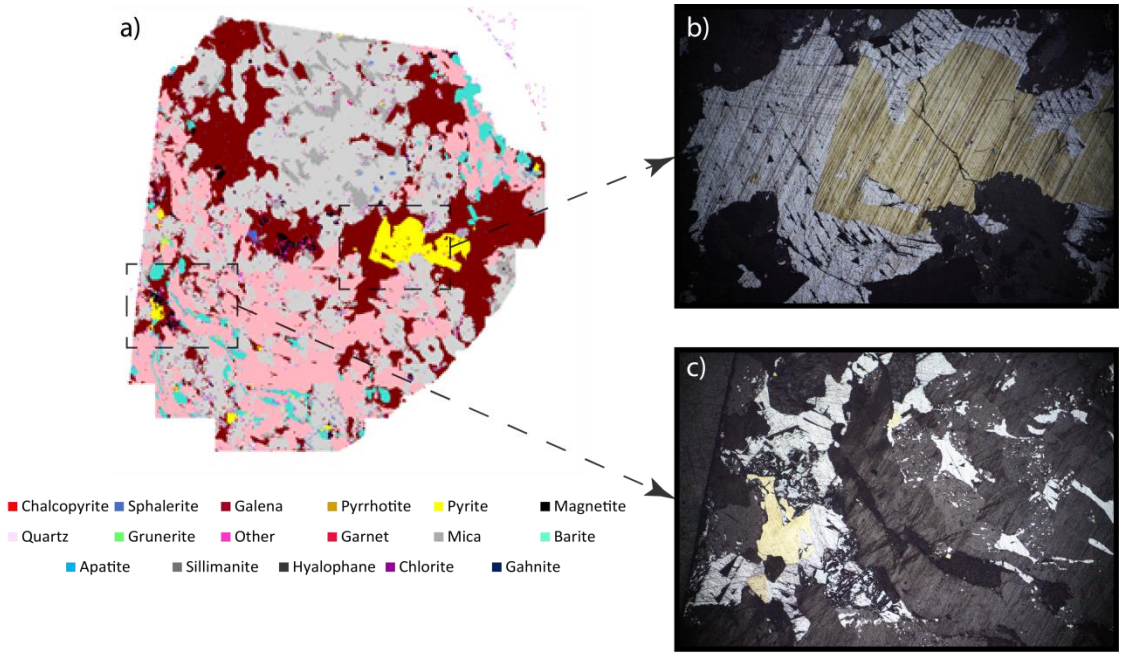

Figure 14: *(a) QEMSCAN false coloured image of ore H quarter core and two (b) and (c) reflected light photomicrographs taken off the same block (field of view of photomicrograph= 5mm). Due to the varying hardness of the minerals in the same ore, smooth polishing of the blocks fit for optical microscopy proved difficult.*

3.3.3 Ore I (HG_055)

Groundmass made up of ranging size (<1 mm - 3 mm) quartz grains. Elongated and foliation defining mica cuts across this sample, with closely associated fibrous sillimanite (Fig. 15a). Magnetite and loosely associated garnet are found to be associated with the mica. Disseminated chalcopyrite and pyrite are found overprinting several minerals (mica, garnet, galena and quartz). The orientation of the mica is less uniform in the top right half of the sample when compared to the well-orientated north-west to south-east conglomeration of mica and sillimanite in the left half of the sample. Triple junctions, together with equilibrated and euhedral mineral grains are largely absent in this sample.

Ore I is made up of minor, fine-grained and disseminated chalcopyrite, galena and sphalerite. The most abundant valuable sulphide mineral in this ore type is galena. The chalcopyrite shows small

amounts of alteration and is associated mostly with silicates. The galena is also mostly associated with silicates, it is however in some cases (Fig. 15c) associated with non-valuable sulphides (pyrite and barite). The overall grainsize of ore I is smaller than the other two ores', the average grainsize of the groundmass is ±1 mm. Ore I shows intermediate to poor grain boundary re-equilibration with almost absent triple junction examples.

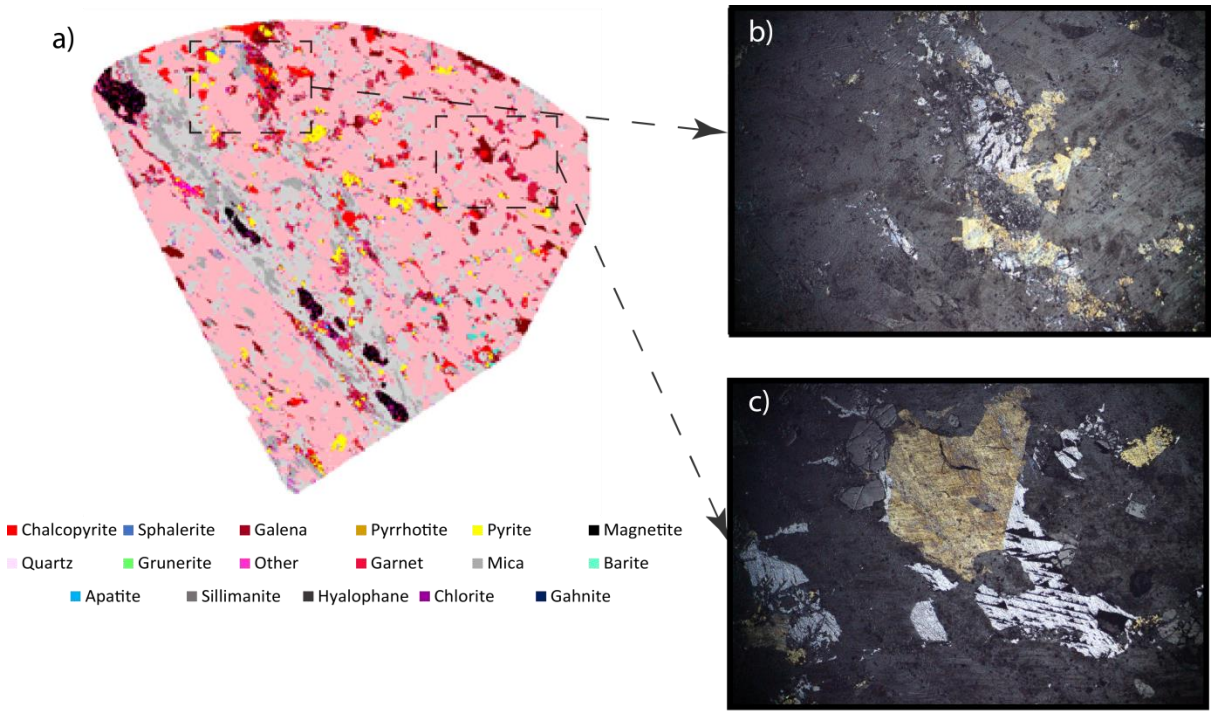

Figure 15: *(a) QEMSCAN false coloured image of ore I quarter core and two (b) and (c) reflected light photomicrographs taken off the same block (field of view of photomicrograph= 5mm). Due to the varying hardness of the minerals in the same ore, smooth polishing of the blocks fit for optical microscopy proved difficult.*

3.4 RESULTS

QXRD analysis (described in section 2.5.1) of the unsized, milled, flotation feed was performed to create a baseline mineral list of each ore type. The QXRD diffractograms for each quartz-dominant ore type can be seen in section 2.6 (Figs. 9-11).

3.4.1 Feed Mineralogy

All ore types were milled to a P80 where 65% sample passes 75 μm. The samples were then split into the four size fractions and run through the QEMSCAN (described section 2.3.3). This section aims to describe the bulk mineralogy (Fig. 16) as well as the distribution of minerals through all four size fractions (Fig. 17). QXRD is a quantitative analytical technique that is prone to stereological bias- thus the data derived from the QXRD (Fig. 12) will thus only be used to qualitatively justify the QEMSCAN mineral list.

The ground mass of all three ores is dominated by quartz, with ore H having more quartz compared to ores G and I. The three other most abundant non-sulphide minerals are magnetite, mica (muscovite,

biotite and chlorite) and garnet. Sample G is the most magnetite and garnet rich ore, of the three quartz-dominant ores. The two LOB ores have similar modal abundances of magnetite (substantially lower than ore G) and mica (slightly higher than ore G). The economic sulphides are made up of chalcopyrite, sphalerite and galena. The detection limit of the QXRD machine, however, precludes the identification of sphalerite. Ore type G has the highest chalcopyrite concentration, ore type I and ore type H, however, have low abundances of chalcopyrite (nearing the detection limit). Ore G has very low, below the detection limit, galena concentrations. The LOB ores, however, have relatively high galena concentrations, nearing a tenth of the sample (on average).

Table 4: *Feed mineralogical breakdown (as seen in Fig. 16), together with mineral group ratios.*

Bulk mineralogy - feed (wt%)			
Mineral	**Ore Type**		
	G	**H**	**I**
Chalcopyrite	5.3	1.1	1.0
Sphalerite	0.1	0.1	0.2
Galena	0.7	9.9	10.1
Total % Economic Sulphides (ES)	6.1	11.1	11.2
Pyrrhotite	1.9	0.5	0.3
Pyrite	10.7	7.6	4.7
Total % Sulphide Gangue (SG)	12.5	8.1	5.1
Magnetite	23.0	5.9	4.4
Gahnite	0.0	0.3	0.2
Quartz	40.6	47.1	45.8
Grunerite	2.2	0.4	0.4
Garnet	10.2	7.4	5.9
Mica	2.1	8.5	12.8
Apatite	1.7	0.3	0.1
Sillimanite	0.1	1.6	0.9
Hyalophane	0.0	0.3	0.7
Barite	0.1	2.4	8.7
Chlorite	0.5	5.6	2.7
Total % Non-Sulphide Gangue (NSG)	80.4	79.8	82.6
ES/SG	0.5	1.4	2.2
ES/NSG	0.1	0.1	0.1
SG/NSG	0.2	0.1	0.1

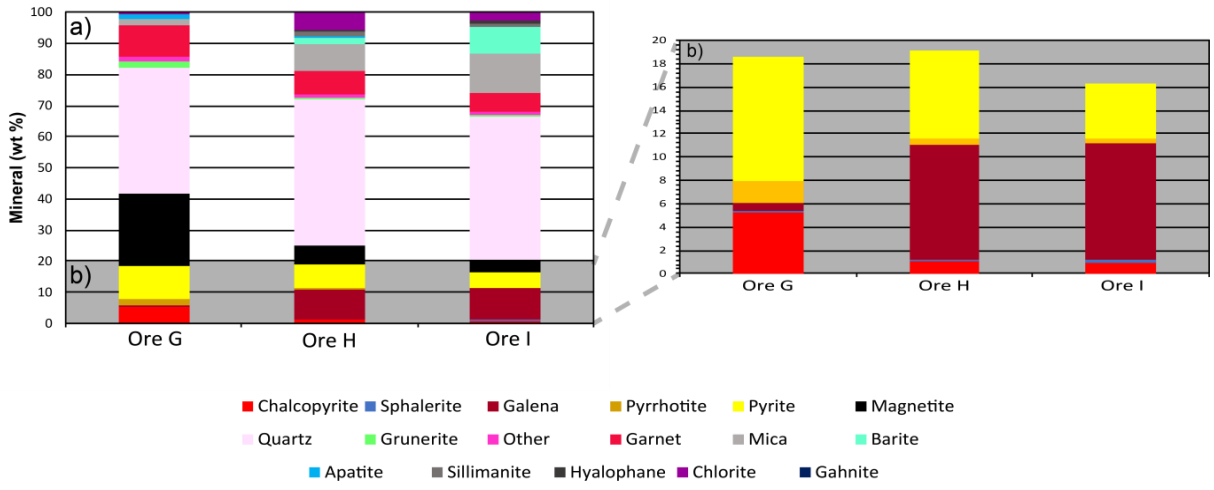

Figure 16: *(a) Bulk mineralogy of the quartz-dominant ore types; (b) Expanded section representing total sulphides in the three quartz-dominant ores. Note the difference in scales between (a) and (b).*

3.4.1.1 Ore G (Garnet Quartzite)

The most abundant gangue, quartz (lowest modal abundance of the three ores, 40.6 wt. %), concentrates in the larger size fractions with decreasing concentration as the size fraction decreases. This is inversely the case with the second most abundant gangue, magnetite (±25 wt. %), which concentrates in the smaller size fractions (Fig. 17a). The garnet abundances (10.2 wt. %) concentrate to the larger size fractions, similar to the other naming mineral in this ore type, quartz. Grunerite (2.2 wt. %), an amphibole-group mineral, and mica (2.1 wt. %, made up of a combination of muscovite and biotite) are both increasingly concentrated in the smaller size fractions (Fig. 17a). The apatite, sillimanite, hyalophane and chlorite abundances are all lower than 2 wt. %. Barite is discussed here as it is a sulphate mineral and will not be discussed with the other sulphide gangue. The minor Barite concentration (<0.1 wt. %) remains relevantly consistent throughout all four size fractions.

The ratio of pyrite to pyrrhotite is largely skewed towards pyrite abundance over pyrrhotite (± 5:1), the combined pyrite and pyrrhotite concentration is highest in G (≈12 wt. %). The overall abundance concentrations of pyrrhotite remain consistent between the four size fractions (Fig. 17b). The pyrite is found to progressively concentrate in the smaller size fractions; this, in turn, increases the pyrite-pyrrhotite ratio through the smaller size fractions (until slightly greater than 5:1).

The economic sulphides found in ore G are: chalcopyrite (5.3 wt. %), galena (0.7 wt. %), and sphalerite (0.08 wt. %). The chalcopyrite concentration progressively increases in smaller size fractions, this is also the case for galena (although in ore G galena is found in minor abundances). The sphalerite is found in very small abundances and shows no distinct distribution through the four size fractions. The total economic sulphide concentration increases by more than a factor of two from the largest to the smallest size fraction (Fig. 17b).

It is important to mention that minor gahnite is found in this ore type (0.03 wt. %) and is concentrated in the two larger of the four size fractions (Fig. 17a). The gahnite modal abundance is of importance, this is due to the refractory nature of this Zn-bearing oxyspinel.

3.4.1.2 Ore H (Mineralised Schist)

The main non-sulphide gangue phase is quartz (47.1 wt. %), the concentration of this quartz decreases through the decreasing size fractions, with similar concentrations found in the two largest size fractions. The second most abundant non-sulphide gangue is mica (8.5 wt. %, a combination of muscovite and biotite). The mica distribution forms an inverse bell curve, with the largest portions found in the largest and smallest size fractions, slightly lower amounts found in the -38µm + 10µm size fraction and the lowest concentration found in the -75 µm + 38 µm size fraction (Fig. 17c). The minor magnetite (5.9 wt. %) is evenly distributed between all four size fractions. The chlorite found in ore H has the highest modal abundance of the three quartz-dominant ores (5.4 wt. %) and is evenly distributed between the four size fractions. Garnet is slightly concentrated in the larger size fractions when compared to the smaller size fractions and has an overall modal abundance of 7.4 wt. %. Sillimanite (1.5 wt. %) has higher concentrations in the larger size fractions (Fig. 17c). Barite (2.4 wt. %) shows the same distribution as in ore type G, with progressively increasing concentrations from

large to small size fractions. The second barium-bearing mineral, hyalophane, shows a similar distribution to barite, however with overall lower concentrations than barite (0.3 wt. %). The almost absent grunerite has an even distribution through the four size fractions.

The non-valuable sulphides (sulphide gangue) present are: pyrite and pyrrhotite, with a pyrite to pyrrhotite ratio of approximately 14:1. This ratio shows that the sulphide gangue constituent of this ore type is made up almost solely of pyrite. The ratio has very slight to no change through the four size fractions (Fig. 17d). Differently to ore type G, this ore type does not concentrate the sulphide gangue to finer grain sizes fractions. The sulphide gangue in this ore type is more evenly distributed, with a slight concentration to the coarser grain sizes/size fractions. The total sulphide gangue constituent of this ore, 8.1 wt. %, has a lower modal abundance than in ore G.

This ore type, H, has low concentrations of chalcopyrite (1.1 wt. %) and sphalerite (0.13 wt. %). The two LOB ores' economic sulphides are dominated by galena. The chalcopyrite and sphalerite concentrations remain consistent through the four size fractions. The galena concentrations are however heavily concentrated in the smaller size fraction (Fig. 17d). Due to galena making up most of the total economic sulphides in this ore type (9.9 wt. %), the total economic sulphides concentration also shows an increases with the decreasing through the size fractions, with a total of over 25% in the -10 μm size category. Slightly larger amounts of gahnite (0.29 wt. %) are found in this ore type and are relatively evenly distributed through the four size fractions in this ore type (Fig. 17c).

3.4.1.3 Ore I (Sulphidic Quartzite)

The main non-sulphide gangue in ore type I is quartz, making up close to 50% of the sample (the most of the three ores). The quartz concentration decreases progressively from the largest size fraction, through the four size fractions, to the smallest size fraction (Fig. 17e). Similarly, to the other LOB ore, the concentration of the second most abundant non-sulphide gangue, mica (12.8 wt. %, as a combination of muscovite and minor biotite), has an inverse bell-shape distribution through the four size fractions. The magnetite (4.4 wt. %) has a relatively equal concentration distribution through the four size fractions (Fig. 17e). The garnet concentrates in the larger size fractions with decreasing concentrations through the four size fractions, with a total abundance of 5.9 wt. %. Ore I has the highest concentration of barite (8.7 wt. %), this barite concentrates in the smallest size fraction (-10 μm), with relative decreasing concentrations with increasing grainsize/size fraction (Fig. 17e). The second barium-bearing mineral, hyalophane, has lower concentrations (0.7 wt. %), but the same distribution as barite. The minor mineral, sillimanite (0.9 wt. %), has higher concentrations in the larger grainsize fractions, with decreasing concentration through the size fractions down to the -10 μm size fraction. Apatite is found in very minor abundances, but similar to the sillimanite, it concentrates in the larger size fractions. The grunerite is the most concentrated in the -10 μm size fraction, decreasing in concentration with an increase in size fraction.

The pyrite:pyrrhotite ratio of this ore type is similar to the other LOB ore type, H, (14:1). Differently to ore type H, the overall non-valuable sulphide concentration is slightly lower (5.1 wt. %). There is no distinct concentration of either pyrite or pyrrhotite through the four size fractions (Fig. 17f).

The low concentration of chalcopyrite (1 wt. %) remains consistent through the four size fractions, with no relative concentration in a particular size fraction; this is also the case for the valuable Zn-sulphide (sphalerite – 0.2 wt. %). The total economic sulphide abundance in this ore type is largely influenced by the total galena abundance (10.1 wt. %). The galena concentration in the finer size fractions is far larger than in the coarse fractions (Fig. 17f). The galena shows a progressive increase in concentration with a decrease in grainsize/size fraction.

This ore type has a minor presence of gahnite (0.2 wt. %), the distribution between the four size fractions is relatively equal (Fig. 17e).

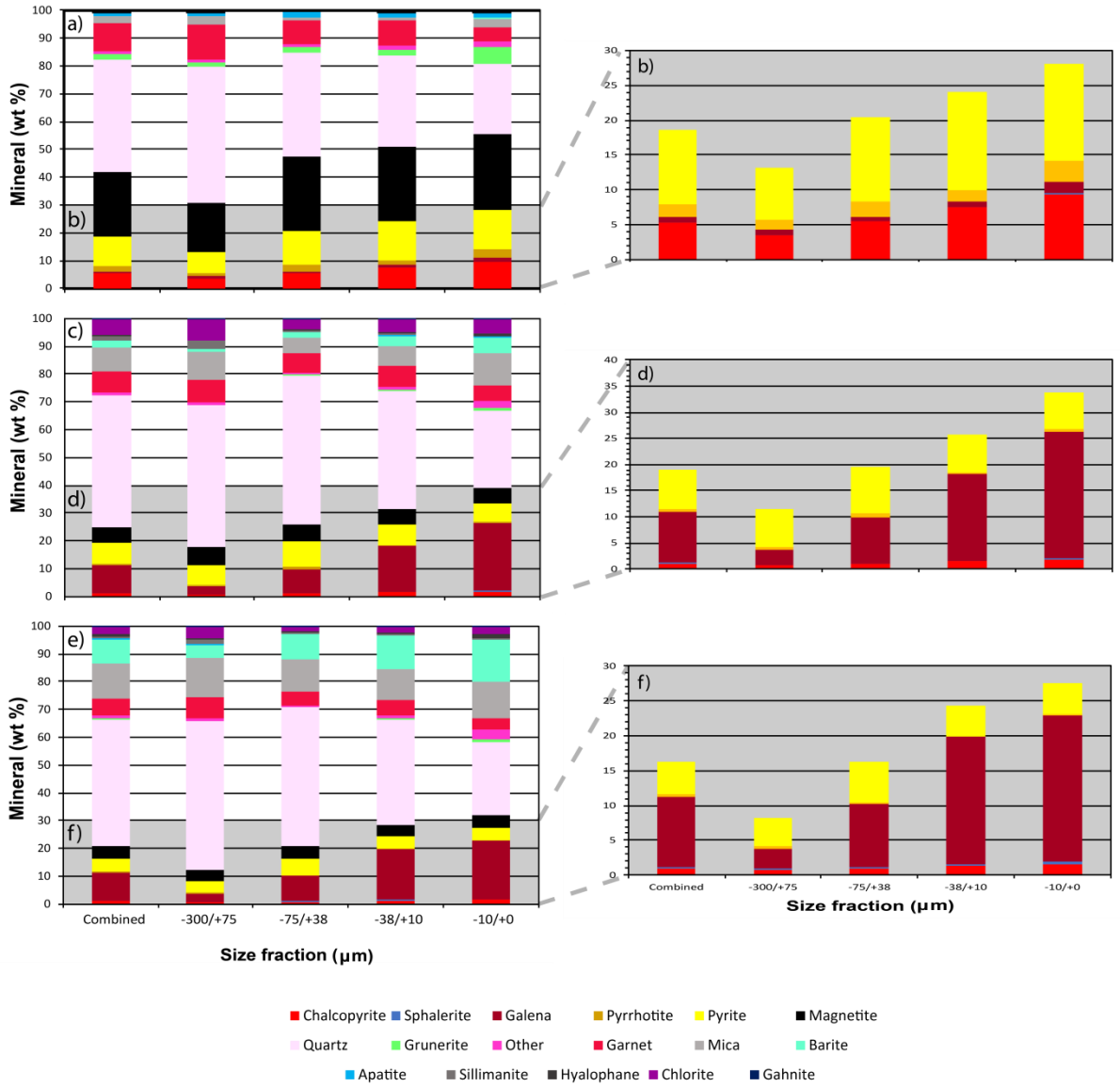

Figure 17: *Size by size feed mineralogy per ore type. (a) Size by size feed ore G and (b) total sulphides. (c) Size by size feed ore H and (d) total sulphides. (e) Size by size feed ore I and (f) total sulphides. The four size fractions are discussed in the methodology section 2.3.3. Note the difference in scales between the bulk and sulphide figures of the same ore type.*

3.4.2 Grainsize distribution

Grainsize distribution data is generated from QEMSCAN analyses of feed samples. The distribution data is in the form of cumulative grainsize plots (Fig. 18), with one µm bins, from one µm (the smallest grainsize to three hundred µm, which is the maximum grainsize. Seven minerals were targeted, three economic sulphides (chalcopyrite, galena and sphalerite), one sulphide gangue mineral (pyrite) and three non-sulphide gangue phases (quartz, magnetite and mica where mica represents muscovite, and biotite grouped together). Brief descriptions will be given on the distributions themselves, with the main focus given to the differences/similarities between the grainsize distributions of the three ore types.

The overall chalcopyrite grainsize distribution for each of the three ore types is similar, with slight variations between the three in the smaller (1 to 50 µm), intermediate (around the 90 µm grainsize fraction) and the large (around the 120 µm grainsize fraction) (Fig. 18a). The two LOB ores (H and I) have slightly more chalcopyrite in the smaller grainsizes compared to ore type G. Around 60 µm the three ore types converge, above that ore type H has slightly more chalcopyrite than G and I. At 120 µm grainsize the three ore types converge again and after that ore types H and I have slightly more chalcopyrite again, compared to G. The three ore types converge again at 150 µm and then move on to cumulative 100% of the sample section.

The two LOB ores show almost identical galena grainsize distribution trends, with a unique trend for ore type G. The LOB ores have higher concentrations of finer galena until the 100 µm grainsize mark. From 100 µm galena grainsize the three ores converge and show similar trends until the 100% cumulative mark (Fig. 18b).

The sphalerite grainsize distribution is slightly more erratic. The LOB ores have a higher percentage of fine sphalerite, until the 90 µm size fraction. At 90 µm ore type G starts showing a slightly higher percentage of finer sphalerite, when compared to ore type I. Ore type H consistently has finer sphalerite than the other two ores (G and I) (Fig. 18c).

The three ore types have similar grainsize distributions of pyrite, until the 80 µm grainsize fraction. From this point ore type H has a noticeably higher percentage of finer pyrite, compared to the other two ore types. All three ore types converge again around the 210 µm pyrite grainsize fraction; this is also nearing the 100% cumulative point (Fig. 18e).

The overall spread of quartz between the three ore types is slightly larger than other minerals. Ore type G has the highest percentage of coarse-grained quartz, ore type H has the highest percentage of fine quartz, with ore type I's grainsize distribution sitting between the two other ore types. The cumulative 100% mark is only obtained at around 270 µm, this speaks to the overall large grain-sized nature of quartz found in the feed samples (Fig. 18f).

The magnetite grainsize distribution between the three ore types is similar until the 60 µm grainsize fraction. At coarser than 60 µm grainsize the two LOB ores follow the same trend, and have a higher

concentration of finer magnetite, compared to the coarser-grained magnetite equivalents of ore type G (Fig. 18d).

The mica (muscovite and biotite) grainsize distribution for the two LOB ores is similar through all grainsize fractions. The LOB ores have a higher concentration of finer grained mica compared to ore type G, this is the case until approximately the 150 µm grainsize fraction. At this point ore type G has a higher concentration of finer grains mica than the two LOB ores. The grainsize distribution of ore type G is slightly erratic, with small jumps in percent amounts over small changes in grainsize increase (Fig. 18g).

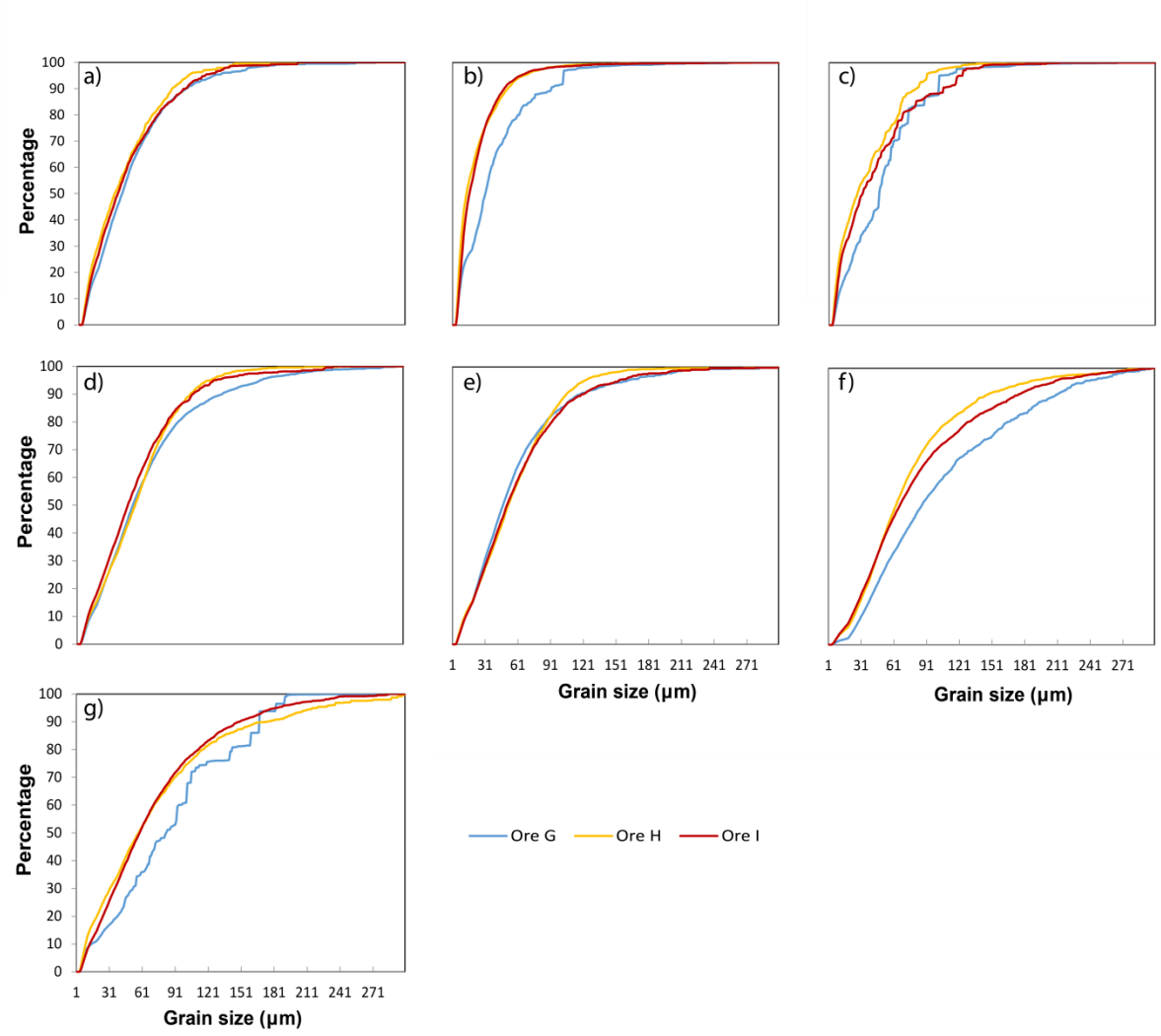

Figure 18: *GSD curves of the three quartz-dominant ores for: (a) chalcopyrite, (b) galena, (c) sphalerite, (d) magnetite, (e) pyrite, (f) quartz and (g) mica. The total number of sulphide grains measured for chalcopyrite (ore G - 79430, ore H – 18303, ore I – 17448), galena (ore G – 10479, ore H – 151553, ore I – 145606), sphalerite (ore G – 2845, ore H – 4569, ore I – 5263) and pyrite (ore G – 117917, ore H – 56556, ore I – 42234) show the confidence at which the GSD measurements were made (the higher the particle count the higher the confidence in the GSD results). The size measurement for a grain was conducted using equivalent spherical diameter as the measuring technique.*

3.4.3 Mineral liberation

This mineral liberation section will focus on the liberation profiles as well as the fraction of the sample that is deemed to be completely liberated (a particle that is made up of 90% or higher of the same mineral, by area) of each ore type, through four size fractions (+75 µm, -75 µm + 38 µm, -38 µm +10 µm and -10 µm). The liberation profiles of interest are the profiles of the three economic sulphides, targeting: chalcopyrite, galena and sphalerite.

Chalcopyrite is 90% liberated in Ore G. The total amount of liberated chalcopyrite increases the finer the size fraction; due to the almost completely liberated nature of the chalcopyrite in this sample the increase in liberation through the smaller size fractions is minor. The total amount of liberated chalcopyrite in ores H and I are lower than that in G, at 75% and 78% liberated respectively. H shows a similar profile of increasing liberation with the decrease in size fraction. The amounts of completely liberated chalcopyrite through the four size fractions does have larger jumps (between size fraction) when compared to G. This increased dispersion between size fractions is well depicted by the spread (in the Y-axis) between profiles of liberation in the four size fractions. The lower total liberation is shown by the more gradual increase in profile of the curve, when compared to G. Ore type I has a very similar profile and total liberation of chalcopyrite compared to ore type H. Ore I has a total chalcopyrite liberation of 78% and a similar increase in liberation with a decrease in size fraction. The wide dispersion in chalcopyrite liberation seen in Table 5 for ore type H is closely paralleled to those seen in Table 5 for ore type I.

The total amount of liberated galena for ore type G is 52%. The general trend for increasing amounts of liberation through fining of size fraction is consistent for this mineral in this ore type. The amount of liberated galena between the size fractions does, however, change drastically as you move between size fractions (21% liberate at +75 µm and 63% liberated at -75 µm + 38 µm). The dispersion of liberation between size fractions is well displayed by the large spread of profiles in Table 5. The gradual profile of the curve speaks to the low amount of overall completely liberated galena in ore type G. The total amount of liberated galena in ore type H is 71%. Similar increase in liberated galena with the decrease in grainsize fraction, the difference in liberated galena between the size fractions is not as drastic as found in G. The distribution of liberation for galena in Table 5, for ore type H, are more condensed, speaking to the similar liberation behaviour of galena in ore H between the four size fractions. The total amount of liberated galena in ore type I is 78%. The same profile for increased liberation of galena with a decrease in size fraction stands true for ore type I. The liberation plot in Appendix A shows a wide dispersion of curves, all with relatively consistent profiles, depicts the change in liberation between size fractions, this can also be seen in Table 5. The largest size fraction has the lowest liberation of galena, and the inverse is true for the smallest size fraction as expected.

The total amount of liberated sphalerite in sample G is 50%. Unlike the above descriptions of economic sulphide liberation for ore G, the liberation of sphalerite is seen to decrease with decreasing grain size. The total amount of liberated sphalerite in ore type H is 22%, with liberation increasing with decreasing grainsize. The wide spread in liberation for sphalerite in Table 5 for ore type H shows

liberation increasing with decreasing size fraction. The total amount of liberated sphalerite in ore type I is 16%, similar to Ore H, meaning that the two LOB ores have similar liberation profiles for sphalerite. Sphalerite liberation in ore type I has the widest dispersion between size fractions, indicating large differences between the liberation profiles of each size fraction (Table 5).

Pyrite liberation for the three ores is similar, with a slight increase in liberation with a decrease in grain size. The spread of liberation profiles between the four size fractions is small in all three ore types, showing that pyrite liberates well, irrespective of the grind size. The total liberation of pyrite for ore G is 70%, for ore H is 66% and for ore I is 72%. This is important because the high liberation of pyrite in the feed relates to pyrite being highly susceptible to suppression should a pyrite depression reagent be added to the flotation reagent suite.

For a graphical representation of the liberation through the four size fractions across the four above stated minerals of the quartz-dominant ores, see Appendix A. The liberation profiles of each ore type through increasing percentages of liberation can be seen in Appendix A.

Table 5: *Mineral liberation across the different quartz-dominant ore types and size fractions for the feed. Liberation here is defined as particles with greater than 90 % of the mineral of interest by area.*

Percentage mineral liberation of minerals of interest in the feed					
Minerals	Ore G				
	Combined	+75µm	-75µm +38µm	-38µm +10µm	-10µm
	Feed	Feed	Feed	Feed	Feed
Chalcopyrite	90	84	92	96	96
	(79430)	*(1509)*	*(6506)*	*(36006)*	*(35409)*
Galena	52	21	63	58	58
	(10749)	*(475)*	*(1067)*	*(4362)*	*(4845)*
Sphalerite	50	63	28	56	56
	(2845)	(275)	(638)	(1371)	(561)
Pyrite	70	71	69	78	78
	(117917)	*(1899)*	*(11204)*	*(57372)*	*(47442)*
Ore H					
Chalcopyrite	75	60	77	87	87
	(18303)	*(1294)*	*(2313)*	*(6215)*	*(8481)*
Galena	71	48	77	86	86
	(151553)	*(3387)*	*(9605)*	*(55714)*	*(82847)*
Sphalerite	22	17	7	25	25
	(4569)	*(389)*	*(811)*	*(1882)*	*(1487)*
Pyrite	66	59	67	82	82
	(56555)	*(2413)*	*(5556)*	*(20099)*	*(28487)*
Ore I					
Chalcopyrite	78	66	83	88	88
	(17448)	*(1326)*	*(1708)*	*(7388)*	*(7026)*
Galena	78	57	88	85	85
	(145606)	*(4814)*	*(8903)*	*(69893)*	*(61996)*
Sphalerite	16	2	6	27	27
	(5263)	*(469)*	*(785)*	*(2519)*	*(1490)*
Pyrite	72	69	74	77	77
	(42234)	*(2076)*	*(3974)*	*(18910)*	*(17274)*

**Value given in brackets represents the amount of sulphide particles analysed.*

3.4.4 Bulk economic mineral association

It is important to note that the associations seen in Figs. 19-21 are somewhat deceptive, as they are associations to a target mineral, but they do not take into account the abundance of that mineral. For

example, sphalerite has close to a 40% association to chalcopyrite in the ore G, but, because of the minuscule modal abundance of sphalerite in ore G, this is not of grave importance. The order of wording is also of utmost importance, for example, 40% of sphalerite is associated with chalcopyrite in ore G, this does not mean that 40% of chalcopyrite is associated to sphalerite, the difference between the two statements is imperative to conceptualise.

3.4.4.1 Chalcopyrite association by size

All three ores show a slight (<6%) chalcopyrite-pyrite, chalcopyrite-magnetite, chalcopyrite-quartz and chalcopyrite-galena association. The chalcopyrite in ore type G is mostly completely liberated, thus through all four size fractions, there is very little chalcopyrite association. The chalcopyrite in ores H and I are mostly liberated (less so than in ore G), resulting in similarly low mineral associations. Chalcopyrite has minor associations to sphalerite (evenly across all four size fractions) in ore I. Chalcopyrite also has low associations with pyrite, mica and quartz (with highest association amounts in the +75µm grainsize fraction). The chalcopyrite-sphalerite and chalcopyrite-mica associations are only evidently seen in the LOB ores (H and I).

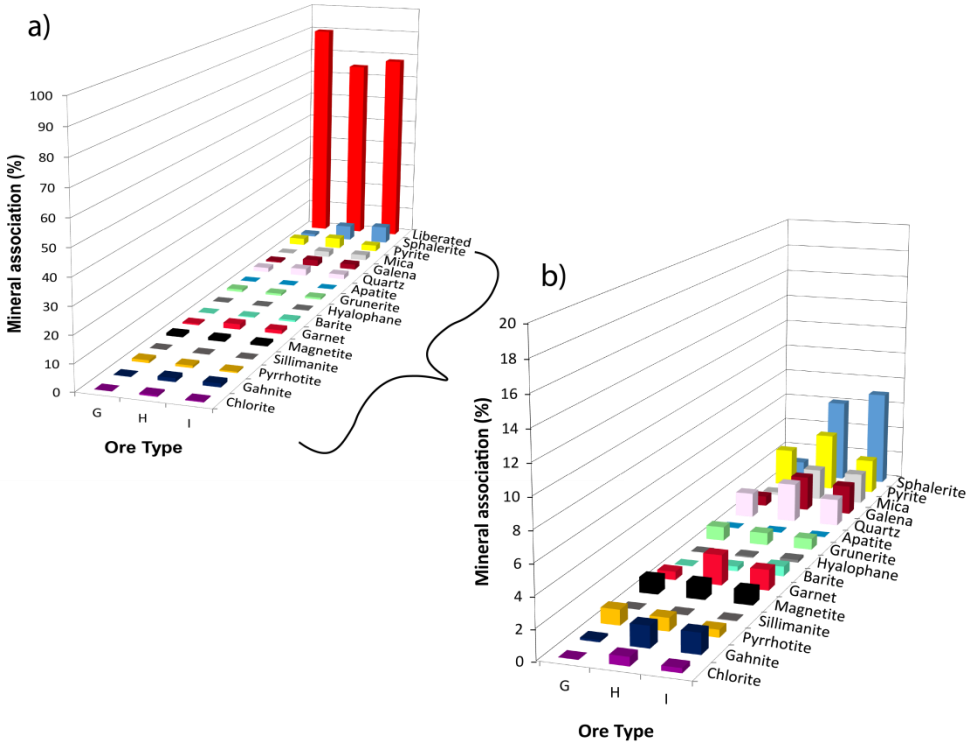

Figure 19: *(a) Bulk chalcopyrite association across the three quartz-dominant ores. (b) Expanded version removing the liberated component from the association profile. Note the difference in scales between (a) and (b).*

3.4.4.2 Galena association by size

Galena is mostly liberated in ores H and I, with a high association to mica, with ore type H having the highest association. The galena in ore type G has only a slight association to mica. All three ores' galena is associated to quartz, ore type H has the lowest galena-quartz association. The galena in ore

type G has a strong association with chalcopyrite; the LOB ores show very little galena-chalcopyrite association. All three ores show a galena-pyrite association, ore type G has the highest association of galena to pyrite, the LOB ore has a lower amount of galena-pyrite association. Ore type G has galena-magnetite, galena-pyrrhotite and galena-grunerite associations, whereas the LOB ores show very little of the three mineral associations. The galena association to mica and quartz in ore type G is concentrated in the +75 μm size fraction. The galena-barite, galena-magnetite and galena-pyrrhotite associations in ore G are evenly distributed through all four size fractions. The galena-quartz and the galena-barite associations are substantially lower than that of the galena-mica association in ores H and I, but also show even distribution across the four size fractions.

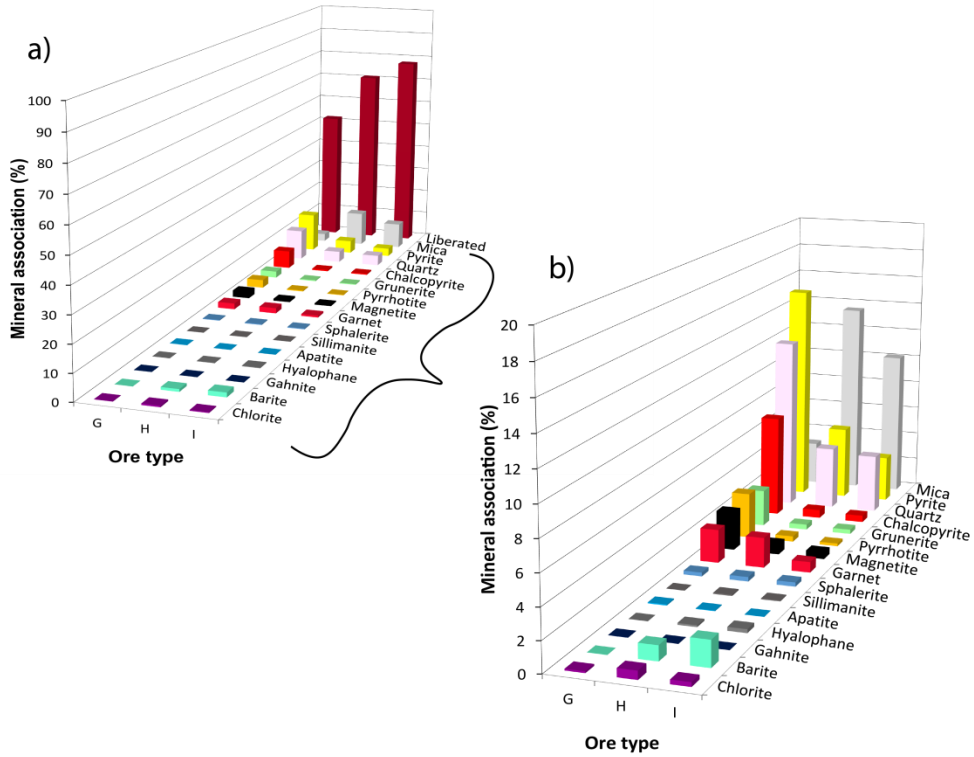

Figure 20: *(a) Bulk galena association across the three quartz-dominant ores. (b) Expanded version removing the liberated component from the association profile. Note the difference in scales between (a) and (b).*

3.4.4.3 Sphalerite association by size

The sphalerite in the three ores is predominantly associated with chalcopyrite (more so in the LOB ores), all other sphalerite associations are minor. The ore type G has minor sphalerite-magnetite and sphalerite-quartz association, and very little other sphalerite association (apart from the association to chalcopyrite). Sphalerite association to chalcopyrite and galena is evenly distributed across the four grainsizes fractions in ores H and I, with lesser amounts of sphalerite-mica, sphalerite-garnet, sphalerite-apatite and sphalerite-magnetite association (all of which decrease in association with decreases in grainsize fraction). A sphalerite-gahnite association is also present (mostly in the LOB ores), with a slight decrease in association with a decrease in size fraction.

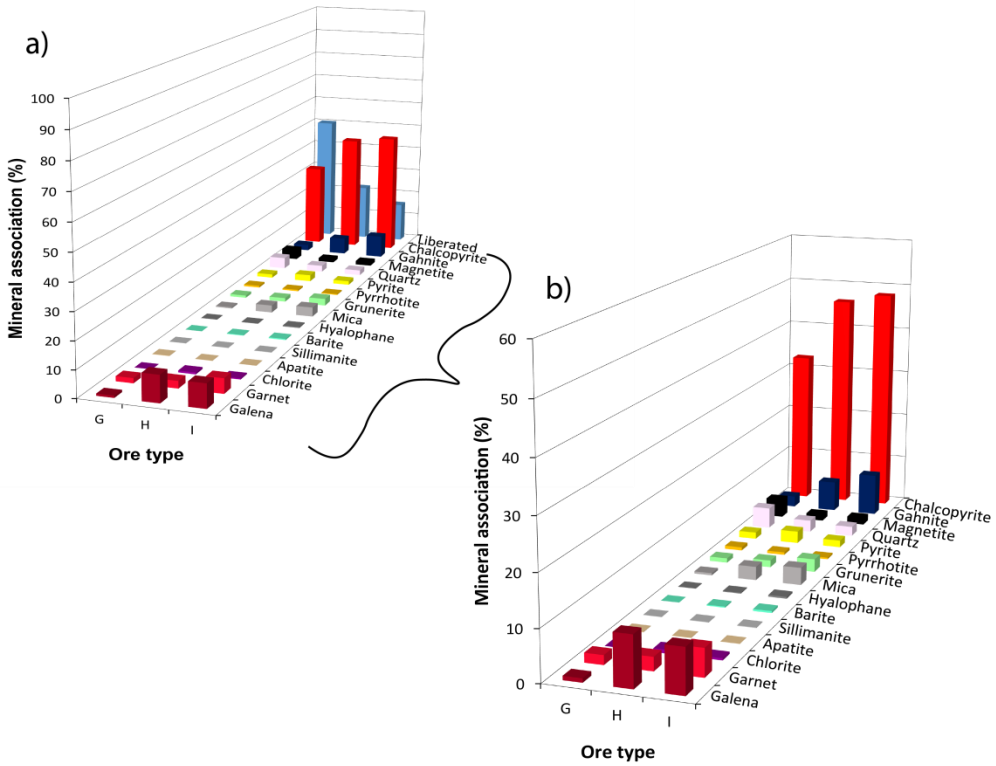

Figure 21: *(a) Bulk sphalerite association across the three quartz-dominant ores. (b) Expanded version removing the liberated component from the association profile. Note the difference in scales between (a) and (b).*

3.5 DISCUSSION

Speed, accuracy and cost-efficiency are the most important aspects of relaying information from a mineralogical level to a minerals processing level. The discussion below will attempt to create metallurgical domains based solely off mineralogical information. Further investigations into the accuracy of these domains will be explored in the minerals processing section (Chapter 4).

3.5.1 Initial geometallurgical domain delineation

The quantity and presence of certain valuable and non-valuable minerals present in each ore type are slightly different, however, general classification and grouping is possible. To create more appropriate groupings of ore types, the ore texture interpretations from the reflected light microscopy need to be included in the rationalisation process necessary for creating purposeful ore groups/ore domains.

The non-sulphide gangue constituents of the quartz-dominant ores vary slightly between the ore found in the GQOB and the ores found in the LOB. The simple difference between the non-sulphide mineral abundance is not the sole discerning factor regarding non-sulphide gangue. The non-sulphide gangue minerals of importance are: quartz, magnetite, garnet and mica. All three ore types have quartz present, in slightly varying proportions. The quartz abundance is thus not a contributing factor in the thinking behind separating/grouping of certain ore types. The combined modal abundance of magnetite and garnet in ore G (33.2 wt. %) is substantially higher than in ores H (13.4 wt. %) and I

(10.3 wt. %). The combined abundance of these two minerals could be of importance in downstream processing due to their high relative hardness. The presence of mica group minerals in the LOB and their absence in the GQOB could also provide issues in processing due to their slaty cleavage.

The notable features/characteristics seen when analysing the ore mineral textures is the grainsize, form and type of economic sulphides present in each ore type. In ore G the chalcopyrite has a medium to large grainsize with a general subhedral grain shape, with minor quantities of other economic sulphides (galena and sphalerite). Ore's H and I have very little chalcopyrite present, the major economic sulphides in these ores are galena. The galena has a more interstitial and anhedral grain shape, with an overall smaller grainsize (compared to the chalcopyrite of ore G).

3.5.2 Domain characterisation through mineralogy by size differences

The mineralogy by size comparison between ore types is an interesting way of classifying groupings; this analysis can provide insights to the manner and behaviour of minerals/mineral groupings once an ore has been subjected to milling. The mineralogy by size information also provides important information; by understanding the mineralogical makeup through the size fractions of the feed the processing team can predict ore behaviour (such as the mechanism of concentration). The processing team can also implement a strategy to target certain minerals, economic or gangue, with the size of the said mineral being an integral piece of information.

In all three ore types, the relative quantity of quartz decreases through the progression from the largest size fraction to the finest size fraction (+75 µm, -75 µm + 38 µm, -38 µm +10 µm and -10 µm), thus making quartz a common characteristic through all four size fractions in all three ore types. The distribution of magnetite between the four size fractions is a unique characteristic that could be used to create ore groupings. In ore type G, magnetite has close to double the relative concentration in the smallest (-10 µm) size fraction when compared to the largest (+75 µm) size fraction (27.5 wt. % and 17.5 wt. %, respectively). This is not the case in the LOB ores (H and I). The equivalent concentrations in H (5.2 wt. % and 6.2 wt. %) and I (4.4wt. % and 4.3 wt. %) do not show a clear concentration of magnetite in the smaller size fractions. The distribution of mica between the four size fractions in the three ore types is similar, although the LOB has far higher mica abundances; the distribution pattern through the size fractions is comparable. The barium sulphate mineral, barite, is concentrated in the smaller size fractions in the LOB ores, with a progressive decrease in concentration with an increase in size fraction. This barite signature is not noticeable when analysing the mineralogy by size of ore G. The decrease in NSG from the largest to smallest size fraction is slightly different between the ores of the two ore bodies. The average total decrease of NSG from the largest to smallest size fraction is ±18 wt. %, ore G has the smallest decrease in NSG, whereas, ores H and I have a similar decrease.

The non-valuable sulphides are a focal point due to the consequential effect they could have on a processing circuit. For simplicity pyrite and pyrrhotite will be combined in the description of their concentrations by size (Non-Valuable Sulphides, NVS). In the ore G the concentration of the NSV increase form the largest (+75 µm) size fraction to smallest (-10 µm) size fraction (12.5 wt. % - 15.8

wt. %), whereas the concentrations of the NVS in the LOB ores do not (H = 8.1 wt. % - 7.5 wt. %, I = 5.1 wt. % - 4.5 wt. %); they decrease slightly.

The total economic sulphide (ES) profiles of all three ore types show a gradual to steep increase with a decrease in size fraction. The main difference between the ore types is not the change in the ratio of economic sulphides through size fractions, but the abundance of specific economic sulphides present in certain ore types. Ore G is rich in the Cu-bearing mineral, chalcopyrite, and poor in the Pb and Zn sulphides (galena and sphalerite). The LOB ores are, however, rich in galena and poor in chalcopyrite and sphalerite.

The mineralogy breakdown through the four size fractions shows similarities between the three ore types. The overall increase in the relative concentration of ES minerals in the smaller size fractions, in all three quartz-dominant ores, provides insights to the milling circuit, and how the milling is achieving the desired efficacy. The overall decrease of NSG in the smaller size fractions is also a desired outcome during the milling process, this is due to the possibility of ultra-fine gangue being entrained in the flotation process.

3.5.3 Grain size implemented ore-domaining

The analysis of the grain size distribution (GSD) of seven minerals (chalcopyrite, galena, sphalerite, pyrite, magnetite, quartz and mica), deemed to be important, between the three ore types may highlight differences/similarities between the three ore types.

The GSD profile of chalcopyrite for the three ore types is similar; this is reiterated by the chalcopyrite description in the above section because GSD does not take into account the abundance of a mineral. The GSD profiles for galena shows two distinct groups, one group made up of the LOB ores and the other made up of the GQOB ore. The GSD profiles for sphalerite are erratic; this could be due to sphalerite being a minor (and possibly accessory) phase, no distinct groupings can be made from looking at these profiles.

The GSD profiles for pyrite are very similar between the three ore types and do not highlight any distinguishing features between the three ores.

The GSD profiles for magnetite have two unique trends. The LOB ores follow the same trend through the intermediate grain sizes (60 μm – 180 μm). The ore G has a lower percent of magnetite in the intermediate grain sizes, compared to the ores of the LOB. The GSD for quartz has three distinct profiles, it could, however, be postulated that two of the profiles are more similar than that of the third. The two “similar” quartz GSD profiles are those of the LOB ores, with ore G presenting a “unique” profile. The overall trend of the quartz GSD indicates that the LOB ores have a higher percentage of fine-grained quartz, compared to ore G. The GSD profiles for mica has two distinctly different groups, but not for the same reason that the other minerals mentioned above did. The first group is made up by the ores of the LOB, these ores have a smooth increasing cumulative curve with an increase in grain size. Ore G, however, has an erratic curve with large percent jumps over small increases in grain size, this ore makes up the second group.

Comparing the grain size distribution of certain minerals in the feed could be a means of separating/grouping ores, should the variance of a mineral's GSD between the ores be substantial enough to the justify a separation/grouping. The GSD of the seven minerals in the three quartz-dominant ores shows unique distribution patterns (depending on the ore body of origin). The unique GSD patterns of ore G compared to ores H and I are, however, not substantial enough to be a discriminatory factor in the groupings of ores into domains. The unique GSD patterns of the GQOB ore compared to the LOB ores show that the degree of foliation (higher degree of metamorphism/foliation exhibited/preserved in the LOB ores) has an impact on the GSD, albeit minor.

3.5.4 Mineral association and liberation as a proxy of feed complexity

The relative association of the three economic sulphide minerals with the other gangue phases found in the ore is shown in Figs. 15-17. The association complexity is inversely dependent on the mineral in question's liberation characteristics (the higher the percentage of liberation the less complex the association characteristics of that mineral are). A culmination of both liberation and association can be used to describe the feed complexity, the higher the liberation percentage (and related low amounts of association) of an ore, the less complex the ore is (at a feed stage), and vice versa for low percentages of liberation and high amounts of association.

The bulk mineral associations of the three economic sulphides show that ore G and the ores of the LOB (H and I) have slightly different association signatures. The chalcopyrite in ore G has very little other minerals associated, whereas the LOB ores' chalcopyrite is associated with small amounts of sphalerite, pyrite, mica, galena and quartz. This is reiterated by looking at the liberation statistics of chalcopyrite in the feed, with ore G having a higher chalcopyrite liberation than the ores of the LOB. Ore G's unique galena association profile is distinguished by the association with: chalcopyrite, magnetite, pyrrhotite and grunerite whereas the LOB ores' galena is not associated with these minerals. The galena liberation in the feed for ore G is substantially lower than the ores of the LOB (H and I). The sphalerite association shows that all three ores have high amounts of sphalerite-chalcopyrite association. The ores of the LOB have distinctly higher sphalerite-galena, sphalerite-apatite, sphalerite-garnet, sphalerite-quartz and sphalerite-pyrite association amounts compared to the GQOB ore. The liberation statistics show that sphalerite is poorly liberated in all three quartz-dominant ores.

From analysing the bulk feed association and liberation it can be seen that all three ores show similar amounts of complexity. The complexity of the ores, however, comes from different minerals in different ores. The complexity of ore G is derived from the poor liberation of galena and sphalerite, and the related complex association patterns of those two minerals. The ores of the LOB find their complexity with the poor liberation of chalcopyrite and sphalerite and the related association complexities.

The size by size economic sulphide associations will be used to further analyse mineral association patterns for minerals that show a similar bulk association between ore types, in particular, the associations of galena-mica, galena-quartz, galena-barite, galena-pyrite, sphalerite-magnetite,

sphalerite-pyrite and sphalerite-quartz. The size by size association will indicate the size of the particles that show associations, this information is important for possible adjustments to be made either to the grinding circuit or flotation circuit (or both), in order to increase liberation/recovery.

Ore G has a decreasing amount of galena-mica association with decreasing size fractions, whereas the LOB ores have a bell-shaped distribution of galena-mica association through the size fractions. All three ore types have a similar decreasing association pattern of galena-quartz as well as galena-pyrite with a size fraction decrease. The galena-barite association in ore G decreases with a decrease in size fraction, the LOB ores show a slight galena-barite association increase with a decrease in size fraction.

The sphalerite-quartz and sphalerite-pyrite association profiles are the same for all three ore types, showing a decrease in association with a decrease in size fraction. The sphalerite-magnetite association profile for ores G and H are similar, with no distinct pattern across the four size fractions. The sphalerite-magnetite association pattern for ore I show a distinct decrease in association with a decrease in size fraction.

3.6 CONCLUSION

The analysis of both qualitative and quantitative mineralogical tools allows one to create a holistic opinion on ore classification. The initially stated similar makeup of the quartz-dominant ore horizon, of this polymetallic base metal sulphide deposit, may be slightly rudimentary.

At face value the quartz-dominant ore horizons have relatively similar bulk compositions; however, the different ore bodies (GQOB and LOB) have intrinsically unique characteristics. The exact delineation of these characteristics could have huge benefits to the processing performances of the quartz-dominant ores, more specifically, grouping of certain ores into unique domains could alleviate, or predict processing disparities.

The GQOB ore (G) and the LOB ores (H and I) have substantially different characteristics in terms of mineralogy, GSD, mineral liberation and mineral association to justify separation, should it be economically viable. The separation of the ores of the two ore bodies into two different domains could result in the processing plant increasing the capability of tailoring the processing circuit to accommodate the differences in the ore characteristics.

Chapter 4: Minerals Processing Characterisation

4.1 INTRODUCTION

The term minerals processing refers to the process that a non-gangue ore undergoes in order to increase the relative concentration of the valuable mineral/element at hand until a financially feasible concentration (grade) is achieved (Abubakre et al., 2007). The chief question faced in minerals processing is how to increase the selectivity, grade and recovery of the processing plant whilst still maintaining, or possibly increasing, the current throughput of ore, and maintaining, or possibly decreasing the current cost of beneficiation (Lotter et al., 2011). The modern practices of metal beneficiation/minerals processing are described as a multifaceted hybrid process, with several well-researched aspects all feeding into a unified and optimised system (Lotter et al., 2011).

The initial stage of minerals processing starts with the implementation of an accurate sampling campaign, followed by a detailed characterisation of mineralogy, morphology and mineral textures. The grouping of ores together into geometallurgical units based on similar mineralogy, textures and potential processing performance is extremely beneficial for several reasons (Lotter et al., 2003). The added benefits for these proposed domains could include: increased recovery and selectivity (through high-level changes in processing conditions for each domain), higher flexibility in processing outcomes through specific domain stockpiling (by only processing certain domains under favourable economic conditions). The implementation of geometallurgical units helps in creating a robust flowsheet whereby predictions of performance and possible areas of complexities/processing-irregularities can be made with a higher level of confidence.

The most common method of base metal sulphide concentration is through a process termed froth flotation, whereby target minerals are “floated” out of a slurry mix (described below) (Lopéz et al., 2019). Commonly in industry a polymetallic deposit will have a succession of flotation cells targeting individual minerals in each cell, this practice is termed sequential flotation. The sequential flotation method is used to tailor-make the flotation environment in each cell in order to optimise the target mineral recovery, which can be potentially difficult due to the polymetallic nature and its related ore complexities (large varieties in mineral associations) of a certain deposit (Bicak, 2019).

In this chapter the processing responses of the three quartz-dominated ores will be analysed. Each ore will undergo laboratory bulk flotation, from which the flotation/processing performance will be measured. The chemical analysis/assay of the flotation concentrate will also be discussed here. The aim is to characterise the minerals processing responses and potentially group the three quartz-dominant ores into one, similar behaving, ore domain.

4.2 METHODS

Ore received from the mine was sized, crushed and split into 1.3 kg aliquots (described in Section 2.2). These aliquots were used for all the processing experiments conducted. PSD and milling analysis were determined on each ore type (described in Section 2.3.1). Elemental deportment was calculated on feed samples using QEMSCAN analysis of sized ores (described in Section 2.4.2). Each ore type underwent triplicate bulk flotation experiments, described in Section 2.3.2. Flotation feeds, concentrates and tails were assayed to determine grade, recovery and enrichment ratio; this chemical assay was done by ICP-OES analysis (described in Section 2.4.4).

4.3 RESULTS

The results from the froth flotation, together with the analytical analysis of the flotation concentrate (XRF, ICP-OES and QEMSCAN) will be presented in this section.

4.3.1 Head grades

The head grades tabulated below are results from feed analysis using an ICP-OES (full dataset can be seen in Appendix B), samples were submitted in duplicates. Ore G has the highest Cu grade and the lowest Pb grade of the three ore types. Ores H and I have substantially higher Pb grades than ore G. All three ores have low, and possibly economically negligible Zn grades.

Table 6: *Head grades of quartz-dominant ores, combined total metal amount and Zn equivalent grade.*

General characteristics	Ore type	% Cu	% Pb	% Zn	Cu+Pb+Zn	Zn Eq*
Garnet quartzite (domain 1, quartz dominant)	G	1.77 (0.04)	0.59 (0.01)	0.08 (0.01)	2.44	5.03
Lower ore body (domain 3, quartz dominant)	H	0.32 (0.01)	5.98 (0.16)	0.13 (0.02)	6.43	6.21
	I	0.32 (<0.01)	6.61 (0.19)	0.12 (0.01)	7.05	6.75

**value given in brackets represents the standard error between the duplicate samples submitted for analysis.*

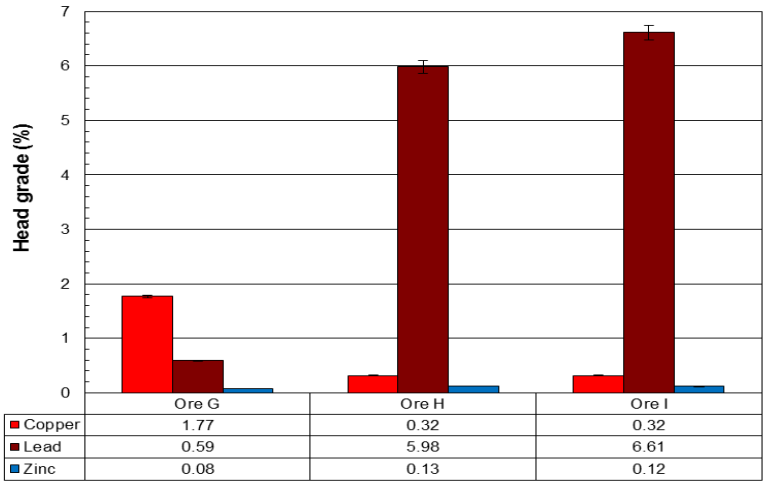

	Ore G	Ore H	Ore I
Copper	1.77	0.32	0.32
Lead	0.59	5.98	6.61
Zinc	0.08	0.13	0.12

Figure 22: *Graphical representation of the feed grades displayed in Table 6. Error bars represent the standard error between the duplicate feed samples sent for ICP-OES analysis.*

4.3.2 Elemental Deportment

Elemental deportment is the measure of what mineral certain elements are deported from (in elemental wt. %), this was done through all four size fractions (+75 µm, -75 µm + 38 µm, -38 µm +10 µm and -10 µm) for five elements of importance (Cu, Pb, Zn, Fe and Mn), for each ore type.

The valuable element deportment should solely be from the targeted base metal sulphide minerals (Cu – chalcopyrite, Pb – galena, Zn – sphalerite). The Cu deportment for all three ores, through all four size fractions, is solely from chalcopyrite. The Pb deportment of all three ore types, through all four size fractions is from galena. The Zn deportment profiles are slightly more complicated than the other two above mentioned metal deportment profiles. The Zn in all three ores is largely concentrated in sphalerite (which is expected), however, significant amounts of Zn is concentrated in gahnite. The amount of Zn concentrated in gahnite decreases with decreasing size fraction, in all three ore types. The Zn-deportment from gahnite is important to note due to the refractory nature of gahnite.

The iron deportment profiles are intrinsically more complicated, this is due to each ore type having a variety of Fe-bearing minerals. There is a distinct difference between the iron deportment profiles of the GQOB ore and the LOB ores, this is directly related to the composition differences between the mineralogy of the ores.

The iron deportment of ore G is between four minerals, namely: magnetite, pyrite, chalcopyrite and pyrrhotite (in decreasing deportment wt. %). A large majority of iron is deported from magnetite (over two thirds, in the two largest size fractions). The final third of the iron deportment is largely from pyrite, with relatively equally minor amounts of deportment from chalcopyrite and pyrrhotite.

The iron deportment of ores H and I are from nine minerals, namely: magnetite, pyrite, garnet, chlorite, mica, chalcopyrite, pyrrhotite and gahnite (in decreasing deportment wt. %). Iron deportment from magnetite and pyrite make up roughly two-thirds of total iron deportment (with magnetite being slightly higher than pyrite). Relatively equal minor contributions of the total deportment are made by: garnet, mica and chlorite. Relatively equal and even smaller than the above listed three minerals,

contributions are made by chalcopyrite and pyrrhotite. The total iron deportment in the LOB ores decreases with a decrease in size fraction, the relative mineral contributions to deportment, however, remain in roughly the same proportions.

The manganese deportment of ore G is made up of two minerals, two-thirds of which being garnet and the other third being magnetite. The Mn deportment of the two LOB ores is similar and will be described together. The Mn deportment of ore H and I are largely made up by deportment from garnet (roughly 70% of total deportment). Magnetite is the second most abundant mineral in Mn deportment. Relatively equal (and smaller than magnetite) amounts of Mn deportment are from mica and chlorite in ore H, whereas manganese deportment of ore I is more concentrated in mica than chlorite.

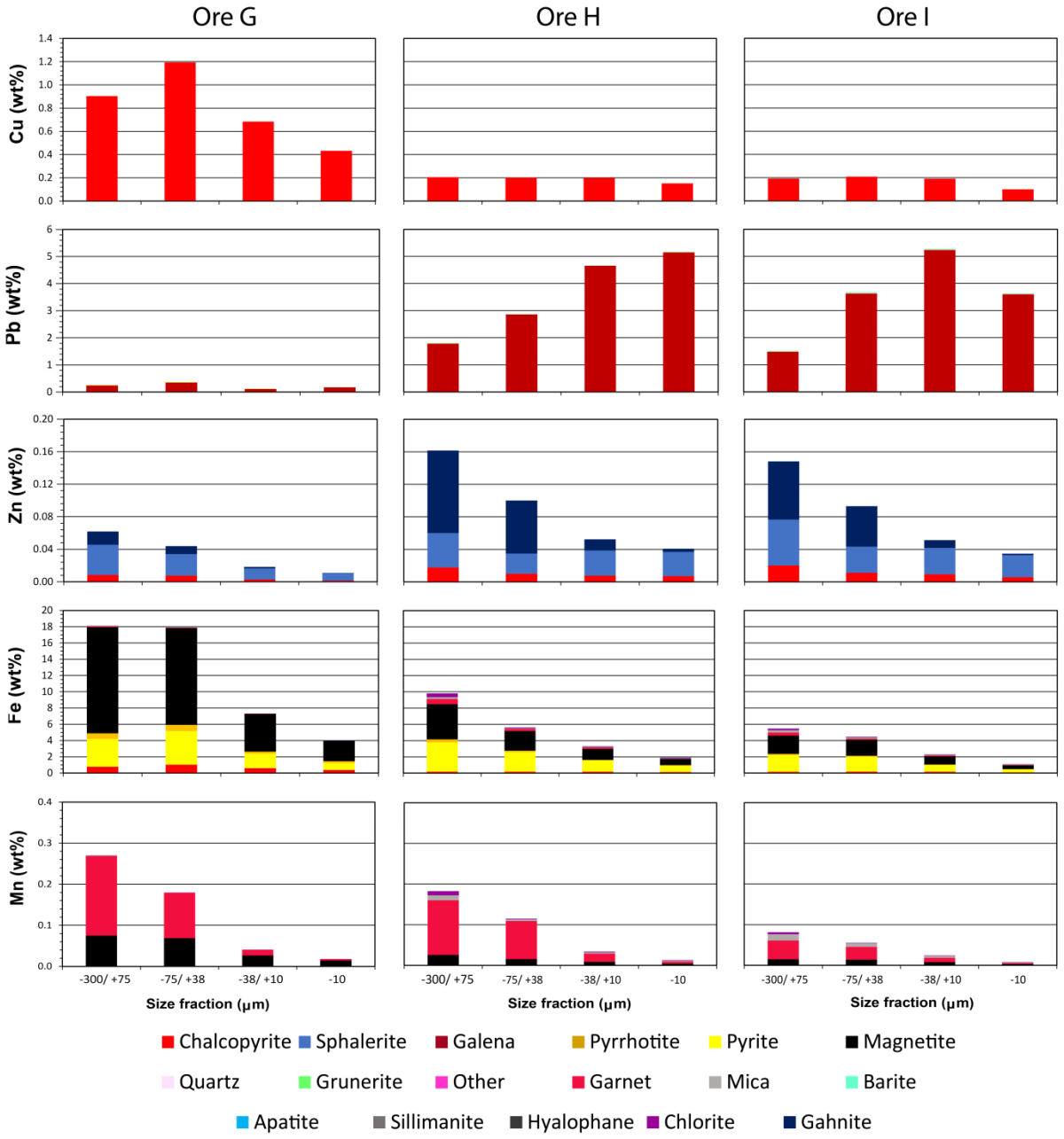

Figure 23: *Flotation feed elemental deportment for the quartz-dominant ores across four size fractions. Note the difference in scales between the figures for each element.*

4.3.3 Solids recovery vs water recovery

The solids recovery vs water recovery graphs are a simplistic first step in identifying and characterising processing performance of an ore type. The solids recovery vs water recovery graphs discussed are averages of triplicate bulk sulphide floats, for each ore type (triplicate solids vs water recovery can be seen in Appendix B). Ore G has an initial solids pull in the first concentrate of 140 g, the cumulative solids pull in the second concentrate is slightly under 192.8 g, the final total cumulative mass pull at the termination of the float is 222 g. The water recovery has the inverse relationship to time compared to solids pull. The water recovery in the first concentrate is 83.6 g and the final cumulative water recovery at the termination of the float is 469.5 g. The amount of ore being recovered becomes negligible midway through the third concentrate. The solids pull of ore H in the first concentrate was 128.7 g, the cumulative solids pull in the second concentrate is 172.5 g, and the final total cumulative solids pull at the termination stage of the flotation process was 220.4 g. The cumulative water recovery increases exponentially as time in the floating process passes. The initial water recovery in the first concentrate was 73.8 g, the final cumulative water recovery for the flotation process of ore H is 436.1 g. The solids pull for ore I is slightly lower than the other two ores. The solids pull for the first concentrate of I was 119 g, the cumulative solids pull for the second concentrate was 162.4 g and the total solids pull for the whole flotation process was 206.7g. The water recovery for ore I in the first concentrate was 62.7 g, with the total water recovery for the duration of the flotation process being 431.5 g. Graphically ore G initially recovers more solids per unit of water, until the end of the float where ore H gives the same solids recovery as ore G. Ore I, while initially on par with ore G, pulls fewer solids per unit of water overall, (Fig. 24). The initial solid pulls and water recoveries are all in a similar region of the graph and this is also the case for the ending points of all three floats.

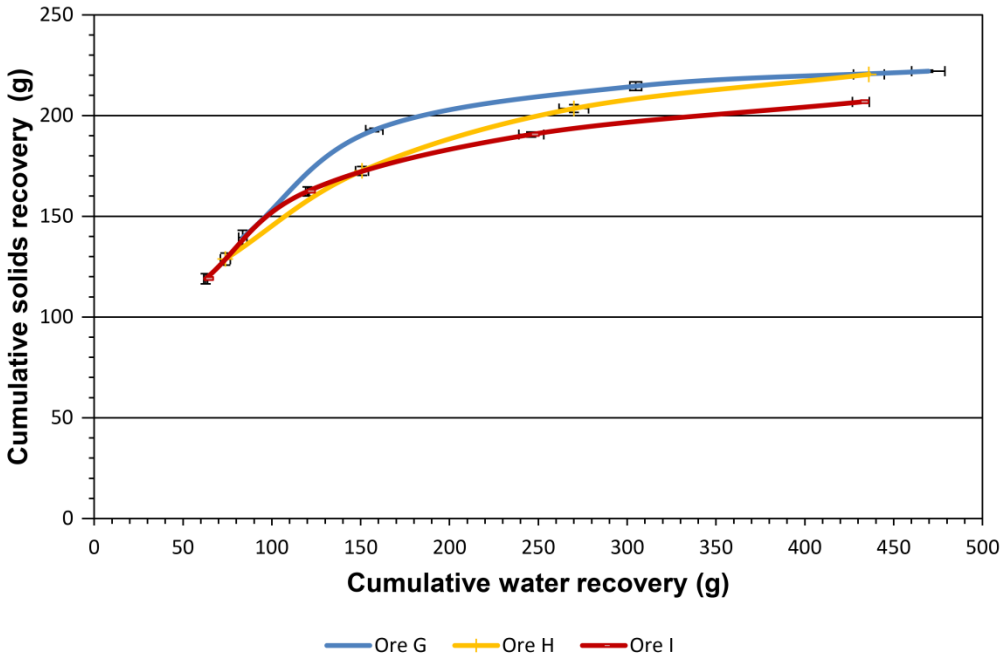

Figure 24: *Cumulative solids vs water recovery for quartz-dominant ores. The error bars on each point represent the standard error between the solids and water recovery at that specific stage in the flotation procedure between the triplicate floats.*

4.3.4 Metal mass vs water recovery

The shape of ore G's curve for the Cu mass vs water has a steep increase in the first two concentrates and then move's horizontal with the increase of water recovery through the four concentrates. The curves for the two LOB ores are sub-horizontal and do not have any Cu mass variation over the four concentrates. A distinct difference in curve shape, as well as curve position, can be seen between the GQOB ore and the LOB ores (Fig. 25a).

The Pb mass vs water recovery curves for the LOB are similar in shape, whereas the curve for ore G is a flat, sub-horizontal line. The LOB curves have steep increases of Pb mass pull in the first two concentrates, the curves then flatten out through the next two concentrates. The curves of the LOB, due to their position on the graph and shape form one group, ore G forms a group by itself (Fig. 25b).

All three ore types have a close grouping of Zn mass vs water recovery curves and exhibit a similar shape. The curves have a steep increase in Zn mass pull in the first two concentrates, thereafter they slightly flatten out, but not to the stage of being described as sub-horizontal. A clear Zn mass pull is present through all four stages of the flotation procedure (Fig. 25c).

Figure 20d for Mn displays interesting profiles for the three ore types. All three ores have similar profiles, which are straight to slightly curved lines with a consistent increase in cumulative Mn mass pull throughout the flotation procedure. Ore G has the highest Mn mass pull, second highest is ore H and the lowest Mn mass pull is ore I (Fig. 25d).

Figure 20e is of particular importance due to a large amount of iron making its way to the flotation concentrate. All three ore types have similar curve shape, speaking to the initial (first two

concentrates of the float) large amounts of Fe mass pull, with a drastic decrease in Fe mass pull through the next two concentrates. The last shape of the curve through the last concentrate could be described as sub-horizontal. The most diagnostic feature of these three curves being split into two groups is the difference in Fe mass pull between ore G and the LOB ores. Ore G has substantially higher Fe mass pull compared to the LOB ores (Fig. 25e).

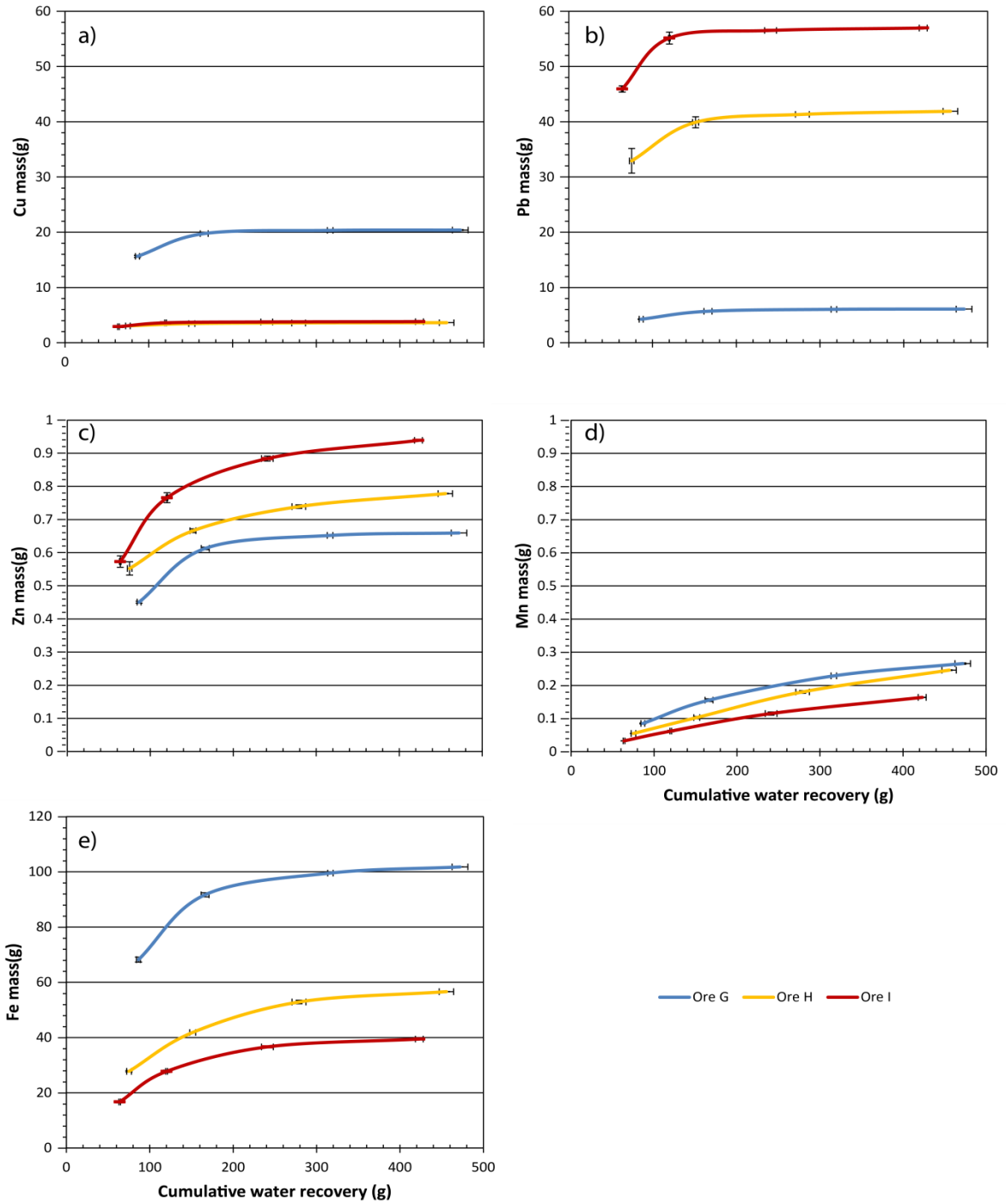

Figure 25: *Metal mass vs water recovery for the quartz-dominant ores. (a) Cu mass vs water recovery, (b) Pb mass vs water recovery, (c) Zn mass vs water recovery, (d) Mn mass vs water recovery and (e) Fe mass vs water recovery. The error bars at each point represent the standard error on the flotation samples sent for ICP-OES and the standard error on the water recovery between the triplicate floats. Note the difference in Y-axis scales for each figure.*

4.3.5 Theoretical mineral grade vs recovery

Theoretical grade recovery curves (Fig. 26) were constructed using QEMSCAN data of sized feed samples of each ore type. The curves look at the theoretical grade vs recovery of the three economic sulphides targeted by the mining operation (chalcopyrite (Fig. 26a), galena (Fig. 26b) and sphalerite (Fig. 26c)). The theoretical curve represents the possible recovery and grade of a certain mineral, the maximum grade represents a completely liberated target mineral grain, and the maximum recovery represents the head grade of that target mineral. The assay on the concentrate, and related grade recovery curve, is limited by the modal abundance of a target element in the target mineral (i.e. Cu in chalcopyrite is 34.63%, this will be the point on the curve at the maximum Cu grade).

Theoretically, ore G is to be the best performing ore out of the three quartz-dominant ores, in the chalcopyrite flotation circuit. Theoretically the worst preforming ore on the chalcopyrite flotation circuit is going to be ore H. In the galena flotation circuit both ore H and I will theoretically be good performers, with ore I performing slightly better than ore H. Ore G, however, theoretically will perform substantially poorer than the ores of the LOB (H and I). In the sphalerite flotation circuit, ore G is the best theoretical performing ore, ore I is the worst. The overall sphalerite theoretical grade and recovery of all three ores exhibit poor potential performance, possibly regrinding of the Zn concentrate prior to flotation might be a solution to this issue.

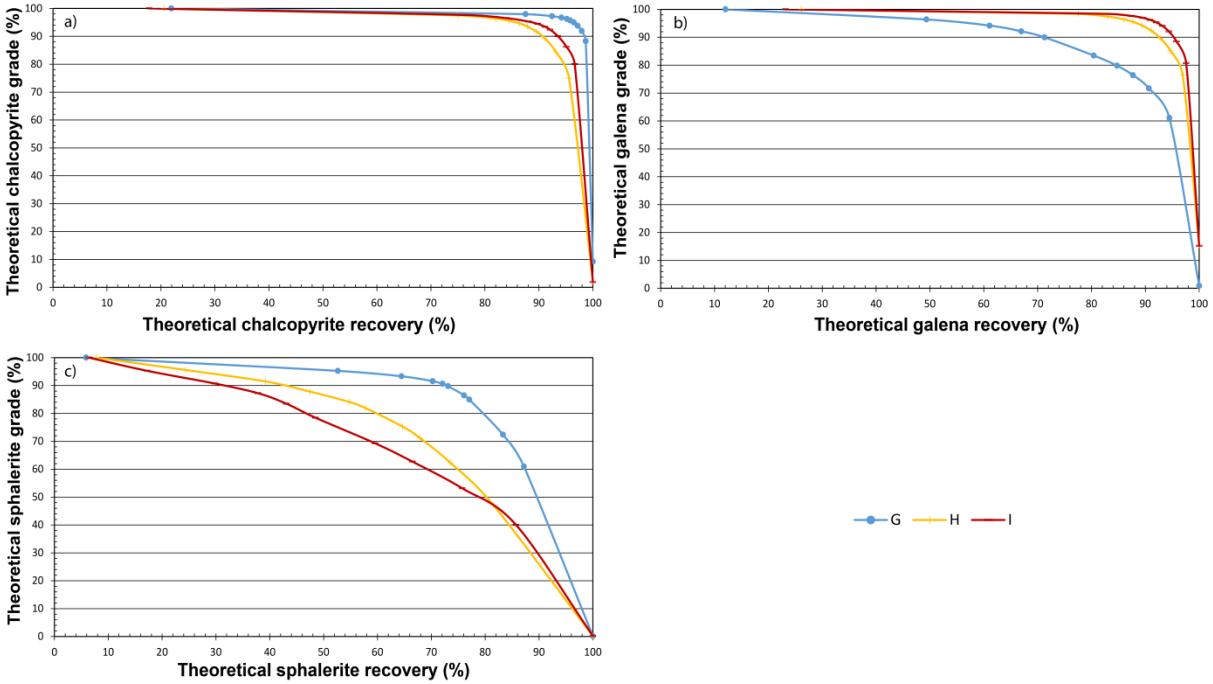

Figure 26: *Theoretical mineral grade vs recovery for: (a) chalcopyrite, (b) galena and (c) sphalerite.*

4.3.6 Elemental grade vs recovery

Elemental grade vs recovery was determined using ICP-OES analysis of flotation concentrates (analysed in duplicates) and related recovery of Cu, Pb, Zn, Fe and Mn (Fig. 27). The Cu grade vs recovery curves for all three ore types have similar shapes, of decreasing grade and increasing recovery through the four concentrates in the flotation process. The Cu grade for ore G in the first

concentrate is over 10%, whereas the Cu grades for the LOB ores (H and I) are below 2.5%. The recovery of Cu in the first concentrate is above 70% for all three ore types and the final recovery nears 100% for all three concentrates.

The spread between the three ore types for the Pb grade vs recovery is more pronounced than Cu grade vs recovery. The grade-recovery curve for ore G is sub-horizontal, with a slight decrease in Pb grade and a typical increase in recovery through the four concentrates of the flotation process. The initial Pb grade in the first concentrate is 3% with a slightly higher than 60% recovery, while the final stage of flotation has a grade of 2.7% with a recovery of 89.5%. The LOB ores have typical grade-recovery curve shapes, with ore I having a slightly higher grade-recovery curve compared to ore H. The first concentrates have grades of 26.6% and 37.9% with recoveries of 72.9% and 78.4%, for ores H and I respectively. The last concentrates have grades of 19% and 27.5% with recoveries of 93% and 97.2%, for ores H and I respectively.

Zn grade-recovery for the quartz-dominant ore horizons is erratic and poor, with very low grades and recoveries most likely due to the minor abundance of Zn (Table 4).

The Fe grade-recovery curve for ore G is sub-horizontal with an overall slight decrease in Fe grade over the spread across increase recovery. The Fe grade of the first concentrate in ore G is 47.5% with a recovery of 20.8%, while the Fe grade for the last concentrate is 45.7% with a recovery of 31%. The Fe grade-recovery curves for the LOB ores are similar in profile, with ore H higher than ore I (Fig. 27e), pointing to higher grades with similar recoveries. The shapes of the LOB curves are straight lines with a positive gradient (Fig. 27e), and curved towards higher recoveries. The grades for the first concentrates are 21.4% and 13.8% with recoveries of 18.2% and 15.5%, for ore H and I respectively. The grades for the final concentrates are 25.6% and 19% with recoveries of 37.2% and 36.7%, for ore H and I respectively.

The Mn grade-recovery curves of all three ores have similar profiles, with the main difference being the change in curve gradient (Fig. 27d). All three ores display straight to straight lines with positive gradients. Ore G has the steepest gradient and ore I has the lowest gradient.

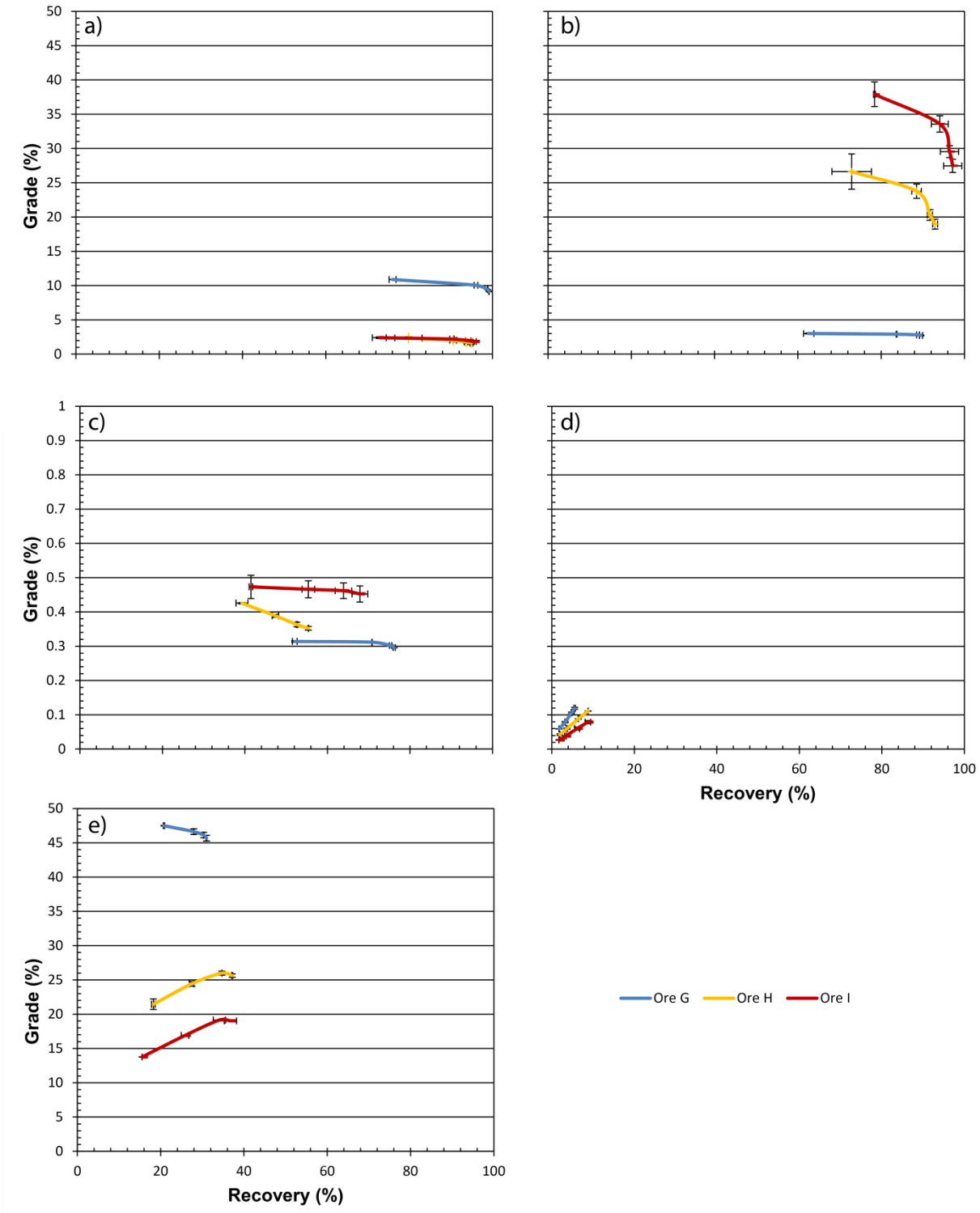

Figure 27: *Elemental grade vs recovery derived from ICP-OES analysis of duplicate flotation experiments for the quartz-dominant ores. (a) Cu grade vs recovery, (b) Pb grade vs recovery, (c) Zn grade vs recovery, (d) Mn grade vs recovery and (e) Fe grade vs recovery. Error bars represent standard error on the duplicate ICP-OES analyses. Note the difference in Y-axis scales between a-b and c-d and e.*

4.3.7 Enrichment ratio

Enrichment ratio graphs are a useful way of comparing elemental concentrations between ore types as they specifically account for the weight disparities between the flotation concentrates of the different ore types. The formula for enrichment ratio is:

$$\boldsymbol{ER} = \frac{\boldsymbol{Ca}}{\boldsymbol{Fa}}$$

where ER is enrichment ratio, Ca is concentrate assay and Fa is feed assay for a given element. This formula has been adapted to have unique abbreviations (Drzymała, 2007).

Cu, Pb and Zn all exhibit expected enrichment ratio vs metal recovery distributions (Fig. 28a-c); however a slight formation of two distinct groups of enrichment curves is seen. A steep positive gradient seen for the first two concentrates followed by a sub-vertical section for the final two concentrates is the expected shape of an elemental enrichment graph. This is due to the distribution of enrichment ratios per percentage recovery increase, meaning, in most cases an element undergoes almost maximum recovery by the second concentrate, thereafter experiencing only a slight increase in recovery (in some cases, no increase) for the remainder of the concentrates in the float. For Cu and Zn enrichment ratios, ore G has a higher recovery and thus lies separately from the ores of the LOB (ores H and I).

Figure 28b for Pb - shows the same shaped curve as Fig. 28a. However, the LOB ores in Fig. 28b have a higher recovery than the ore G, and thus, again, making two distinct groups.

All three ores have, for the most part, very similar Mn enrichment ratio profiles and enrichment-recovery values (Fig. 28d). The fourth concentrate of ore G has a slightly higher enrichment ratio, allowing it to veer off the trends of the LOB ores.

The distinction of groups/similar-trends from Fig. 28e is slightly more ambiguous than the other enrichment graphs. All three ores have comparable Fe enrichment ratios, there is, however, slight changes in percentage recovery through the four concentrates between the three ore types. Ore G has a typical curve shape with a maximum Fe recovery of approximately 30%, the ores of the LOB have a slightly more atypical curve shape, with a maximum Fe recovery closer to 40%. Ores H and I have very similar curve shapes and enrichment-recovery values.

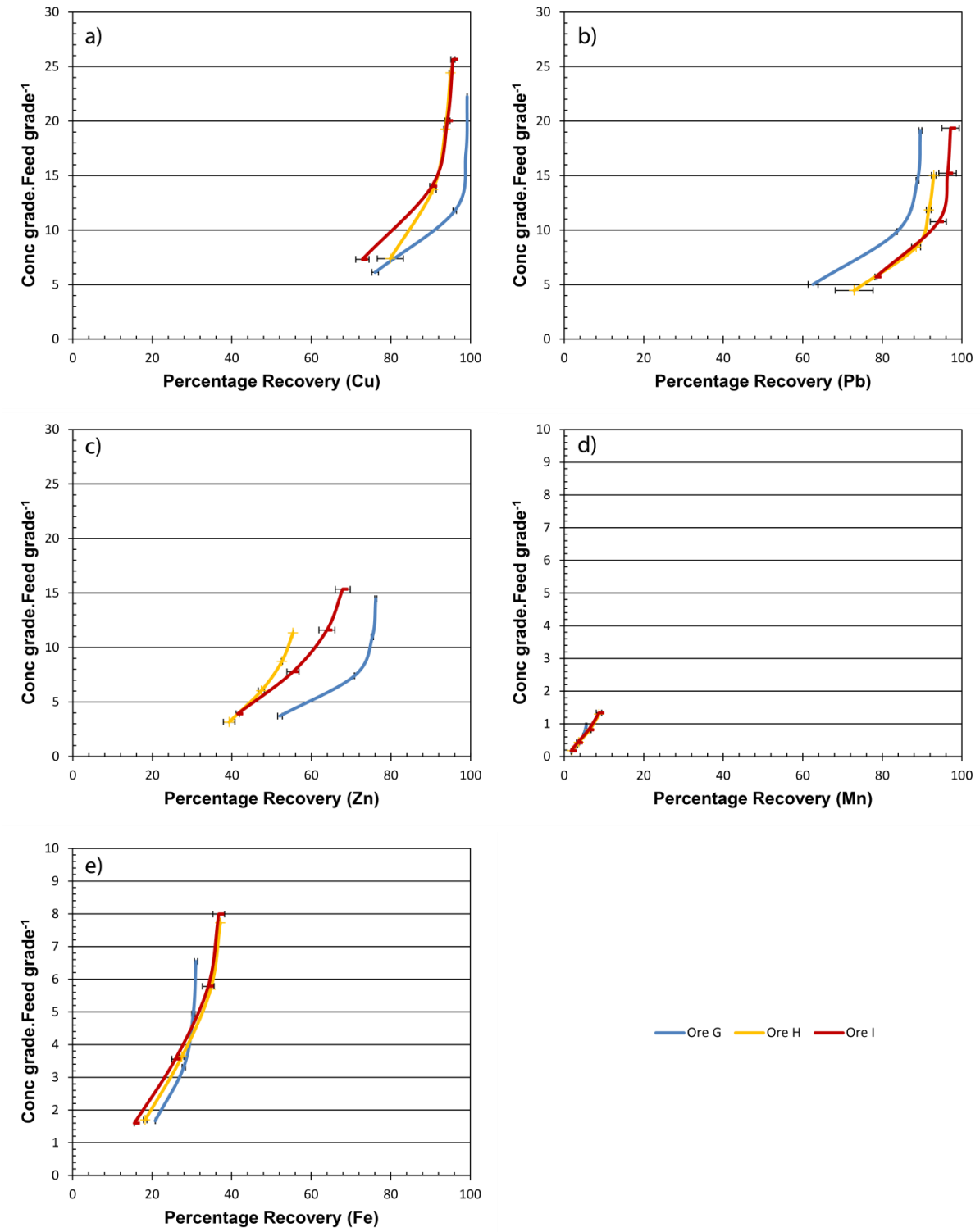

Figure 28: *Enrichment ratio vs recovery for the quartz-dominant ores. (a) Cu enrichment ratio, (b) Pb enrichment ratio, (c) Zn enrichment ratio, (d) Mn enrichment ratio and (e) Fe enrichment ratio. The error bars represent the standard error between duplicate ICP-OES analysis of recovery for each flotation concentrate. Note the difference in Y-axis scale between a-b-c and d-e.*

4.3.8 Zn equivalent grade

The Zn equivalent grade (ZnEG) is a way to assign a "real world" value to each ore and to compare them to each other. The ZnEG value is calculated according to the equation below, is derived from the relative grade of each valuable target element (e.g. CuG, PbG and ZnG) and their current metal price (CuP, PbP and ZnP) expressed in US$ per kilogram relative to the Zn metal price (ZnP) in US$ per kilogram.

$$ZnEG = \left(\frac{CuP}{ZnP} \times CuG\right) + \left(\frac{PbP}{ZnP} \times PbG\right) + \left(\frac{ZnP}{ZnP} \times ZnG\right)$$

To calculate the ZnEG for a specific ore all the above variables must be known for each specific ore; the ZnEG calculated here uses the assay grade of each ore done on ICP-OES (Appendix B). Ore G has a ZnEG of 25.6, ore H has a ZnEG of 21.2 and ore I has a ZnEG of 29.3 (as of the commodity prices on 16/09/2019).

4.4 DISCUSSION

4.4.1 Implications of ore-hardness and breakability

The two topics being discussed in the pre-flotation section are: particle size distribution (PSD) and milling. These two processes are centralised around an ore's hardness, breakability and grindability characteristics. The PSD is more a function of breakability of an ore, three ores from the same deposit, with similar mineralogy, are expected to display comparable breakability and a related PSD. This is the case for all three of the quartz-dominant ores, as the profiles in the PSD graphs are similar (Appendix A), with slight variance between the ore of the GQOB and the ore of the LOB. The milling curve results are directly related to ore hardness and ore grindability. The difference in milling duration, necessary for the required grind P80 of 65% passing 75 μm, is the main focal point of the milling section. This is the case because the milling environment was kept the same throughout all mill cycles; there was no change in milling medium or change in milling type (e.g. rod mill vs ball mill). Ore G (21 mins 42 sec) has a noticeably longer mill time compared to the more similar milling times of ore H (18 mins 12 sec) and I (17 mins 18 sec). The only parameter that is different between the three ores is the mineralogy, by this rationale, the difference in milling time is a function of mineralogical disparities between the ores, and their related mineral characteristics (mineral hardness, grainsize and interlocking capabilities) (Chenje et al., 2004).

4.4.2 Flotation performance based ore-domaining

The mass vs water flotation chart is an important illustration of the total mass pull throughout the flotation process. The froth height was kept to an average height of 15 mm above the surface of the slurry. In many industry flotation circuits an activator is used (e.g. Cu-sulphate), in these bulk sulphide flotation experiments no activator was used. The mass-water recovery curves for the three quartz-dominant ore are typical for a polymetallic base metal sulphide ore, with a majority of mass recovery at the beginning stages of the float, thereafter levelling off, indicating that the ore has been "floated out". This term indicates that at the end of the flotation experiment all the hydrophobic and

hydrophobic-induced minerals in the ore have been recovered. All three quartz-dominant ores form one group indicating that there can be no separation of the ore, based solely on the results of the mass vs water recovery. A clear delineation between the two ore bodies is possible when looking at the head grades of valuable elements in each ore type. Ore G has the highest and the only economically viable Cu grade (1.77%) between the three ores. Ore G is, however, relatively speaking, void of any other valuable target elements (Pb – 0.56%, Zn – 0.08%). Ore H has substantially lower amounts of Cu compared to ore G (0.32%). The value in ore H lies in its Pb abundance (0.59%). This is also the case for the second LOB ore, I, which has 0.32% Cu and 6.61% Pb. The LOB ores are also relatively devoid of Zn, they do have slightly higher Zn grades, compared to ore G, but the Zn grades are not high enough for Zn to be economically targeted (H - 0.13%, I – 0.12%).

Knowing the head grades of an ore is imperative to determining the ore's value and setting up an efficient processing circuit. Elements are, however, not found in their native form, they are locked in minerals (target minerals), and in this ore body's case, they are locked in sulphides (economic sulphides). In order to create a processing circuit that does not incur penalties related to entrainment of gangue one must know which minerals contain the target elements. This is done by looking at the elemental deportment of each ore. Elemental deportment can also be used to see which phases are most likely recovered should you know you have an above regular assay amount for a deleterious element in your concentrate. The economic elemental deportment is located in three economic sulphides, Cu is deported from chalcopyrite, Pb is deported from galena and Zn is deported from sphalerite. The non-valuable element that is cause for investigation in this ore is Fe. From looking at Fe-deportment in Fig. 23, one can derive that the minerals that are most likely being concentrated; and resulting in high iron recovery are magnetite and pyrite.

The grade recovery curves (Fig. 27) are a fundamental cornerstone in the analysis of ore performance. They can, at times, be slightly misleading when two ores have different head grades, but similar recovery. One may assume that these two ores are unique from each other, but this may not make processing sense. For Cu, the ore G has a higher grade than the ores of the LOB and thus make two different groups. For Pb, the spread between the three ores is larger, and no one group can be easily defined, however, ores H and I have substantially higher grades than ore G (which has a flat grade recovery curve). The flat nature of G's Pb grade recovery curve speaks to a consistent grade of Pb being recovered and thus points towards Pb not being completely floated out. For Zn, all three ores display similar curve profiles and cannot be split into different groupings. For Fe, the grade in ore G is higher than in ore H and I, this being significant enough to form two separate groups. The Fe grade recovery curves for the LOB ores show a steady increase in grade with duration of float, this points to a mineral being recovered in the float that is a late floater and is high in iron concentration. For Mn, the profiles of the three ores are similar, with a consistent increase in grade with an increase in recovery, also point towards the concentration of a late floating Mn-rich mineral in the latter stages of the flotation process.

Enrichment ratio values can provide an interesting insight into ore recovery performance, due to this value negating for the grade of the element in question. Figure 28a and 28c show two distinct groups,

ore G and the ores of the LOB (H and I), with ore G having higher Cu recovery values. This is inversely the case with Fig. 28b, but the same grouping applies. Figure 28e is slightly more ambiguous, but groupings can still be made between ore G and the ores of the LOB, the ores of the LOB have higher enrichment ratio and recovery end amounts. The enrichment ratio profiles for manganese are similar between the three ores, this speaks to a similar form of manganese-bearing phases being present in all three ores.

4.4.3 Elemental recovery based ore-domaining

The shape of metal mass vs water recovery curves (Fig. 25) can speak to the type of recovery the said metal undergoes (normal flotation, entrainment, etc.). The Cu mass recovery of all three ore types shows a large mass pull in the initial stages of the float, thereafter the mass pull flattens out. The Cu mass of ore G is expectedly higher than that of the LOB, this is due to the higher Cu head grade in ore G. The inverse is the case for the Pb recovery, with the larger Pb mass pull by the LOB ores. Figure 25c for all three ores is similar. Figure 25c also shows a typical curve shape, pointing toward normal flotation responses of the Zn-bearing mineral that is recovered (typically sphalerite). For iron, the mass recovery curves of all three ores have a typical curve shape, showing that iron is being recovered through flotation. The Fe mass pull of ore G is higher than that of the LOB ores, also to be expected due to ore G's higher Fe head grade. Figure 25d for Mn - shows all three ore types grouped close together, the curve shape is however atypical for normal flotation, as they have a consistent gradient. The shape of these curves is more of a straight line with a relatively consistent gradient. This points to manganese-bearing minerals possibly being entrained in the flotation process.

4.5 CONCLUSION

The milling and particle size distribution data points to a separation of two ore groupings, the first group made up solely of ore G and the second group made up of the LOB ores, H and I. This is the case due to the similarities of PSD and milling times of ore H and I, and the clearly unique PSD and milling time of ore G. Figure 24 does not point towards any separation between the ores. This result is a slightly rudimentary way of viewing mass pull, as the composition of the concentrate between the three ores is dissimilar, the total mass pull is, however, similar, therefore the total mass pull is reflected as being similar between the three ores.

The low recoveries for Zn in all three ore types can largely be related to the presence of gahnite. Gahnite is a Zn bearing oxy-spinel, it is, however, a refractory mineral, unlike sphalerite. The presence of a refractory Zn phase (which typically does not float) results in decreased recovery because the Zn head grade is misleadingly split between a naturally floating mineral (sphalerite) and a refractory mineral (gahnite).

The analytical results from the flotation concentrates show a clear division between ore G and ores H and I. The elemental mass pull, grade recovery, elemental deportment and enrichment ratios of the different ore bodies show a division between them. A general conclusion is that ores of the different ore bodies have enough of a separation in results to rationalise the separation of the two ore bodies (GQOB and LOB) ores in a pre-processing environment.

Chapter 5: Mineralogical Classification of Concentrate

5.1 INTRODUCTION

The mineralogical classification of the flotation concentrate is an important aspect of minerals processing, as through this analysis an exact mineralogical break down can be understood. The characterisation of economic sulphide recovery along with the characterisation of gangue (naturally floating, true floating and entrained) can be analysed and possible steps can be proposed to the processing team to try and maximise the economic outcome of the processing circuit (Becker et al., 2009; Chetty et al., 2009). Certain aspects of the flotation concentrate are more relevant than others, quantifying the grade, liberation and association of the mineral phases in the concentrate are of utmost importance (Chetty et al., 2009). The understanding of the mineral grades helps the processing team understand the quantity and proportions of economic, gangue and deleterious minerals that are being recovered, it can also provide downstream smelting operation with valuable insights into the mineralogical makeup of the ore concentrate (Mwase et al., 2012; Nel et al., 2005). The mineral liberation statistics give an insight into the nature of the concentrated minerals, if they are locked, semi-locked or completely liberated, this is important information for further mineral/element concentration (Lastra, 2007). The association statistics give an insight to the makeup of composite grains, if chalcopyrite is associated with pyrite in the concentrate further steps need to be undertaken to try and liberate the chalcopyrite from the non-valuable pyrite.

5.2 METHODS

The data presented in this chapter is the mineralogy of the C_1 concentrate from the flotation test work. The C_1 concentrate was chosen because the majority of the total recoverable solids had been recovered by this stage of the float (Fig. 24). The C1 concentrate was then split into four size fractions (as described in the methods section, Chapter 2.3.3), in order to analyse if certain minerals were concentrating into specific size fractions during the floatation process. Each size fraction was then set into epoxy mounts, for QEMSCAN analysis. Vertical sections were taken of each sample to avoid gravitational settling based on differential mineral densities. The mounts were then run through the

QEMSCAN, at the Department of Chemical Engineering (UCT), the running conditions are described in the Methods section (Chapter 2.4.2). The data was then analysed using the, already refined, Species Identification Protocol (SIP) list that was created and modified on the feed samples. The analysis of this data was done using iDiscover. For simplicity, in this chapter, the C1 concentrate will just be referred to as the concentrate

5.3 RESULTS

5.3.1 Concentrate mineralogy

The total non-sulphide gangue component of the three quartz-dominant ores (Fig. 29b) makes up a minor portion of the total concentrate, ore G has 4 wt. %, ore H has 4.4 wt. % and ore I has 4.1 wt. % non-sulphide gangue. The economic sulphide versus sulphide gangue ratios between the two ore bodies and their related ores is, however, unique. The ratio of economic sulphide:sulphide gangue for the three ores is as follows: G – 0.6:1, H – 2.1:1 and I – 3.5:1. These values show a clear concentration of sulphide gangue over economic sulphides in ore G, and vice versa for the LOB ores (H and I).

The GQOB ore concentrate (Fig. 29a) is chalcopyrite rich (Cu rich) whereas the LOB ore's concentrates are galena rich (Pb rich), all three ores have comparable amounts of sphalerite (Zn mineral) in the concentrates. Ore G has a chalcopyrite concentration of 30.7 wt. %, galena concentration of 3.8 wt. % and sphalerite concentration of 0.4 wt. %. Ore H has a chalcopyrite concentration of 5.9 wt. %, galena concentration of 57.4 wt. % and sphalerite concentration of 0.6 wt. %. Ore I has a chalcopyrite concentration of 6 wt. %, galena concentration of 67.3 wt. % and sphalerite concentration of 0.8 wt. %. Intuitively these mineral abundances relate to the feed abundances of each economic sulphide mineral.

The total non-valuable sulphide fraction of the concentrates (Fig. 29a) in all three ore types are dominated by pyrite, with minor amounts of pyrrhotite in the concentrate. Ore G has 56.7 wt. % pyrite and 2.1 wt. % pyrrhotite, ore H has 29.8 wt. % pyrite and 0.6 wt. % pyrrhotite and ore I have 20.7 wt. % pyrite and 0.3 wt. % pyrrhotite. These values reiterate the above comment to how the LOB ores have substantially less sulphide gangue when compared to ore G.

No particular NSG phase is concentrated in any sample (Fig. 29b). The concentrated hierarchy of gangue phases in ore G is: quartz > magnetite > grunerite > sillimanite > garnet (other gangue phases all have less than 0.1% concentration). The gangue hierarchy of ore H and I is: quartz > grunerite ≥ garnet > magnetite > mica ≥ barite > sillimanite (where gangue phases are all lower concentrations than 0.1 wt. %).

Table 7: *Bulk mineralogy of concentrate C_1 and mineral group ratios. Note that the totals exclude the "other" group of minerals, and thus do not add up to 100%.*

Bulk mineralogy - concentrate C1 (wt%)			
Mineral	**Ore Type**		
	G	**H**	**I**
Chalcopyrite	30.7	5.9	6.0
Sphalerite	0.4	0.6	0.8
Galena	3.8	57.4	67.3
Total % Economic Sulphides (ES)	35.0	63.8	74.1
Pyrrhotite	2.1	0.6	0.3
Pyrite	56.7	29.8	20.7
Total % Sulphide Gangue (SG)	58.8	30.4	21.0
Magnetite	0.94	0.5	0.4
Gahnite	0.07	0.0	0.0
Quartz	1.60	1.4	1.3
Grunerite	0.74	0.7	0.9
Garnet	0.29	0.7	0.8
Mica	0.00	0.2	0.4
Apatite	0.01	0.1	0.0
Sillimanite	0.59	0.1	0.1
Hyalophane	0.00	0.0	0.0
Barite	0.07	0.6	0.2
Chlorite	0.06	0.1	0.1
Total % Non-Sulphide Gangue (NSG)	4.4	4.4	4.1
ES/SG	0.6	2.1	3.5
ES/NSG	8.0	14.4	18.1
SG/NSG	13.5	6.9	5.1

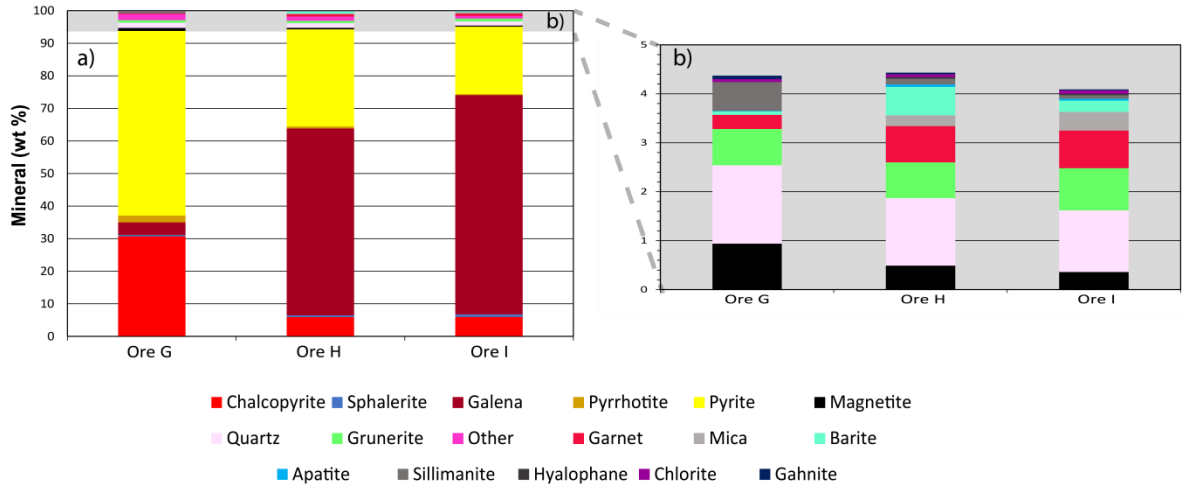

Figure 29: *(a) Bulk flotation concentrate C_1 mineralogy for quartz-dominant ores. (b) Total NSG component of flotation concentrate C_1. Note the difference in scales between (a) and (b).*

5.3.2 Concentrate mineralogy by size

Of the NSG phases the only two minerals that show distinct concentration patterns across the four size fractions are garnet and mica (Fig. 30). In ore type G (Fig. 30b) the garnet concentration

decreases whereas the mica concentration increases as you move from the largest size fraction to the smallest fraction, this is not the case for the LOB ores. The LOB ores show similar patterns for garnet and mica concentration through the four size fractions, both the garnet and mica mineral groups decrease in concentration with a decrease in size fraction from the +75 μm to the -10 μm size fractions.

Ore G shows a clear increase in concentration with a decrease in size fraction for the economic sulphides (Fig. 30a), with the total economic sulphide concentration in the +75 μm size fraction being < 30%, compared to a total economic sulphide concentration of > 50% in the -10 μm size fraction. This is inversely the case for the total sulphide gangue concentration, ore G showing a general decrease in sulphide gangue concentration with a decrease in size fraction (> 20%) difference in sulphide gangue concentration between the biggest and smallest size fraction. The total sulphides in ore G exhibit a consistent concentration through all four size fractions, of < 95% but > 90%.

The ores of the LOB (H and I) have similar concentration patterns (Fig. 30) (increases or decreases of certain mineral abundances through the size fractions) to ore G through the four size fractions, however, the changes in concentrations between the size fractions for both the economic sulphides and the sulphide gangue are more distinct than in ore G. The ore H shows an increase in economic sulphide concentration of over 60% and the ore I of over 50%, from the largest size fraction to the smallest size fraction (Fig. 30c and 30e respectively). This is inversely the case for the sulphide gangue phases in the LOB ores (by the same margin) (Fig. 30d and 30f respectively). The total sulphide concentration of both LOB ores across the four size fractions remains consistently above 90%.

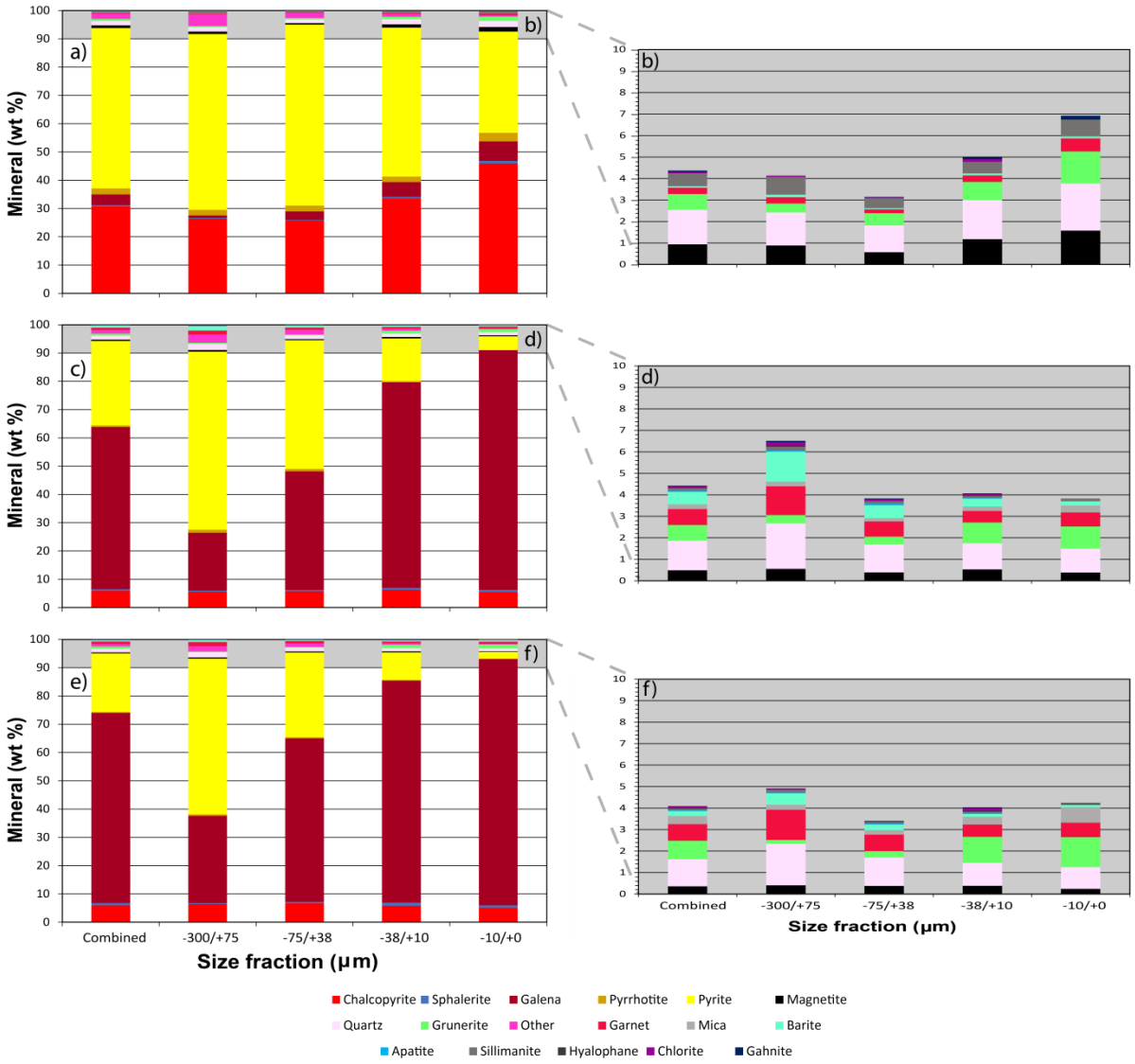

Figure 30: *Flotation concentrate C mineralogy by size for: (a) ore G bulk mineralogy and (b) NSG, (c) ore H bulk mineralogy and (d) NSG, (e) ore I bulk mineralogy and (f) NSG. Note the difference in scales between bulk NSG graphs for the same ore type.*

5.3.3 Grain size distribution (GSD)

The chalcopyrite GSD for the three ores have minor grouping formation, with the two LOB ores having more similar curves compared to the curve of ore G. Ore G has a slightly higher proportion of fine chalcopyrite grains than ores H and I, the three ores, however, have similar GSD curves (Fig. 31a). The grouping pattern for the GSD of galena is similar to that of chalcopyrite, with a slightly more prominent distinction between the two ore bodies (Fig. 31b). The GSD curves for sphalerite are similar for all three ore types, showing erratic jumps in percentage for certain sphalerite grain sizes (Fig. 31c). These erratic jumps are a function of the small sample size (small relative amount of sphalerite particles analysed).

A clear distinction between ore bodies can be seen in the GSD curves for magnetite and pyrite, with ore G (GQOB) having a higher percentage of finer-grained magnetite and pyrite compared to ores H

and I (LOB) (Fig. 31d and e respectively). The GSD curves for quartz are more erratic, but throughout the grain size spectrum ore G has slightly finer-grained quartz compared to the quartz of ore H and ore I (Fig. 31f). A clear split can be seen between the grain sizes of mica for ore G and ore H/I, the LOB ores have a higher proportion of larger grained mica when compared to the GSD of ore G (Fig. 31g). The erratic nature of the NSG GSD curves can be attributed to the low modal proportions of these minerals in the flotation concentrate.

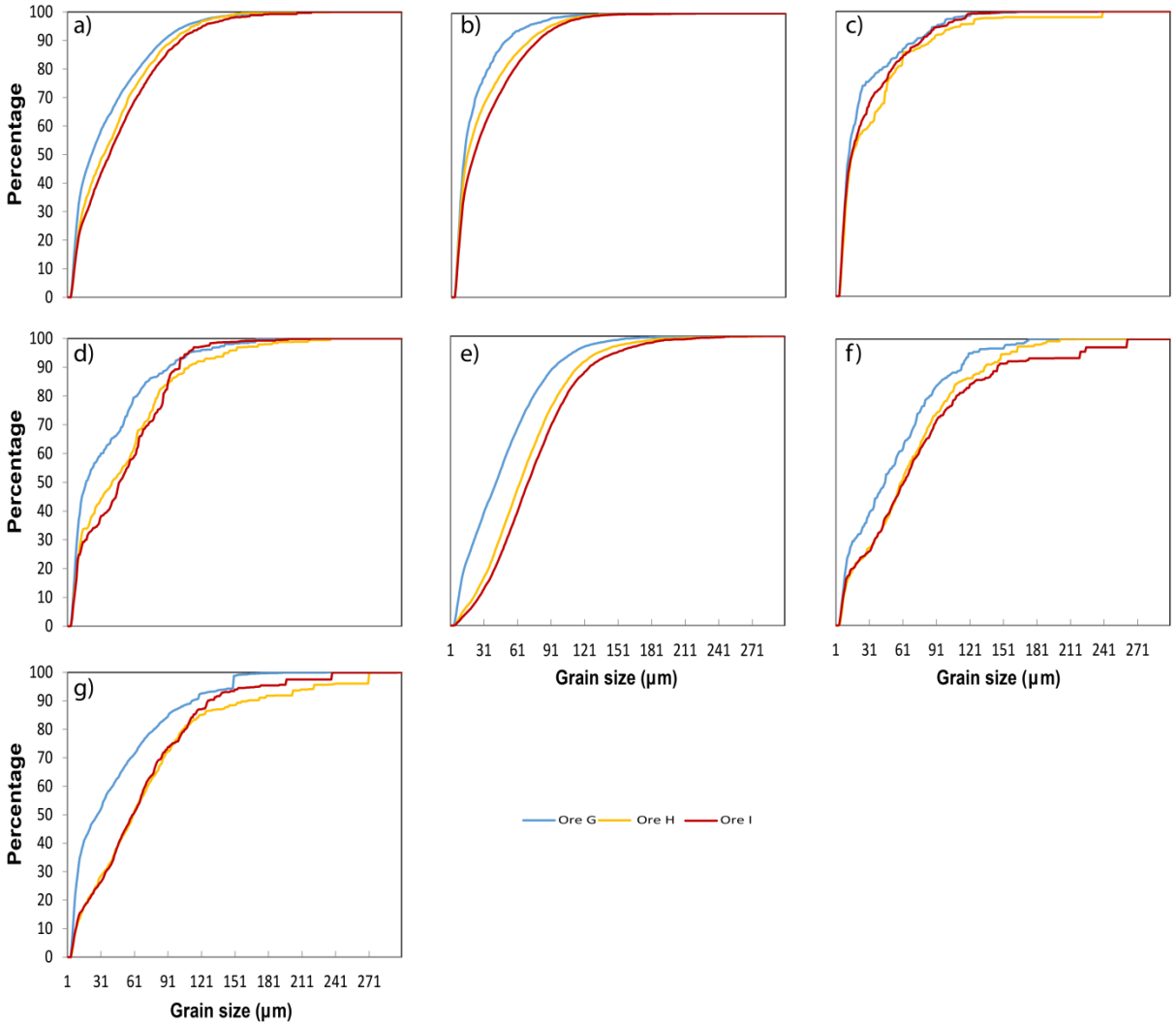

Figure 31: *Flotation concentrate C_1 GSD for minerals: (a) chalcopyrite, (b) galena, (c) sphalerite, (d) magnetite, (e) pyrite, (f) quartz and (g) mica.*

5.3.4 Mineral liberation

The chalcopyrite for all three ore types is, as expected, well liberated (Fig. 32). The highest liberation is found in ore G (85% is totally liberated), with chalcopyrite in the LOB ores being slightly less, but still well liberated (H – 75% and I – 77%). The galena for ore G is semi-liberated (53%) whereas the LOB ores galena is well liberated (H – 86% and I – 89%) (Fig. 32). The sphalerites, much like the sphalerite in the feed, is poorly liberated, with ore G's concentrate showing the best liberation (35%). Ore H and I have poor sphalerite liberation and may be considered to have locked sphalerite (H –

15% and I – 13%) (Fig. 32). The only sulphide gangue to be discussed, in terms of mineral liberation, will be pyrite. This is the case due to the high amount of pyrite concentration in the flotation concentrate, understanding the pyrite liberation may give valuable insights into the mechanisms of pyrite recovery (i.e. liberated – true flotation, locked – flotation by association). The pyrite in all three ore types is well liberated, particularly in terms of the concentrate relative to the feed; with all three ore types showing pyrite liberation between 84% and below 90%. The pyrite liberation is not governed by the amount of pyrite recovery (and vice versa), as the three ore types have varying amounts of pyrite recovery but similar pyrite liberation.

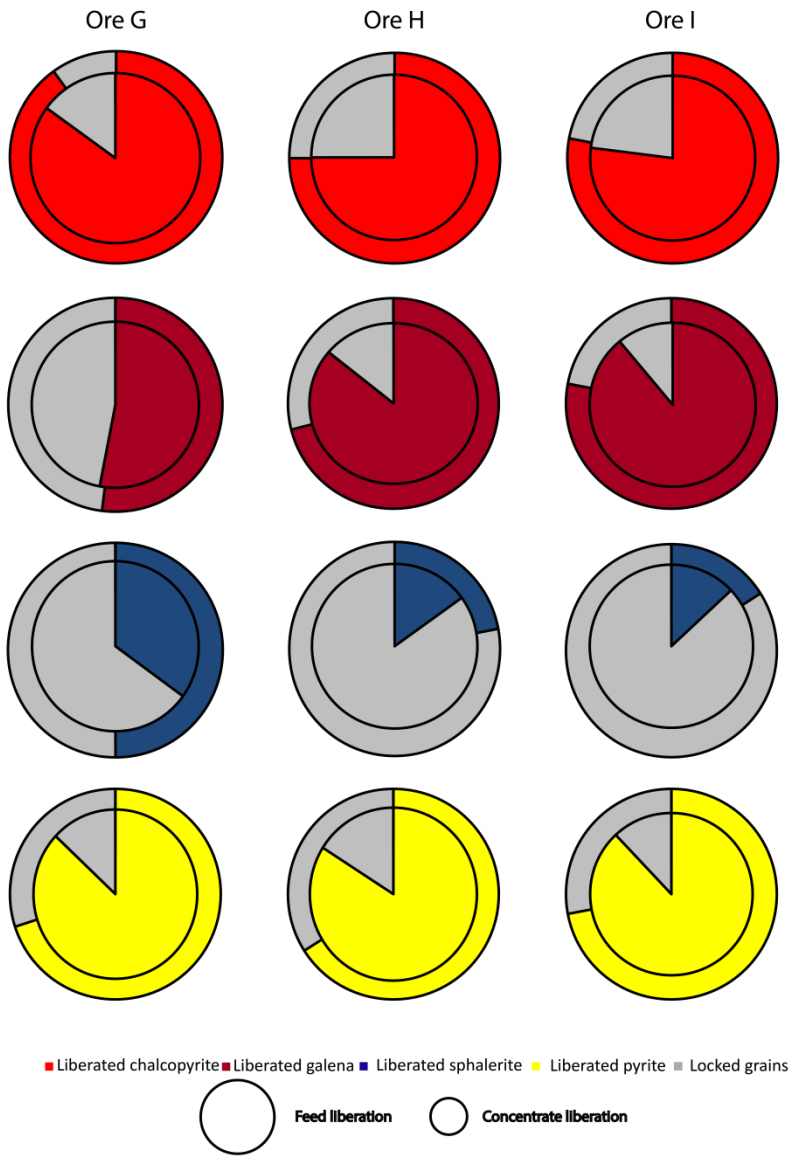

Figure 32: *Sulphide mineral liberation of feed vs concentrate C_1. A liberated sulphide in this chart is defined by a particle having 90% area or higher covered by one mineral. The outer ring represents the mineral liberation in the feed and the inner ring represents the liberation in the concentrate C_1*

Table 8: *Mineral liberation across the different quartz-dominant ore types and size fractions for concentrate.C_1. Liberation here is defined as particles with greater than 90 % of the mineral of interest by area. The combined liberation values here are represented by the inner ring in Fig. 27. Analytical inaccuracies in the -10 µm liberation fraction resulted in the assumption that the -10 µm liberation fraction is the same or more liberated than the -38 µm liberation fraction.*

Percentage mineral liberation of minerals of interest (concentrate C1)					
Minerals	Ore G				
	Combined	+75µm	-75µm +38µm	-38µm +10µm	-10µm
	Concentrate	Concentrate	Concentrate	Concentrate	Concentrate
Chalcopyrite	85	80	89	94	94
	(31418)	*(3548)*	*(3782)*	*(5124)*	*(18964)*
Galena	53	30	62	74	74
	(5777)	*(727)*	*(1142)*	*(869)*	*(3039)*
Sphalerite	35	29	38	43	43
	(2027)	*(572)*	*(467)*	*(246)*	*(742)*
Pyrite	87	90	92	91	91
	(29560)	*(5279)*	*(6496)*	*(5089)*	*(12696)*
Ore H					
Chalcopyrite	75	73	85	84	84
	(6522)	*(1672)*	*(1841)*	*(1257)*	*(1752)*
Galena	86	75	90	93	93
	(27845)	*(3605)*	*(5714)*	*(7562)*	*(10964)*
Sphalerite	15	3	10	13	13
	(2498)	*(548)*	*(1178)*	*(362)*	*(410)*
Pyrite	84	87	87	74	74
	(14954)	*(5613)*	*(5908)*	*(2006)*	*(1427)*
Ore I					
Chalcopyrite	77	81	86	88	88
	(10014)	*(1752)*	*(3807)*	*(2477)*	*(1978)*
Galena	89	86	95	96	96
	(45189)	*(3930)*	*(13435)*	*(16058)*	*(11766)*
Sphalerite	13	3	14	21	21
	(4539)	*(590)*	*(2549)*	*(930)*	*(551)*
Pyrite	88	90	90	82	82
	(19403)	*(5129)*	*(9984)*	*(3010)*	*(1280)*

**Value given in brackets represents the total amount of sulphide particles analysed.*

Graphical representation of the liberation in flotation concentrate C_1 through the four size fractions can be seen in Appendix C.

5.3.5 Mineral association

Due to the high liberation in most of the minerals of interest (chalcopyrite, galena and pyrite) the mineral association values are low. Chalcopyrite shows an association to pyrite, galena and sphalerite in all three ore types (Fig. 33). The chalcopyrite association to pyrite is similar in all three ore types (Fig. 33b), however, the chalcopyrite association to galena and sphalerite is most pronounced in the LOB ores (H and I) (Fig. 33b). The galena association profiles (Fig. 33c) show a clear delineation between the ores of the two ore bodies, with higher galena association to pyrite and chalcopyrite in the GQOB ore. The galena-pyrite association in ores H and I is similar and higher than the galena-chalcopyrite association (which is also similar between the two LOB ores) (Fig. 33d). Sphalerite has a poor liberation in all three ore types, in particular the LOB ores (Fig. 33e). This results in high

sphalerite association values, in particular the sphalerite association to chalcopyrite. The LOB ores also show a strong sphalerite-galena association, higher than that of ore G (Fig. 33f).

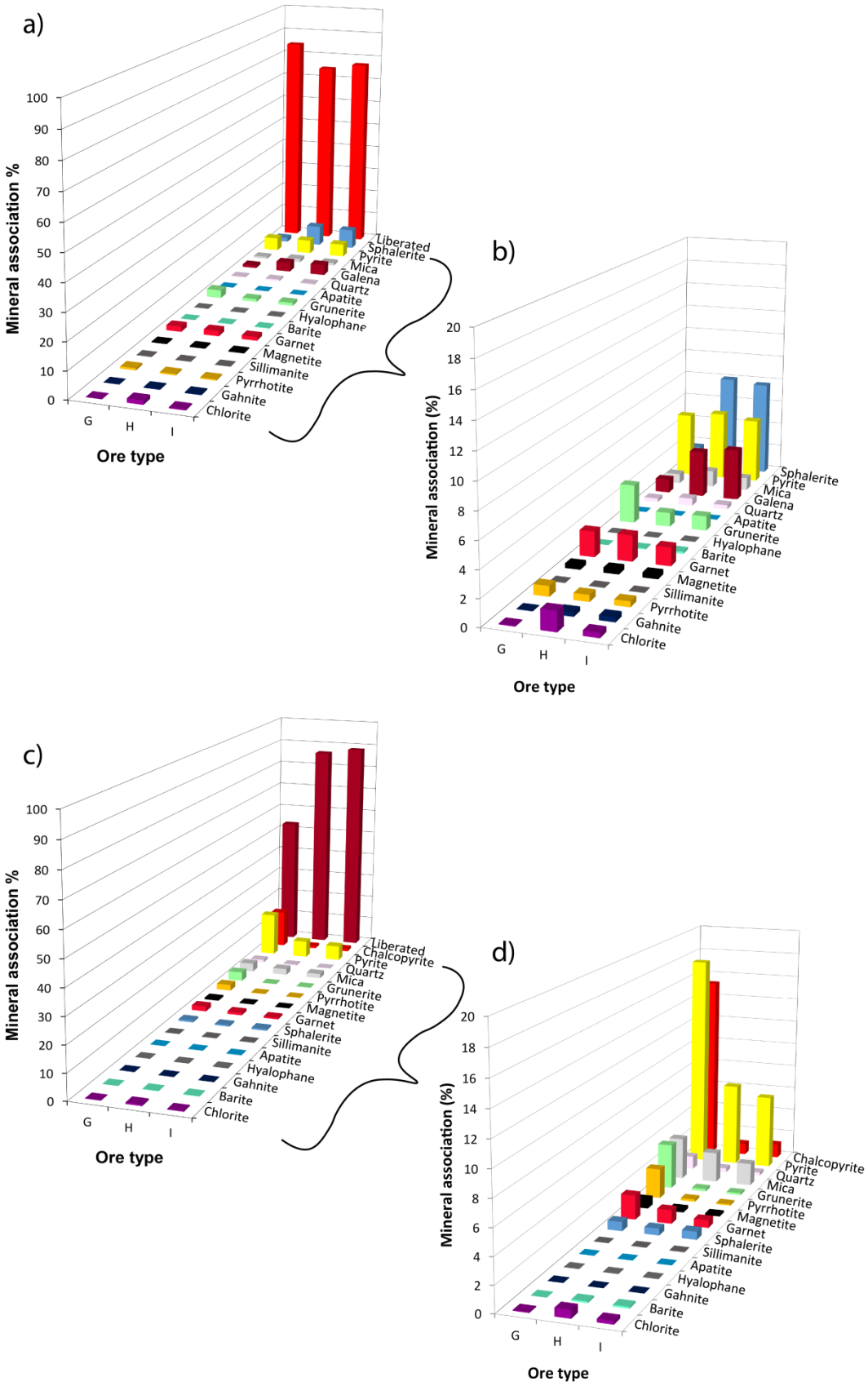

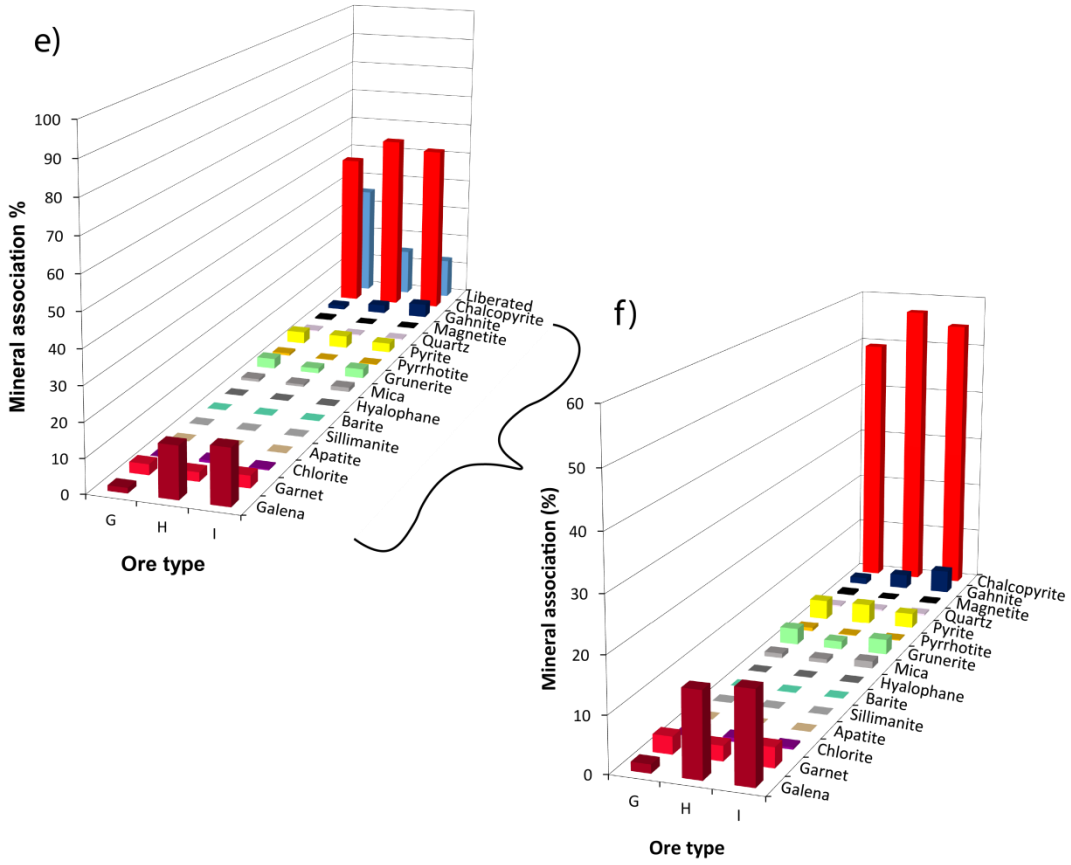

Figure 33: *(a) Bulk chalcopyrite, (c) galena and (e) sphalerite association of flotation concentrate C_1 for the quartz-dominant ores. Expanded version removing the liberated component from the association profile (b), (d) and (f). Note the difference in scales between figures with and without the liberated component for each sulphide association.*

5.3.6 Mineral association by size

Chalcopyrite does not show any preference in association through the size fractions for all three ore types, with an exception to the chalcopyrite-galena association in the -10 µm size fraction in the LOB ores. This chalcopyrite-galena association is slightly elevated in the -10µm size fraction. The galena-pyrite, galena-grunerite and galena-garnet association decreases with a decrease in size fraction of ore G. The galena-chalcopyrite association for ore G remains relatively consistent throughout all four size fractions, with minor fluctuations. The galena association for the LOB ores show no increase in abundance as you move through the four size fractions. The sphalerite association (which is dominated by the sphalerite-chalcopyrite association) has no discernible pattern through the four size fractions for all three quartz-dominant ore types.

5.3.7 Elemental deportment

The Cu in all three ore types is solely deported from the mineral chalcopyrite, similarly, the Pb is solely deported from galena in all three ore types. Zn is deported from sphalerite (chiefly) and chalcopyrite (minor, as an accessory trap phase described in section 2.5.2), with a slight increase in Zn deportment from chalcopyrite in the finer grain size fractions, this is the case for all three ore types (Fig. 34). The iron deportment in ore G is from pyrite and chalcopyrite, with a majority of the

deportment coming from pyrite. The ratio of iron deportment from pyrite to the iron deportment from chalcopyrite decreases with a decrease in size fraction (more iron is deported from chalcopyrite the smaller the size fraction is). The iron deportment for the LOB ores does not show the same profiles as the iron deportment for ore G (Fig. 34). The total iron deportment drastically decreases from the largest to the finest size fraction (over 25% total iron deportment decrease from the +75 µm to the -10 µm size fractions). The iron deportment is dominated by the deportment from pyrite (this deportment controls the drastic total deportment decrease). The iron deportment from chalcopyrite is minor and *remains* relatively consistent through the four size fractions. The manganese deportment is dominantly from garnet in each ore type, ore G has deportment from magnetite and sphalerite (this is not as pronounced in the manganese deportment for the LOB ores). The LOB ores show manganese deportment from chlorite (decreasing deportment from chlorite with a decrease in size fraction).

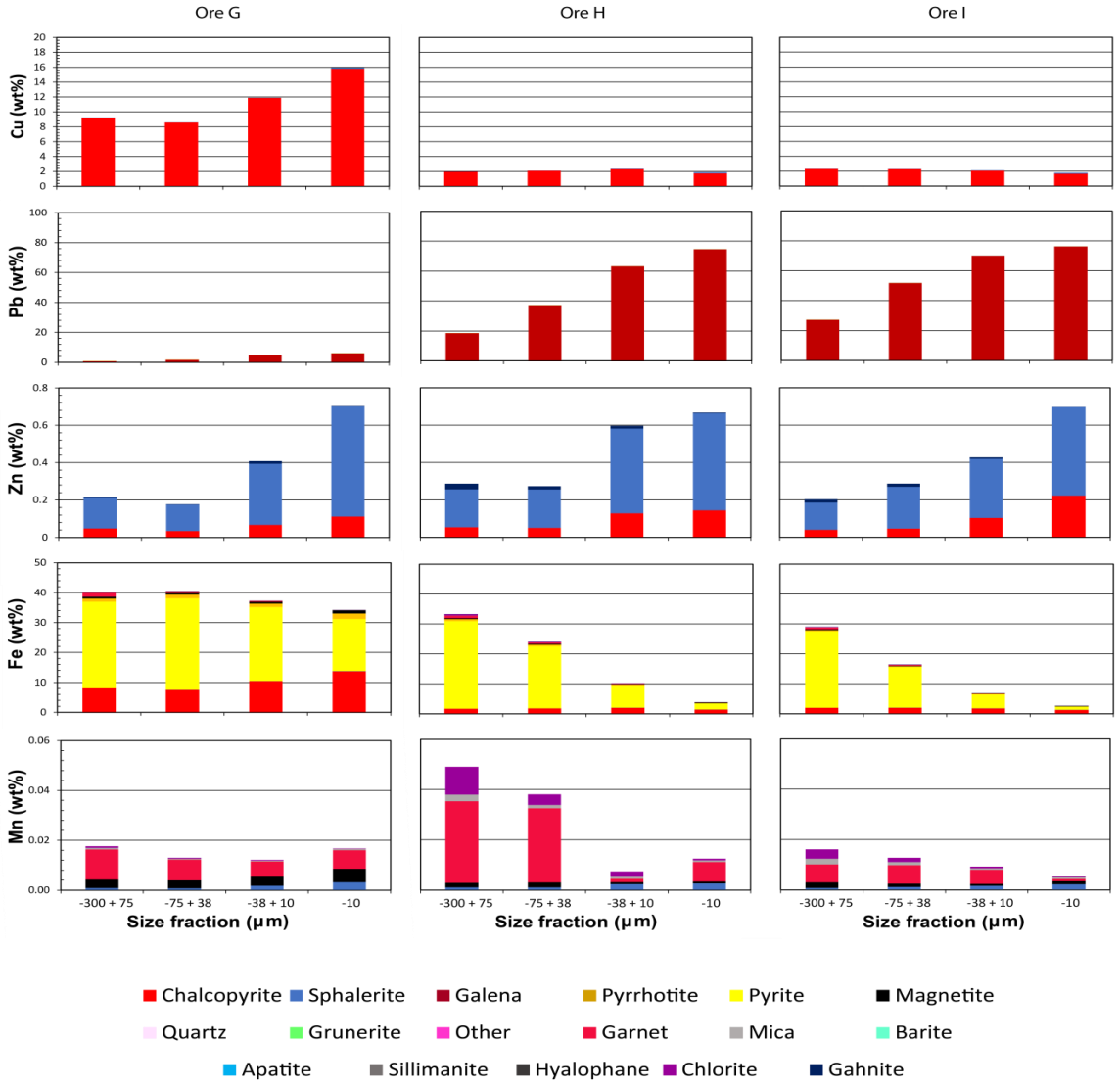

Figure 34: *Flotation concentrate C elemental deportment through four size fractions. Note the change in scale between the figures for each element.*

5.4 DISCUSSION

5.4.1 Concentrate mineralogy characterisation insights

The expected concentration of economic minerals in the flotation concentrate was recovered, in correlation with respective ore head grades of these economic targets. The head grades depict that ore G has the highest chalcopyrite (Cu head grade) and the lowest galena (Pb head grade) concentration amongst the three quartz-dominant ore varieties. This is seen in the concentrate mineralogy, as ore G has ≈30 mass percent chalcopyrite in the concentrate, compared to ores H and I which both have less than 5 mass percent chalcopyrite. This is also the case for the respective galena head grades and the resultant galena concentration in the flotation concentrate. Ores H and I have a higher galena head grade than ore G, the galena concentration in the LOB ores is substantially higher than the galena concentration in the GQOB ore (LOB ores – average of 62 wt. % galena and ore G - 3.82 wt. % galena in the concentrate). Although the Zn head grade is low, it is important to note that the recovered sphalerite percentage through flotation does not correlate to this head grade. This is because some of the Zn measured in the feed, in some cases almost half (LOB ores display higher feed percentages of Zn deportment from gahnite), is locked in gahnite. The gahnite concentration in the concentrate can be considered null, this is due to the refractory nature of this mineral, and its related recalcitrant behaviour in flotation conditions. This results in an unexpected decrease in Zn grade and recovery in the concentrate when compared to the Zn grade and potential recovery in the feed. This “Zn loss” is represented by the comparison of Zn deportment between the feed and the concentrate, where it can be seen that the feed has a contingent of Zn deportment from gahnite whereas the concentrate has no Zn deported from gahnite. Large concentrations (in ore G particularly) of pyrite is found in the flotation concentrate, due to the liberated nature of this pyrite it can be assumed that it is being concentrated through true flotation. All other minerals are in very low concentrations (2 wt. % or lower) and can be assumed to either be entrained in the froth with the target minerals or recovered as composite particles (NSG-ES composites).

5.4.2 Morphology of concentrated minerals

The fundamentals of flotation predict that certain minerals will be selectively concentrated in the flotation froth, this ability/willingness to be concentrated is largely (but not solely) influenced by the specific mineral liberation statistics. The more liberated a target mineral is, the higher the likelihood that mineral will be concentrated in the flotation froth (should that mineral be hydrophobic or have hydrophobicity induced upon it), it is for that reason that mineral liberation is such a pivotal aspect of minerals processing. In the same vein, the minerals found in the concentrate are expected to have high degrees of liberation, due to this being such an influential aspect in the flotation process. The concentration of minerals in the flotation process with low degrees of liberation point to other mechanisms of concentration - as opposed to true flotation (i.e. entrainment, flotation by association, etc.).

The liberation of chalcopyrite and galena in the concentrate is very high and points to the recovery of these minerals by true flotation. The liberation of sphalerite, on the other hand, is not as high as the

other two economic sulphides. The liberation together with the association data, which shows a high degree of sphalerite-chalcopyrite association, points toward the possibility of sphalerite being recovered through flotation by association. Sphalerite is usually activated in the flotation cell, through the addition of an activator (e.g. Cu sulphate, $CuSO_4$). The quartz-dominant ores are not sphalerite rich, this can be seen looking at the head grades of Zn, it is for that reason (along with trying to avoid unnecessary/unwanted gangue activation) that an activator was not added. This lack of sphalerite in the concentrate is the most likely reason for the poor sphalerite liberation and recovery seen. The other mineral that deserves attention is pyrite, largely due to the extremely high, in some cases (ore G), concentration. The liberation data for pyrite along with the association data shows that pyrite has low amounts of mineral association and high degrees of liberation. This, in turn, means that pyrite is being concentrated through true flotation, and due to the gangue (and potentially deleterious) nature of pyrite this is cause for concern and needs to be addressed in the flotation procedure.

The GSD of the minerals of interest (chalcopyrite, galena, sphalerite, pyrite, quartz, magnetite and mica) of the three quartz-dominant ores is distinctly unique when comparing the feed to the concentrate C_1 of an ore. The feed GSD plots (Fig. 18) show that ore G has an overall larger grainsize (compared to ores H and I) in all of the seven minerals when comparing this to the concentrate C_1 GSD plots (Fig. 31), this is not the case. Ore G, more actively than ores H and I, concentrates finer-grained minerals. This is seen by the GSD curves - how ore G has the finer-grained curve (out of the three ore types). Ores H and I also concentrate finer-grained mineral specimens, the change between the feed and concentrate C_1 are, however, not as radicle as it is with ore G. This speaks to or G having a higher breakability propensity, than the other two ores.

5.4.3 Potential concentrate dilution and its implications

The potential dilution of the flotation concentrate through the recovery of unwanted minerals is substantially problematic for a mining operation, this issue results in penalties being accrued by the mine for concentration impurities. The unwanted recovery of pyrite in these flotation experiments, however, has massive environmental ramifications, due to the acid generating potential of pyrite. The recovery and concentration of pyrite, which will need to be removed from the economic sulphide concentrates, will result in raw, concentrated and liberated pyrite being reported to tailings. This is a particular issue when processing ore G, as the concentration of pyrite in ore G was the highest (56.7 wt. %) between the three quartz-dominant ores. The liberated nature of the pyrite in concentrate C_1 (between 84 and 88%) is both cause for concern, as well as, a positive attribute. The drawbacks of the high liberation of pyrite found in the flotation concentrate, is that the pyrite grains have very little, to no, association minerals that may decrease the speed (or even buffer) of pyrite generating acid (through acid rock drainage). The beneficial aspect of this high liberation value is that the implementation of pyrite suppression in the flotation circuit will be received with a high probability of success. Due to the pyrite being almost completely liberated, with no accessory phases present, reduces the possibility of association based suppression complications. The potential for concentrate dilution by other minerals is minor, as all other minerals concentrations don't individually exceed 2 wt. %.

5.5 CONCLUSION

The bulk mineralogy of the concentrates only substantially varies between three minerals in the three ore types. The concentrations of chalcopyrite, galena and pyrite are the main minerals of varying concentrations. The chalcopyrite grade in ore G is substantially higher than the chalcopyrite grade in the LOB ores (H and I). The galena grade between the two ore bodies has an equal but opposite contrast, with the LOB ores having a substantially higher galena grade compared to the GQOB ore. The pyrite grade is unique to each ore type, with a decrease in grade from ore G through ore H to ore I. These mineralogical differences are not a function of the difference in mineral liberation or mineral association, as all three ores have similar liberation and association statistics, but more so a difference in feed mineralogy.

The separation of the ore bodies exhibited in Fig. 25 (metal mass vs. water recovery) can be further interpreted with the knowledge of the concentrate mineralogy. The higher Cu mass vs water recovery shown by ore G, compared to ores H and I, is due to the higher chalcopyrite grade of chalcopyrite in ore G's concentrate. The spread in Fig. 25b is explained by the spread in galena grade between the three ores. The relatively similar Zn and mass vs water recovery curves for the three ores is explained by the similar sphalerite grade in the three ores' concentrates. The difference in iron mass vs water recovery between the two ore bodies is due to the substantially higher grade of pyrite in ore G compared to ores H and I.

The recovery of the potentially deleterious mineral, pyrite, is of importance. Pyrite is a chief mineral in acid rock drainage, due to its extremely high acid generating potential. The recovery of pyrite can be avoided through its suppression in the flotation circuit with the addition of a depressant (i.e. guar gum). This does not, however, alleviate the possibility for acid rock drainage to take place, pyrite neutralisation is needed in the tailings due to the high pyrite content of the ore.

Chapter 6: Conclusions and Recommendations

6.1 CONCLUSIONS

At the beginning of this thesis, four key objectives and associated key questions were identified to guide the research. The first three key objectives were each addressed in the first three chapters, whilst the fourth objective served to indicate the overall significance of the resultant work. In the sections below, the main findings of each chapter are placed in the context of the stated first three key objectives. The last key objective is addressed by the discussion of the overall recommendations of the thesis.

- **Key Objective One: To characterise the mineralogy and texture of the LOB and GQOB ore types.**

  Quartz makes up the main bulk gangue mineral for all three ores. However, thereafter the comparability of the ore's mineralogy between the three ores becomes more complex. The two ore bodies (LOB and GQOB) are dissimilar in most mineral concentrations, barring equivalent mineral concentrations in minor mineral phases. The most important mineral discrepancies between the ores come about when considering economic and deleterious mineral concentrations, as the ramifications for beneficiation are amplified when processing ores with these discrepancies through the same minerals processing system. A clear division between the ores of the two ore bodies can be seen when solely analysing the bulk feed mineralogy. Ore G of the GQOB has a high chalcopyrite and pyrite concentration whereas ores H and I (of the LOB) have high galena concentrations with lesser pyrite concentrations. The main gangue phase in ore G is magnetite, whereas mica is the main gangue phase in the LOB ores. The LOB ores have a higher concentration of gahnite, which is detrimental to Zn recovery. The LOB ores are more foliated than the GQOB, which has a more isotropic fabric. The two ore bodies show distinct behaviour during crushing and milling resulting in different GSDs, mineral liberation and mineral association profiles between the LOB and the GQOB. The mineral liberation of the two main ES minerals (chalcopyrite and galena) in all three quartz-dominant ore types is high (Table 5). However, a clear separation between the three

quartz-dominant ore types can be seen as ore G has a higher chalcopyrite liberation than ores H and I. This is inversely the case with galena liberation, as ores H and I have higher galena liberation than ore G. The differences in specific mineral liberation are primarily a function of mineralogy and texture, and hence these differences are expected.

- **Key Objective Two: To characterise the mineral processing performance of the LOB and GQOB ore types.**

  The PSD and milling time of ores are functions of both an ore's hardness as well as its breakability. Both these properties relate to mineralogy and texture. From the flotation test work carried out, a slight division is seen between the ores of the different ore bodies. The total mass pull and water recovery of all three ores are similar, pointing towards the foliation of the LOB ores playing little to no role in the total recovery. The theoretical mineral grade recovery curves (Fig. 26) for the three ore types show that ore G is theoretically the best performing chalcopyrite (Cu) ore and ore I is theoretically the best performing galena (Pb) ore. Comparison of theoretical grade recovery curves (Fig. 26) with actual grade recovery curves (Fig. 27) for Zn, shows that ore G will be the best performing ore of the three ore types but that the grade recovery is not as maximised as it is with chalcopyrite and galena. However, the actual grade recovery curve for Zn (Fig. 27c), is not as easy to interpret as the Cu or Pb equivalents (Fig. 27a and 27b, respectively). This is interpreted to be a function of Zn deportment from gahnite, as some of the Zn in the sample is locked in gahnite which is refractory and cannot be recovered using conventional methods. The inability to recover all the gahnite, in turn, decreases the Zn recovery. In comparison, with Cu and Pb, all the Cu is found in chalcopyrite and all the Pb is found in galena, both of which are almost completely recovered. This decrease in available Zn for recovery affects the grade recovery curves, and as a result, ores G and I have comparable curves, ore G has a higher grade but lower recovery and vice versa for ore I.

  Another parameter defining the flotation performance of these ores is the gangue recovery (both sulphide and non-sulphide). In the metal mass vs water recovery curves (Fig. 25), it can be clearly seen that the iron recovery in ores G and H is high, particularly in ore G. This is a cause for concern from both an economic and an environmental perspective. The iron recovery will decrease the relative concentration of valuable elements in the concentrate and depending on what mineral the iron is present in, could be a major cause of acid-rock drainage generation.

- **Key Objective Three: To characterise the mineralogy of the bulk flotation concentrate C_1**

  The characterisation of the flotation concentrates helps identify which mineral phases certain elements are concentrating in, in the flotation concentrate. Properly characterising, the flotation concentrates also helps understand the nature of concentrated minerals, i.e. if they

are liberated and floated or floated by association. Understanding these characteristics can also feed back into the initial stages of the processing circuit, i.e. if the liberation of economic sulphides is not high enough, then appropriate changes could be made to the fineness of the feed grind going into the flotation circuit in order to try and increase the liberation. The main minerals concentrated in all three ores is similar but the concentrations of these minerals are, however, unique. Ore G has the highest concentration of chalcopyrite and pyrite out of the three ores. Ore H has a lower concentration of both pyrite and chalcopyrite, but a higher concentration of galena. Ore I has the lowest concentration of pyrite and the highest concentration of galena, with an equivalent chalcopyrite concentration to ore H. The other minor minerals found in the concentrates are present in very minor amounts (<2%), with the total non-sulphide gangue recovered being <5% in all three ores. The division between the economic minerals recovered points towards the grouping of the LOB ores and separation of the GQOB ore, in terms of mineralogical similarities. The liberation of chalcopyrite, galena and pyrite are all high, with lower amounts of sphalerite liberation, in all three ores. The liberation of each mineral between the ores is however unique to the ore bodies, with ore G having higher chalcopyrite liberation compared to the chalcopyrite liberation in ores H and I (which are comparable). The same is the case for the galena liberation, with galena being better liberated in ores H and I in comparison to ore G. The economic element deportments are as expected, with Cu being deported from chalcopyrite, Pb being deported from galena and Zn being deported from sphalerite (due to the non-floating nature of gahnite). The iron deportment is of importance, due to the high iron recovery, with iron overwhelmingly deported from the liberated pyrite found in the concentrate. The GSD of recovered minerals is unique to each ore body because although the morphology of individual grains does not change during the process of concentration, the mineralogy of the concentrate is different to that of the feed and hence the bulk morphology of the concentrate in comparison to the feed is different. In summary, the mineralogy and quantitative statistics of the flotation concentrate indicate that the ores of the two ore bodies are different from each other.

6.2 RECOMMENDATIONS

- **To assess the possible implementation and relevance of creating a geometallurgical domain for the quartz-dominant ores.**

  The implementation of geometallurgical domains is aimed at better control over the processing performance of the ores going through the processing circuit. The geometallurgical domains can also help with forecasting processing outcomes, and better identify processing irregularities. However, the identification of geometallurgical domains though does not imply that it will be practical to implement such domains on a mine site. Implementation would involve much wider considerations regarding the logistics of mining different sections of the ore body in such a way that the identified ore domains are preserved through the physical mining process and the process of extracting the mined ore from the mine. This would be particularly problematic in the case of underground workings where

space and access restrictions would complicate extraction of ore material in individual domains.

Nevertheless, and although further work is needed to precisely define the parameters of each domain, it would be recommended here that ores G, H and I are not grouped together solely based on the fact that these three ore types are quartz dominate. The mineralogical characterisation of the three ore types indicates ore G is unique in comparison to ores H and I, which are alike. The processing performance shows that the total solids-water recoveries of the three ore types is similar but that ore G clearly has unique processing qualities in comparison to ores H and I. Similarly and as previously stated, the same behaviour is observed for the flotation response and the concentrate mineralogy.

The implementation of geometallurgical domains would be beneficial to the mining practice if it was practical to implement. Of the three quartz-dominant ore horizons, ore G should make up its own geometallurgical domain, and ores H and I should be grouped together to make up the second geometallurgical domain. These groupings should result in more consistent processing performance, concentrate grade and recovery of the economic sulphides. The grouping of the different ore types into these two domains would also contribute to more reliable forecasting and allow the mining practice to better manage and anticipate future changes, both economic and geological.

This study has been conducted in parallel with a comparable study on the magnetite-dominant ore types of the Upper Ore Body (UOB) in the same deposit (Gordon, 2019). That study identified six ore types that were grouped into three ore domains but identified similar issues with the feasibility of implementing a domain-orientated mining process. Although it has not been the explicit intention here to directly compare and contrast these studies, it is worth considering the scale of the differences noted between the various different ore types. For example, it would be necessary to evaluate whether the differences between the ore types from the LOB and the GQOB identified in this study, are greater than or less than the differences between the quartz-dominant ores of the LOB and the magnetite-dominant ores of the UOB. Comparison of the mineralogical and textural character as well as the minerals processing response based on the work done in this study and that of Gordon (2019) is quite complex because of fundamental differences in the basic mineralogy of the three ore bodies and would require additional work to do this properly. Nevertheless, the differences in the geological (mineralogy and texture) and minerals processing (flotation response) behaviour of the different quartz-dominant ore types suggests that geometallurgical domaining may provide a means of optimising efficiency of mining operations. Although this may prove costly in implementation for existing mines, the benefits to newly discovered ore deposits could be significant both in terms of mining efficiency and financial longevity.

References List

Abubakre, O.K., Muriana, R.A., Nwokike, P.N., 2007. Characterization and Beneficiation of Anka Chromite Ore Using Magnetic Separation Process. J. Miner. Mater. Charact. Eng. 6, 143–150.

Albijanic, B., Amini, E., Wightman, E., Ozdemir, O., Nguyen, A. V., Bradshaw, D.J., 2011. A relationship between the bubble–particle attachment time and the mineralogy of a copper–sulphide ore. Miner. Eng. 24, 1335–1339. https://doi.org/10.1016/j.mineng.2011.06.005

Amini, E., Hosseini, T.R., Oliazadeh, M., Kolahdoozan, M., 2009. Application of Acidithiobacillus Ferrooxidans in Coal Flotation. Int. J. Coal Prep. Util. 29, 279–288. https://doi.org/10.1080/19392690903558314

Bailie, R.H., Reid, D.., 2005. Ore textures and possible sulphide partial melting at Broken Hill, Aggeneys, South Africa I: Petrography. South African J. Geol. 108, 51–70.

Becker, M., Harris, P.J., Wiese, J.G., Bradshaw, D.J., 2009. Mineralogical characterisation of naturally floatable gangue in Merensky Reef ore flotation. Int. J. Miner. Process. 93, 246–255. https://doi.org/10.1016/j.minpro.2009.10.004

Beers, D., Bossilkov, A., Corder, G., Berkel, R., 2008. Industrial Symbiosis in the Australian Minerals Industry: The Cases of Kwinana and Gladstone. J. Ind. Ecol. 11, 55–72. https://doi.org/10.1162/jiec.2007.1161

Beeson, R., 1990. Broken Hill-type lead-zinc deposits - an overview of their occurrence and geological setting. Trans. Inst. Min. Metall. Sect. B 99, 163–175.

Bicak, O., 2019. A technique to determine ore variability in a sulphide ore. Miner. Eng. 142, 105927. https://doi.org/10.1016/j.mineng.2019.105927

Bicak, O., Ekmekci, Z., Bradshaw, D.J., Harris, P.J., 2007. Adsorption of guar gum and CMC on pyrite. Miner. Eng. 20, 996–1002. https://doi.org/10.1016/j.mineng.2007.03.002

Boger, D.V., 2000. Rheology and the Minerals Industry. Miner. Process. Extr. Metall. Rev. 20, 1–25. https://doi.org/10.1080/08827509908962460

Boisvert, J.B., Rossi, M.E., Ehrig, K., Deutsch, C. V., 2013. Geometallurgical Modeling at Olympic Dam Mine, South Australia. Math. Geosci. 45, 901–925. https://doi.org/10.1007/s11004-013-9462-5

Bradshaw, D., 2014. The role of process mineralogy in improving the process performance of complex sulphide ores, in: XXVII International Mineral Processing Congress (IMPC) Santiago Chile: The Role of Process Mineralogy in Improving the Process Performance of Complex Sulphide Ores. pp. 1–23.

Bulatovic, S.M., 1999. USE OF ORGANIC POLYMERS IN THE FLOTATION OF POLYMETALLIC

ORES: A REVIEW. Miner. Eng. 12, 341–354.

Calvo, G., Mudd, G., Valero, Alicia, Valero, Antonio, 2016. Decreasing Ore Grades in Global Metallic Mining: A Theoretical Issue or a Global Reality? Resources 5, 36. https://doi.org/10.3390/resources5040036

Cao, Y.-J., Xia-Hui, G., Zi-Long, M.A., Xiao-Xia, Y.U., Xiao-Dong, C., Zhang, X.-P., 2009. Process mineralogy of copper-nickel sulphide flotation by a cyclonic-static micro-bubble flotation column. Min. Sci. Technol. 19, 784–787. https://doi.org/10.1016/S1674-5264(09)60143-5

Chandra, A.P., Gerson, A.R., 2009. A review of the fundamental studies of the copper activation mechanisms for selective flotation of the sulfide minerals, sphalerite and pyrite. Adv. Colloid Interface Sci. 145, 97–110. https://doi.org/10.1016/j.cis.2008.09.001

Chandraprabha, M.N., Natarajan, K.A., Modak, J.M., 2004. Selective separation of pyrite and chalcopyrite by biomodulation. Colloids Surfaces B Biointerfaces 37, 93–100. https://doi.org/10.1016/j.colsurfb.2004.06.011

Chauhan, M., Napier-Munn, T., Keeney, L., Bradshaw, D.J., 2013. Progress in Developing a Geometallurgy Flotation Indicator, in: The Second Ausimm International Geometallurgy Conference. Brisbane, pp. 1–6.

Chenje, T.W., Simbi, D.J., Navara, E., 2004. Relationship between microstructure, hardness, impact toughness and wear performance of selected grinding media for mineral ore milling operations. Mater. Des. 25, 11–18. https://doi.org/10.1016/S0261-3069(03)00168-7

Chetty, D., Gryffenberg, L., Lekgetho, T.., Molebale, I.., 2009. Automated SEM study of PGM distribution across a UG2 flotation concentrate bank: implications for understanding PGM floatability. J. South. African Inst. Min. Metall. 109, 587–593.

Chipfunhu, D., Bournival, G., Dickie, S., Ata, S., 2019. Performance characterisation of new frothers for sulphide mineral flotation. Miner. Eng. 131, 272–279. https://doi.org/10.1016/j.mineng.2018.11.014

Colliston, A.E., Praekelt, W.P., Schoch, A.E., 1989. A broad perspective (Haramoep) of geological relations established by sequence mapping in the Proterozoic Aggeneys terrane, Bushmanland, South Africa. South African J. Geol. 92, 42–48.

Colliston, W.P., Praekelt, H.E., Schoch, A.E., 1991. A progressive ductile shear model for the Proterozoic Aggeneys Terrane, Namaqua mobile belt, South Africa. Precambrian Res. 49, 205–215. https://doi.org/10.1016/0301-9268(91)90032-6

Colliston, W.P., Schoch, A.E., 2006. The distribition and diagnostic features of deformed plutonic rocks in two terranes of the Namaque mobile belt along the Orange (Gariep) River , South Africa. South African J. Geol. 109, 369–392.

Colliston, W.P., Schoch, A.E., 2003. A mid-Proterozoic Valcano-Sedimentary sequence in the Aggeneys Hills Duplex, Namaqua Metamorphic Complex. South African J. Geol. 106, 343–360.

Colliston, W.P., Schoch, A.E., 2000. Mid-Proterozoic tectonic evolution along the Orange River on the border between South Africa and Namibia. Communs geol. Surv. Namibia 12, 57–66.

Cook, N.J., 2000. Mineral characterisation of industrial mineral deposits at the Geological Survey of Norway: a short introduction. NORGES Geol. UNDERSOKELSE 436, 189–192.

Cornell, D.., Pettersson, A., Whitehouse, M.J., Schersten, A., 2009. A New Chronostratigraphic Paradigm for the Age and Tectonic History of the Mesoproterozoic Bushmanland Ore District , South Africa. Eco 104, 385–404.

Cornell, D.H., Thomas, R.T., Moen, H.F.G., Reid, D.L., Moore, J.M., Gibson, R.L., 2006. The Geology Of South Africa, 1st ed. Geological Society of South Africa/Council for Geoscience, Johannesburg/Pretoria.

Coward, S., Vann, J., Dunham, S., Stewart, M., 2009. The primary-response framework for geometallurgical variables, in: Seventh International Mining Geology Conference. Perth, WA, pp. 109–113.

Crockford, P.W., Wing, B.A., Paytan, A., Hodgskiss, M.S.W., Mayfield, K.K., Hayles, J.A., Middleton, J.E., Ahm, A.-S.C., Johnston, D.T., Caxito, F., Uhlein, G., Halverson, G.P., Eickmann, B., Torres, M., Horner, T.J., 2019. Barium-isotopic constraints on the origin of post-Marinoan barites. Earth Planet. Sci. Lett. 519, 234–244. https://doi.org/10.1016/j.epsl.2019.05.018

Cropp, A., Goodall, W., 2005. The Influence of Rock Texture on Mineral processing. Min Assist 1–9.

Cropp, A.F., Goodall, W.R., Bradshaw, D.J., 2013. The Influence of Textural Variation and Gangue Mineralogy on Recovery of Copper by Flotation from Porphyry Ore – A Review, in: The Second Ausimm International Geometallurgy Conference. pp. 279–291.

Drzymała, J., 2007. Atlas of upgrading curves used in separation and mineral science and technology. Physicochem. Probl. Miner. Process. 41, 27–35.

Eglington, B., 2006. Evolution of the Namaqua-Natal Belt, southern Africa - A geochronological and isotope geochemical review. J. African Earth Sci. 46, 93–111. https://doi.org/10.1016/j.jafrearsci.2006.01.014

Elshkaki, A., Graedel, T.E., Ciacci, L., Reck, B., 2016. Copper demand, supply, and associated energy use to 2050. Glob. Environ. Chang. 39, 305–315. https://doi.org/10.1016/j.gloenvcha.2016.06.006

Eshel, G., Levy, G.J., Mingelgrin, U., Singer, M.J., 2004. Critical Evaluation of the Use of Laser Diffraction for Particle-Size Distribution Analysis. Soil Sci. Soc. Am. J. 68, 736–743. https://doi.org/10.2136/sssaj2004.0736

Gaines, L., 2014. The future of automotive lithium-ion battery recycling: Charting a sustainable course. Sustain. Mater. Technol. 1, 2–7. https://doi.org/10.1016/j.susmat.2014.10.001

Gong, J., Peng, Y., Bouajila, A., Ourriban, M., Yeung, A., Liu, Q., 2010. Reducing quartz gangue entrainment in sulphide ore flotation by high molecular weight polyethylene oxide. Int. J. Miner.

Process. 97, 44–51. https://doi.org/10.1016/j.minpro.2010.07.009

Goodall, W.R., Scales, P.J., 2007. An overview of the advantages and disadvantages of the determination of gold mineralogy by automated mineralogy. Miner. Eng. 20, 506–517. https://doi.org/10.1016/j.mineng.2007.01.010

Gordon, H.J.J., 2019. A mineralogical approach to quantifying ore variability within a polymetallic Cu-Pb-Zn broken hill-type deposit and its implications for geometallurgy. Stellenbosch University.

Gordon, H.J.J., Miller, J.A., Becker, M., 2018. Using Mineralogy for Early Stage Geometallurgical Domain Definition : a Case Study of the Swartberg Polymetallic Sulphide Deposit, in: Proceedings of Geometallurgy 2018. pp. 121–132.

Groves, I.M., Bierlein, D.I., Broome, J., Penhall, J., 2008. Recognition of the hydrothermal feeder to the structurally inverted, giant broken hill deposit, new South Wales, Australia. Econ. Geol. 103, 1389–1394. https://doi.org/10.2113/gsecongeo.103.7.1389

Gu, Y., Schouwstra, R.P., Rule, C., 2014. The value of automated mineralogy. Miner. Eng. 58, 100–103. https://doi.org/10.1016/J.MINENG.2014.01.020

Gustafson, J.K., Burrell, H.C., Garretty, M.D., 1950. GEOLOGY OF THE BROKEN HILL ORE DEPOSIT, BROKEN HILL, N.S.W., AUSTRALIA. GSA Bull. 61, 1369–1438. https://doi.org/10.1130/0016-7606(1950)61[1369:gotbho]2.0.co;2

Hope, G.A., Woods, R., Munce, C.G., 2001. Raman microprobe mineral identification. Miner. Eng. 14, 1565–1577. https://doi.org/10.1016/S0892-6875(01)00175-3

Höy, T., 2001. Sedex and Broken Hill-Type Deposits , Northern Monashee Mountains , Southern British Columbia. Br. Columbia Geol. Surv. 85–114.

Johnson, N.W., 2006. Liberated 0–10μm particles from sulphide ores, their production and separation—Recent developments and future needs. Miner. Eng. 19, 666–674. https://doi.org/10.1016/j.mineng.2005.09.025

Khoso, S.A., Hu, Y., Lyu, F., Liu, R., Sun, W., 2019. Selective separation of chalcopyrite from pyrite with a novel non-hazardous biodegradable depressant. J. Clean. Prod. 232, 888–897. https://doi.org/10.1016/j.jclepro.2019.06.008

Klinglmair, M., Sala, S., Brandão, M., 2014. Assessing resource depletion in LCA: a review of methods and methodological issues. Int. J. Life Cycle Assess. 19, 580–592. https://doi.org/10.1007/s11367-013-0650-9

Lamberg, P., Rosenkranz, J., Wanhainen, C., 2013. Building a geometallurgical model in iron ores using a mineralogical approach with liberation data, in: Proceedings of the Second AusIMM International Geometallurgy Conference, Brisbane, Australia. pp. 317–324.

Lastra, R., 2007. Seven practical application cases of liberation analysis. Int. J. Miner. Process. 84, 337–347. https://doi.org/10.1016/j.minpro.2006.07.017

Lipson, R.D., 1980. The granitic rocks surrounding the aggeneysberge - A metamorphosed Rapakivi Suite. Trans. Geol. Soc. South Africa 83, 179–192.

Lishchuk, V., Koch, P.-H., Ghorbani, Y., Butcher, A.R., 2020. Towards integrated geometallurgical approach: Critical review of current practices and future trends. Miner. Eng. 145, 106072. https://doi.org/10.1016/j.mineng.2019.106072

Lopéz, R., Jordão, H., Hartmann, R., Ämmälä, A., Carvalho, M.T., 2019. Study of butyl-amine nanocrystal cellulose in the flotation of complex sulphide ores. Colloids Surfaces A Physicochem. Eng. Asp. 579, 123655. https://doi.org/10.1016/j.colsurfa.2019.123655

López Valdivieso, A., Celedón Cervantes, T., Song, S., Robledo Cabrera, A., Laskowski, J.., 2004. Dextrin as a non-toxic depressant for pyrite in flotation with xanthates as collector. Miner. Eng. 17, 1001–1006. https://doi.org/10.1016/j.mineng.2004.04.003

Lotter, N.O., Kormos, L.J., Oliveira, J., Fragomeni, D., Whiteman, E., 2011. Modern Process Mineralogy: Two case studies. Miner. Eng. 24, 638–650. https://doi.org/10.1016/j.mineng.2011.02.017

Lotter, N.O., Kowal, D.L., Tuzun, M.A., Whittaker, P.J., Kormos, L., 2003. Sampling and flotation testing of Sudbury Basin drill core for process mineralogy modelling. Miner. Eng. 16, 857–864. https://doi.org/10.1016/S0892-6875(03)00207-3

Lund, C., Lamberg, P., 2014. Geometallurgy – A tool for better resource efficiency. Eur. Fed. Geol. 37, 39–43.

Macey, P.H., Bailie, R.H., Miller, J.A., Thomas, R.J., de Beer, C., Frei, D., le Roux, P.J., 2018. Implications of the distribution, age and origins of the granites of the Mesoproterozoic Spektakel Suite for the timing of the Namaqua Orogeny in the Bushmanland Subprovince of the Namaqua-Natal Metamorphic Province, South Africa. Precambrian Res. 312, 68–98. https://doi.org/10.1016/j.precamres.2018.02.026

Macey, P.H., Thomas, R.J., Minnaar, H.M., Gresse, P.G., Lambert, C.W., Groenewald, C.A., Miller, J.A., Indongo, J., Angombe, M., Shifotoka, G., Frei, D., Diener, J.F.A., Kisters, A.F.M., Dhansay, T., Smith, H., Doggart, S., Le Roux, P., Hartnady, M.I., Tinguely, C., 2017. Origin and evolution of the ~1.9 Ga Richtersveld Magmatic Arc, SW Africa. Precambrian Res. 292, 417–451. https://doi.org/10.1016/j.precamres.2017.01.013

Mainza, A.N., Simukanga, S., Witika, L.K., 1999. Evaluating the performance of new collectors on feed to Nkana concentrator's flotation circuit. Miner. Eng. 12, 571–577. https://doi.org/10.1016/S0892-6875(99)00039-4

McClung, C., Viljoen, F., 2011. Mineralogical Assessment of the Metamorphosed Broken Hill Sulfide Deposit, South Africa: Implications for Processing Complex Orebodies. Proc. 10th Int. Congr. Appl. Mineral. 434–472. https://doi.org/10.1007/978-3-642-27682-8

McClung, C.R., Gutzmer, J., Beukes, N.J., Mezger, K., Strauss, H., Gertloff, E., 2007. Geochemistry

of bedded barite of the Mesoproterozic Aggeneys-Gamsberg Broken Hill-type district, South AFrics. Min. Depos. 42, 537–549.

Mehrabani, J.V., Noaparast, M., Mousavi, S.M., Dehghan, R., Rasooli, E., Hajizadeh, H., 2010. Depression of pyrite in the flotation of high pyrite low-grade lead–zinc ore using Acidithiobacillus ferrooxidans. Miner. Eng. 23, 10–16. https://doi.org/10.1016/j.mineng.2009.08.008

Mikhlin, Y., Vorobyev, S., Romanchenko, A., Karasev, S., Karacharov, A., Zharkov, S., 2016. Ultrafine particles derived from mineral processing: A case study of the Pb–Zn sulfide ore with emphasis on lead-bearing colloids. Chemosphere 147, 60–66. https://doi.org/10.1016/j.chemosphere.2015.12.096

Morland, R., Webster, A.E., 1998. Broken Hill lead-zinc-silver deposit. Geol. Aust. Papua New Guinean Miner. Depos. 6, 619–626.

Mu, Y., Peng, Y., Lauten, R.A., 2016. The depression of pyrite in selective flotation by different reagent systems – A Literature review. Miner. Eng. 96–97, 143–156. https://doi.org/10.1016/j.mineng.2016.06.018

Mwase, J.M., Petersen, J., Eksteen, J.J., 2012. A conceptual flowsheet for heap leaching of platinum group metals (PGMs) from a low-grade ore concentrate. Hydrometallurgy 111–112, 129–135. https://doi.org/10.1016/j.hydromet.2011.11.012

Nel, E., Valenta, M., Naude, N., 2005. Influence of open circuit regrind milling on UG-2 ore composition and mineralogy at Impala's UG-2 concentrator. Miner. Eng. 18, 785–790. https://doi.org/10.1016/j.mineng.2005.01.031

Oleynik, I.S., 2005. Australia : mineral & mining sector investment and business guide. International Business Publications.

Olubambi, P.A., Ndlovu, S., Potgieter, J.H., Borode, J.O., 2008. Mineralogical characterization of Ishiagu (Nigeria) complex sulphide ore. Int. J. Miner. Process. 87, 83–89. https://doi.org/10.1016/j.minpro.2008.02.008

Pascoe, R.D., Power, M.R., Simpson, B., 2007. QEMSCAN analysis as a tool for improved understanding of gravity separator performance. Miner. Eng. 20, 487–495. https://doi.org/10.1016/j.mineng.2006.12.012

Piercey, S.J., 2015. A semipermeable interface model for the genesis of subseafloor replacement-type volcanogenic massive sulfide (VMS) deposits. Econ. Geol. 110, 1655–1660.

Pinto, A., Gaspar, O., 1991. The ore textures of the Neves-Corvo volcanogenic massive sulphides and their implications for ore beneficiation. Mineral. Mag. 55, 417–422.

Praekelt, H., Schoch, A., 1997. Stratigraphical synthesis of the metasediments of the Aggeneys terrane in the Namaqua mobile belt. South African J. Geol. 100, 85–100.

Praekelt, H.E., Colliston, W.P., Schoch, A.E., 1983. The stratigraphic interpretation of a highly deformed proterozoic region in central bushmanland, south africa: first correlation of structurally

separated metasediments of the aggeneys subgroup. Precambrian Res. 23, 177–185.

Praekelt, H.E., Schoch, A., Visser, J.N.J., 1997. The metasediments of the Aggeneys terrane in the Namaqua Mobile Belt: Sedimentary response to extensional-compressional variations in a continental environment. South African J. Geol. 100, 101–110.

Raith, J.G., Cornell, D.H., Frimmel, H.E., De Beer, C.H., 2003. New Insights into the Geology of the Namaqua Tectonic Province , South Africa , from Ion Probe Dating of Detrital and Metamorphic Zircon. J. Geol. 111, 347–366. https://doi.org/10.1086/373973

Rath, R.K., Subramanian, S., Pradeep, T., 2000. Surface Chemical Studies on Pyrite in the Presence of Polysaccharide-Based Flotation Depressants. J. Colloid Interface Sci. 229, 82–91. https://doi.org/10.1006/jcis.2000.6990

Reid, D.L., WELKE, H.J., ERLANK, A.J., BETTON, P.J., 1987. Composition, age and tectonic setting of amphibolites in the central Bushmanland Group, western Namaqua Province, southern Africa. Precambrian Res. 36, 99–126.

Richardson, S., Glücksman, E., Beveridge, A., Daffern, T., Ellis, R., King, P., 2017. NI 43-101 Technical report for the Zinkgruvan mine, Sweden.

Roache, T.J., 2004. Shear zone versus fold geometries at the Cannington Ag-Pb-Zn deposit: Implications for the genesis of BHT deposits. J. Struct. Geol. 26, 1215–1230. https://doi.org/10.1016/j.jsg.2003.11.013

Robb, L.J., 2005. Introduction to ore-forming processes, 1st ed. Blackwell Publishing.

Robb, L.J., Armstrong, R.A., Waters, D.J., 1999. The History of Granulite-Facies Metamorphism and Crustal Growth from Single Zircon U – Pb Geochronology : J. Petrol. 40, 1747–1770.

Rodrigues, R.T., Rubio, J., 2007. DAF–dissolved air flotation: Potential applications in the mining and mineral processing industry. Int. J. Miner. Process. 82, 1–13. https://doi.org/10.1016/j.minpro.2006.07.019

Rothery, E., 2001. Tectonic origin of the shape of the Broken Hill lodes supported by their structural setting in a high- grade shear zone. Aust. J. Earth Sci. 48, 201–220. https://doi.org/10.1046/j.1440-0952.2001.00852.x

Rozendaal, A., Rudnick, T.K., Heyn, R., 2017. Mesoproterozoic base metal sulphide deposits in the Namaqua Sector of the Namaqua-Natal Metamorphic Province , South Africa : a review. South African J. Geol. 120, 153–186. https://doi.org/10.25131/gssajg.

Rudnick, T.K., 2016. The genesis of the Swartberg base-metal sulphide deposit, South Africa. Stellenbosch University.

Ryan, P.J., Lawrence, A.L., Lipson, R.D., Moore, J.M., Paterson, A., Stedman, D.P., Van Zyl, D., 1986. The Aggeneys Base Metal Sulphide Deposits, Namaqualand District, in: Mineral Deposits of Southern Africa. pp. 1447–1473.

Sangster, D.F., 2018. Toward an integrated genetic model for vent-distal SEDEX deposits. Miner. Depos. 53, 509–527. https://doi.org/10.1007/s00126-017-0755-3

Sant'Agostino, L.M., Alves, P.R., Shimabukuro, N., Bonás, T.B., 2001. Applied mineralogy as a tool for mine planning of phosphate rock. Miner. Eng. 14, 1649–1657. https://doi.org/10.1016/S0892-6875(01)00183-2

Schipper, B.W., Lin, H.-C., Meloni, M.A., Wansleeben, K., Heijungs, R., van der Voet, E., 2018. Estimating global copper demand until 2100 with regression and stock dynamics. Resour. Conserv. Recycl. 132, 28–36. https://doi.org/10.1016/J.RESCONREC.2018.01.004

Spencer, S., Sutherland, D., 2000. Stereological correction of mineral liberation grade distributions estimated by single sectioning of particles. Image Anal. Stereol. 19, 175–182.

Stalder, M., Rozendaal, A., 2004. Apatite nodules as an indicator of depositional environment and ore genesis for the Mesoproterozoic Broken Hill-type Gamsberg Zn-Pb deposit, Namaqua Province, South Africa. Miner. Depos. 39, 189–203. https://doi.org/10.1007/s00126-003-0394-8

Steenberg, E., Harris, P.J., 1984. Adsorption of carboxymethylcellulose, guar gum, and starch onto talc, sulphides, oxides, and salt-type minerals. South African J. Chem. 37, 85–90.

Tankard, A.J., Jackson, M.P.A., Eriksson, K.A., Hobday, D.K., Hunter, D.R., Minter, W.E. I, 1982. Crustal Evolution Of Southern Africa, 1st ed. Springer-Verlag, New York, Heidelberg, Berlin.

Thomas, R.J., Macey, P.H., Spencer, C., Dhansay, T., Diener, J.F.A., Lambert, C.W., Frei, D., Nguno, A., 2016. The Sperrgebiet Domain, Aurus Mountains, SW Namibia: A ~2020–850Ma window within the Pan-African Gariep Orogen. Precambrian Res. 286, 35–58. https://doi.org/10.1016/j.precamres.2016.09.023

Tilton, J.. ., 2003. On borrowed time: assessing the threat of mineral depletion, 1 st. ed. New York.

Valdes-Nodarse, E.L., 1998. Pb-Zn "SEDEX" deposits and their copper stockwork roots, western Cuba. Miner. Depos. 33, 560–567. https://doi.org/10.1007/s001260050172

Van Schijndel, V., Cornell, D.H., Anczkiewicz, R., Scherstén, A., 2019. Evidence for Mesoproterozoic collision, deep burial and rapid exhumation of garbenschiefer in the Namaqua Front, South Africa. Geosci. Front. https://doi.org/10.1016/j.gsf.2019.06.004

Walters, S., Bailey, A., 1998. Geology and Mineralization of the Cannington Ag-Pb-Zn Deposit: An Example of Broken Hill-Type Mineralization in the Eastern Succession, Mount Isa Inlier, Australia. Econ. Geol. 93, 1307–1329.

Wei, D., Craig, I.K., 2009. Economic performance assessment of two ROM ore milling circuit controllers. Miner. Eng. 22, 826–839. https://doi.org/10.1016/j.mineng.2009.02.013

Wiese, J., Harris, P., Bradshaw, D., 2007. The response of sulphide and gangue minerals in selected Merensky ores to increased depressant dosages. Miner. Eng. 20, 986–995. https://doi.org/10.1016/j.mineng.2007.03.008

Wiese, J., Harris, P., Bradshaw, D., 2005. The influence of the reagent suite on the flotation of ores from the Merensky reef. Miner. Eng. 18, 189–198. https://doi.org/10.1016/j.mineng.2004.09.013

Xiao, Z., Laplante, A.R., 2004. Characterizing and recovering the platinum group minerals—a review. Miner. Eng. 17, 961–979. https://doi.org/10.1016/j.mineng.2004.04.001

Appendix A: Feed mineralogy

Bulk mineralogy - feed (wt%)					
Mineral	**Ore G size fraction (µm)**				
	Combined	**-300/+75**	**-75/+38**	**-38/+10**	**-10/+1**
Chalcopyrite	5.3	3.5	5.5	7.4	9.4
Sphalerite	0.1	0.1	0.1	0.1	0.1
Galena	0.7	0.7	0.6	0.7	1.6
Total % Economic Sulphides (ES)	6.1	4.3	6.1	8.3	11.1
Pyrrhotite	1.9	1.4	2.2	1.6	3.1
Pyrite	10.7	7.6	12.1	14.1	13.9
Total % Sulphide Gangue (SG)	12.5	8.9	14.4	15.7	17.0
Magnetite	23.0	17.5	26.8	26.8	27.5
Gahnite	0.0	0.0	0.0	0.0	0.0
Quartz	40.6	49.0	37.6	33.0	25.2
Grunerite	2.2	1.6	1.8	2.2	6.2
Garnet	10.2	12.7	8.8	9.0	5.3
Mica	2.1	3.0	1.0	1.4	3.2
Apatite	1.7	1.3	2.1	1.7	1.7
Sillimanite	0.1	0.1	0.1	0.1	0.1
Hyalophane	0.0	0.0	0.0	0.0	0.0
Barite	0.1	0.1	0.0	0.0	0.2
Chlorite	0.5	0.5	0.3	0.5	0.8
Total % Non-Sulphide Gangue (NSG)	80.4	85.9	78.5	74.8	70.3
ES/SG	0.1	0.0	0.1	0.1	0.2
ES/NSG	0.1	0.0	0.1	0.1	0.2
SG/NSG	0.2	0.1	0.2	0.2	0.2

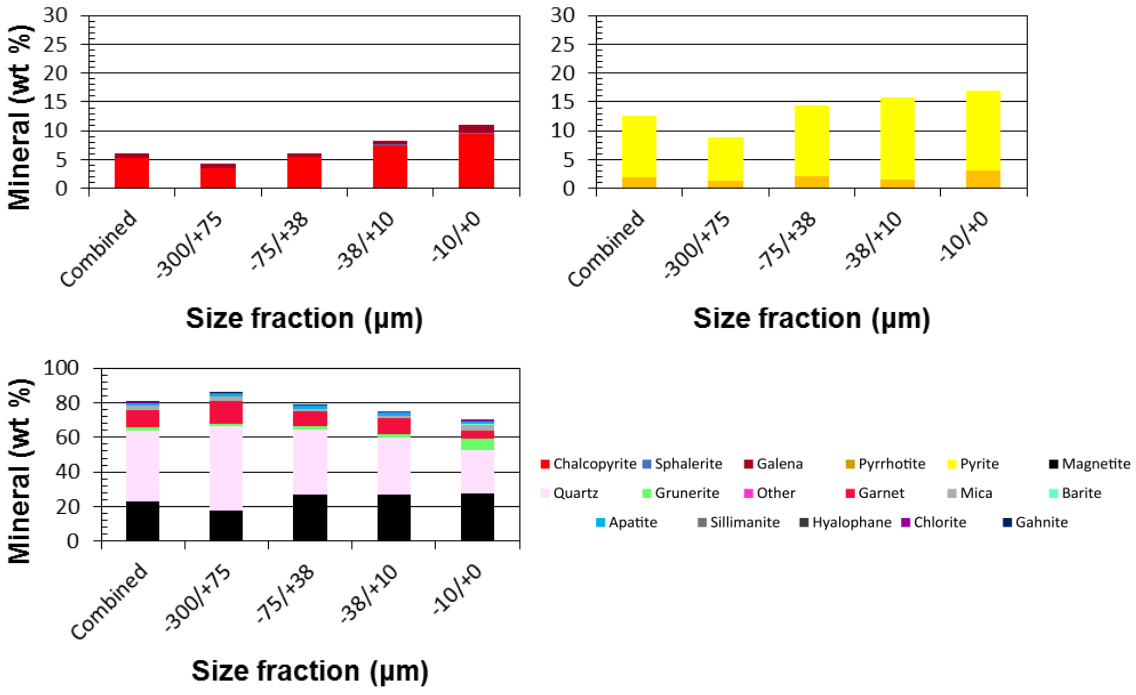

Note: Bulk mineralogy by size, ore G. Top left graph (total ES by size), top right graph (total SG by size) and bottom graph (total NSG by size).

Bulk mineralogy - feed (wt%)					
Mineral	**Ore H size fraction (µm)**				
	Combined	**-300/+75**	**-75/+38**	**-38/+10**	**-10/+1**
Chalcopyrite	1.07	0.68	1.01	1.49	1.85
Sphalerite	0.13	0.12	0.12	0.17	0.21
Galena	9.85	3.03	8.83	16.53	24.24
Total % Economic Sulphides (ES)	11.1	3.8	10.0	18.2	26.3
Pyrrhotite	0.5	0.54	0.66	0.29	0.43
Pyrite	7.6	7.07	9.06	7.23	6.97
Total % Sulphide Gangue (SG)	8.1	7.6	9.7	7.5	7.4
Magnetite	5.93	6.16	6.14	5.68	5.19
Gahnite	0.29	0.40	0.27	0.23	0.21
Quartz	47.06	51.09	53.81	42.54	27.86
Grunerite	0.41	0.26	0.27	0.40	1.14
Garnet	7.43	8.21	7.00	7.52	5.69
Mica	8.5	10.11	5.25	7.12	11.23
Apatite	0.25	0.23	0.23	0.34	0.28
Sillimanite	1.58	2.96	0.54	0.57	0.43
Hyalophane	0.34	0.14	0.31	0.40	0.85
Barite	2.38	1.00	2.14	3.39	5.76
Chlorite	5.64	7.35	3.62	4.82	5.12
Total % Non-Sulphide Gangue (NSG)	79.8	87.9	79.6	73.0	63.8
ES/SG	0.1	0.0	0.1	0.2	0.4
ES/NSG	0.1	0.0	0.1	0.2	0.4
SG/NSG	0.1	0.1	0.1	0.1	0.1

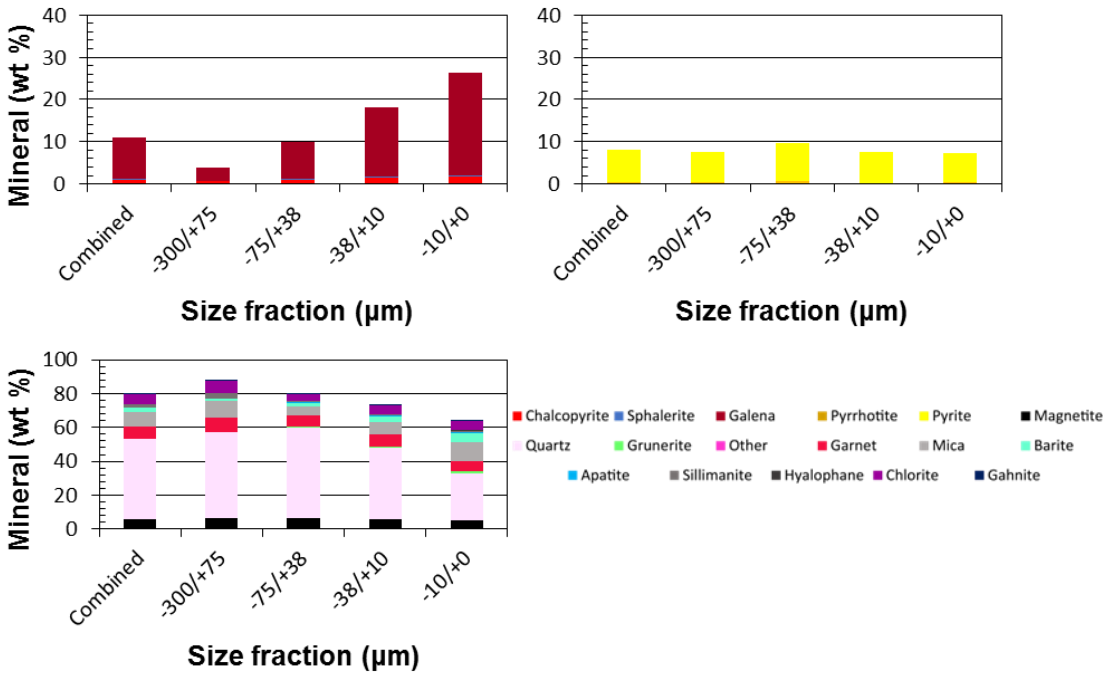

Note: Bulk mineralogy by size, ore H. Top left graph (total ES by size), top right graph (total SG by size) and bottom graph (total NSG by size).

Bulk mineralogy - feed (wt%)					
Mineral	**Ore I size fraction (µm)**				
	Combined	**-300/+75**	**-75/+38**	**-38/+10**	**-10/+1**
Chalcopyrite	1.0	0.7	0.9	1.4	1.6
Sphalerite	0.2	0.2	0.2	0.1	0.3
Galena	10.1	2.8	9.1	18.3	21.0
Total % Economic Sulphides (ES)	11.2	3.7	10.2	19.8	22.8
Pyrrhotite	0.3	0.4	0.3	0.2	0.3
Pyrite	4.7	4.0	5.9	4.3	4.5
Total % Sulphide Gangue (SG)	5.1	4.5	6.2	4.5	4.8
Magnetite	4.4	4.3	4.7	4.3	4.4
Gahnite	0.2	0.2	0.2	0.1	0.1
Quartz	45.8	53.2	49.8	37.6	26.4
Grunerite	0.4	0.3	0.2	0.4	1.0
Garnet	5.9	7.6	4.7	5.5	4.3
Mica	12.8	14.5	11.6	11.2	13.0
Apatite	0.1	0.1	0.1	0.1	0.1
Sillimanite	0.9	1.9	0.3	0.3	0.3
Hyalophane	0.7	0.5	0.5	0.8	1.8
Barite	8.7	4.5	9.3	11.7	15.2
Chlorite	2.7	4.0	1.5	2.2	2.6
Total % Non-Sulphide Gangue (NSG)	82.6	91.1	83.0	74.3	69.3
ES/SG	0.1	0.0	0.1	0.3	0.3
ES/NSG	0.1	0.0	0.1	0.3	0.3
SG/NSG	0.1	0.0	0.1	0.1	0.1

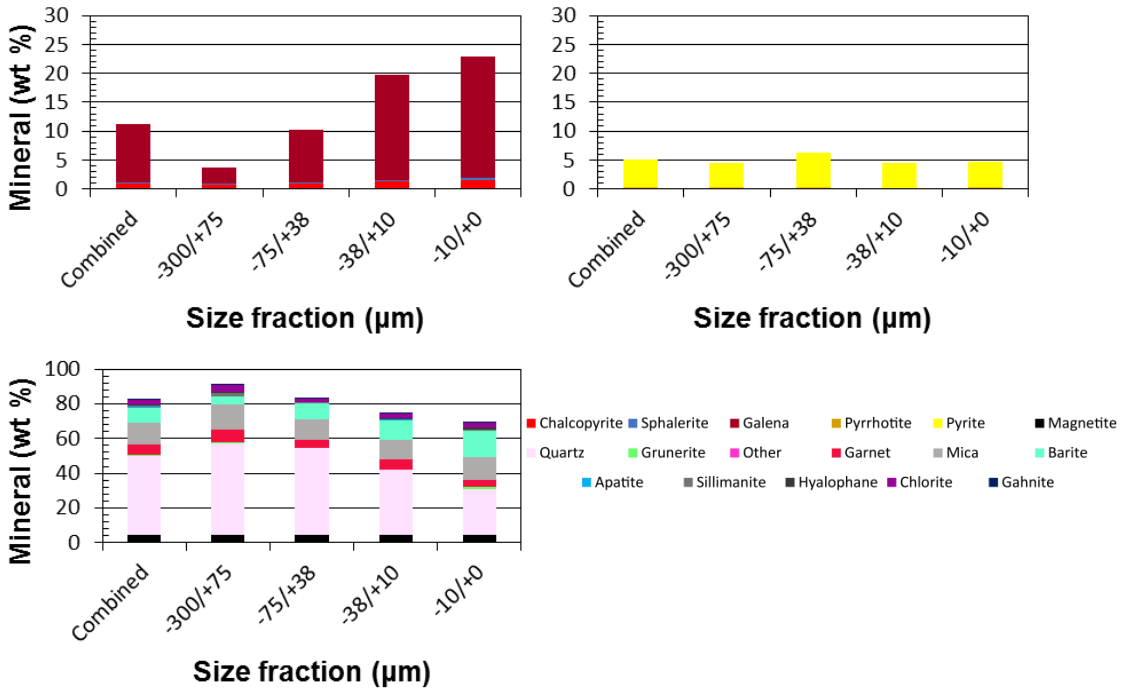

Note: Bulk mineralogy by size, ore I. Top left graph (total ES by size), top right graph (total SG by size) and bottom graph (total NSG by size)

Mineral liberation of ES minerals												
	Ore G											
Ore Type	Combined		+75µm		-75µm +38µm		-38µm +10µm		-10µm			
	Feed	Concentrate	Feed	Concentrate	Feed	Concentrate	Feed	Concentrate	Feed	Concentrate		
Chalcopyrite	90	85	84	80	92	89	96	94	96	94		
	(79430)	*(31418)*	*(1509)*	*(3548)*	*(6506)*	*(3782)*	*(36006)*	*(5124)*	*(35409)*	*(18964)*		
Galena	52	53	21	30	63	62	58	74	58	74		
	(10749)	*(5777)*	*(475)*	*(727)*	*(1067)*	*(1142)*	*(4362)*	*(869)*	*(4845)*	*(3039)*		
Sphalerite	50	35	63	29	28	38	56	43	56	43		
	(2845)	*(2027)*	*(275)*	*(572)*	*(638)*	*(467)*	*(1371)*	*(246)*	*(561)*	*(742)*		
Pyrite	70	87	71	90	69	92	78	91	78	91		
	(117917)	*(29560)*	*(1899)*	*(5279)*	*(11204)*	*(6496)*	*(57372)*	*(5089)*	*(47442)*	*(12696)*		
Ore Type	Ore H											
Chalcopyrite	75	75	60	73	77	85	87	84	87	84		
	(18303)	*(6522)*	*(1294)*	*(1672)*	*(2313)*	*(1841)*	*(6215)*	*(1257)*	*(8481)*	*(1752)*		
Galena	71	86	48	75	77	90	86	93	86	93		
	(151553)	*(27845)*	*(3387)*	*(3605)*	*(9605)*	*(5714)*	*(55714)*	*(7562)*	*(82847)*	*(10964)*		
Sphalerite	22	15	17	3	7	10	25	13	25	13		
	(4569)	*(2498)*	*(389)*	*(548)*	*(811)*	*(1178)*	*(1882)*	*(362)*	*(1487)*	*(410)*		
Pyrite	66	84	59	87	67	87	82	74	82	74		
	(56555)	*(14954)*	*(2413)*	*(5613)*	*(5556)*	*(5908)*	*(20099)*	*(2006)*	*(28487)*	*(1427)*		
Ore Type	Ore I											
Chalcopyrite	78	77	66	81	83	86	88	88	88	88		
	(17448)	*(10014)*	*(1326)*	*(1752)*	*(1708)*	*(3807)*	*(7388)*	*(2477)*	*(7026)*	*(1978)*		
Galena	78	89	57	86	88	95	85	96	85	96		
	(145606)	*(45189)*	*(4814)*	*(3930)*	*(8903)*	*(13435)*	*(69893)*	*(16058)*	*(61996)*	*(11766)*		
Sphalerite	16	13	2	3	6	14	27	21	27	21		
	(5263)	*(4539)*	*(469)*	*(590)*	*(785)*	*(2549)*	*(2519)*	*(930)*	*(1490)*	*(551)*		
Pyrite	72	88	69	90	74	90	77	82	77	82		
	(42234)	*(19403)*	*(2076)*	*(5129)*	*(3974)*	*(9984)*	*(18910)*	*(3010)*	*(17274)*	*(1280)*		

Note: Total sulphide liberation (liberated defined as a particle having >90% area covered by one mineral). Value given in brackets represents the total amount of sulphides analysed.

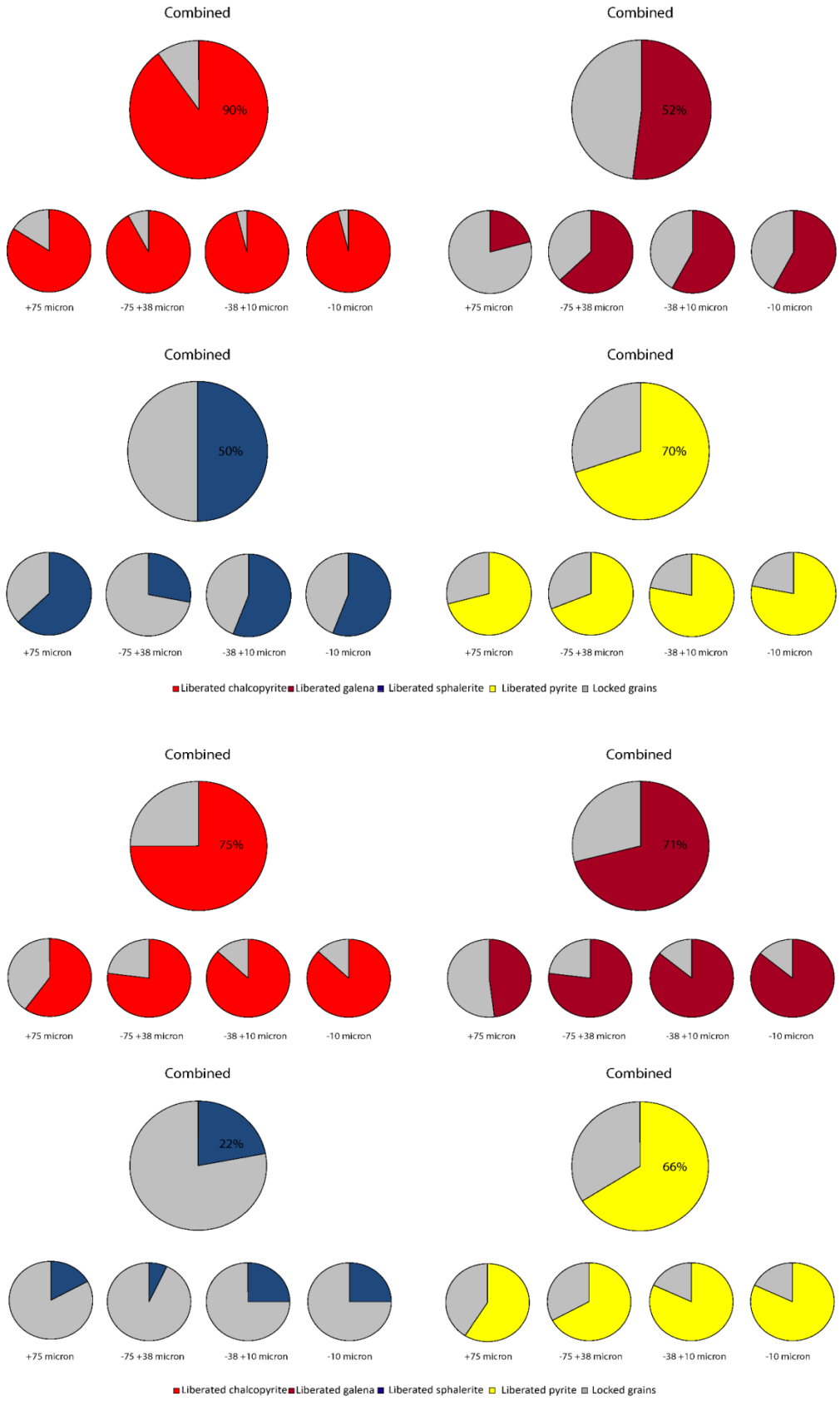

Note: Liberation pies showing percentage of sulphides totally liberated in all three quartz-dominant ores, across all four size fractions. Top group (Ore G), second group (ore H) last group (ore I).

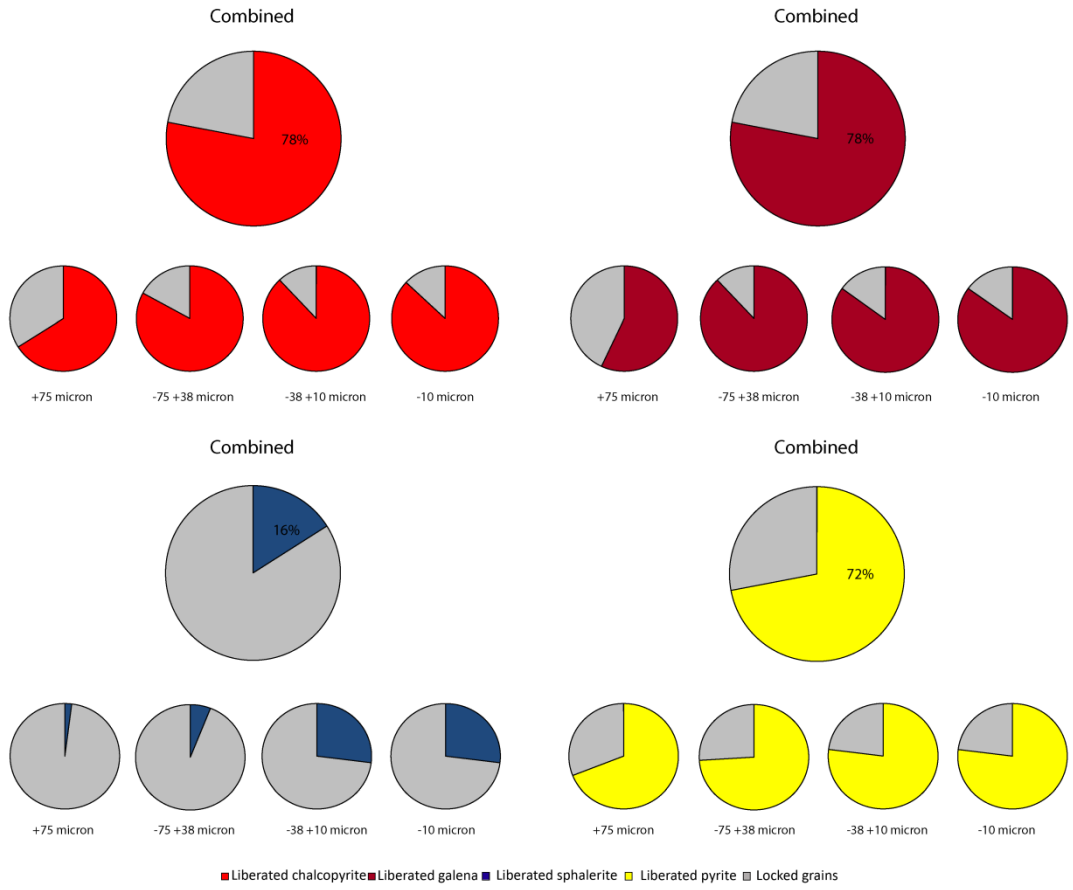

Note: Continued

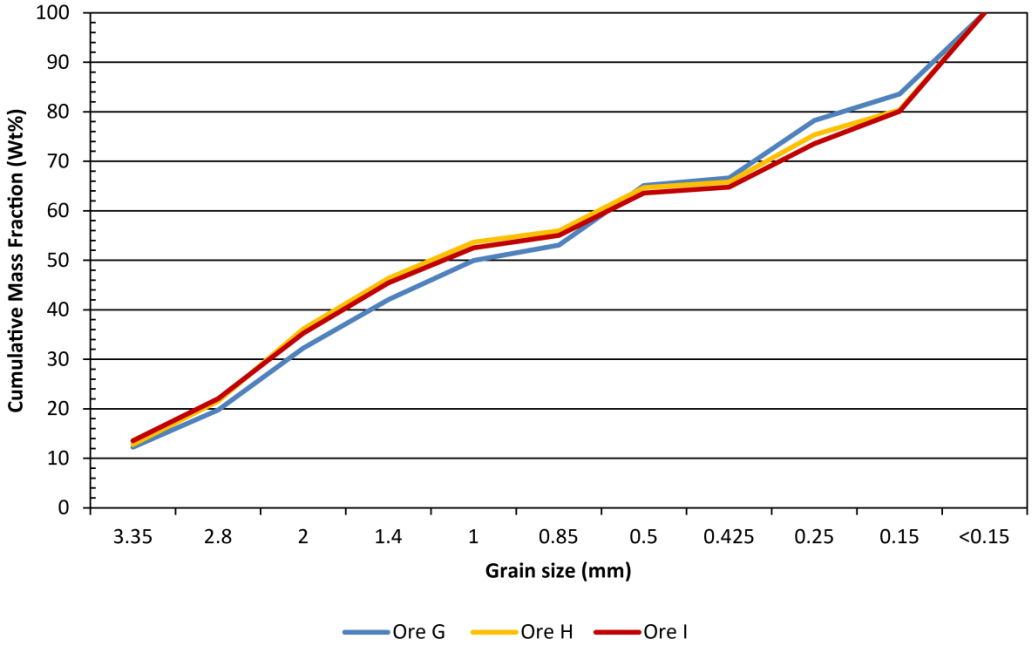

Note: Particle Size Distribution (PSD) of the three quartz-dominant ores post crushing.

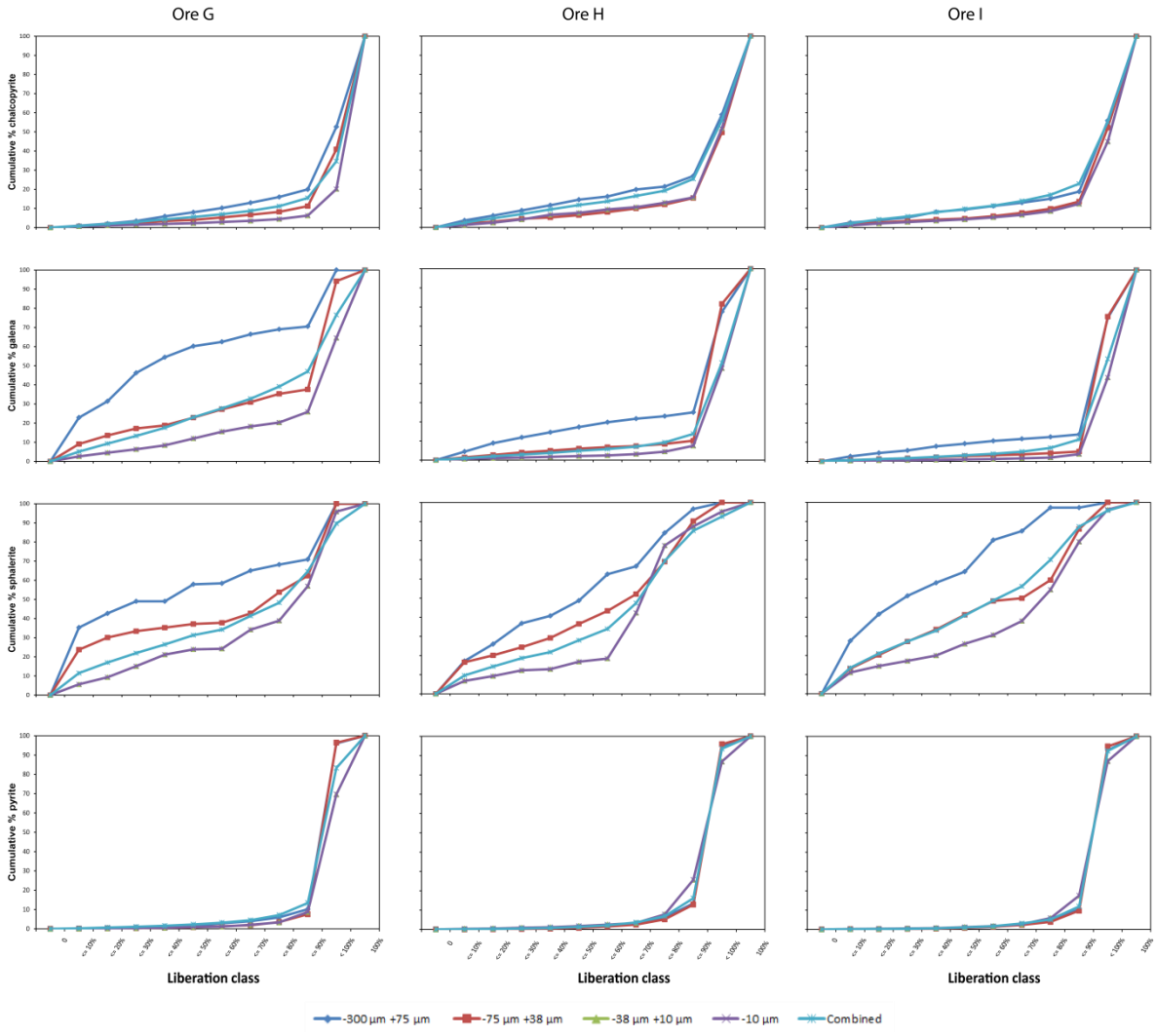

Note: Mineral liberation line charts showing a cumulative function of liberation for all three ores in four sulphides (chalcopyrite, galena, sphalerite and pyrite).

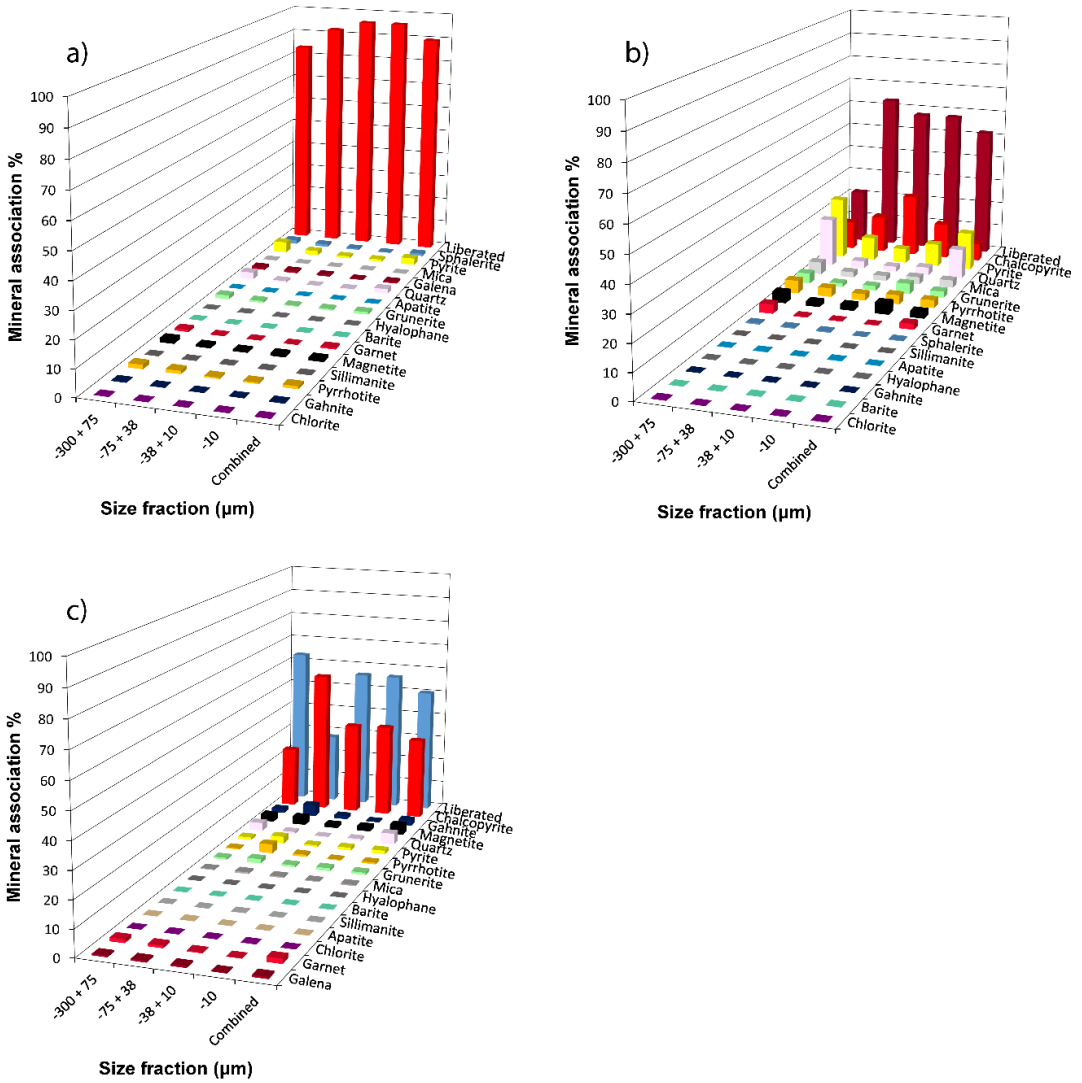

Note: Total (a) chalcopyrite association by size, (b) galena association by size and (c) sphalerite association by size for ore G.

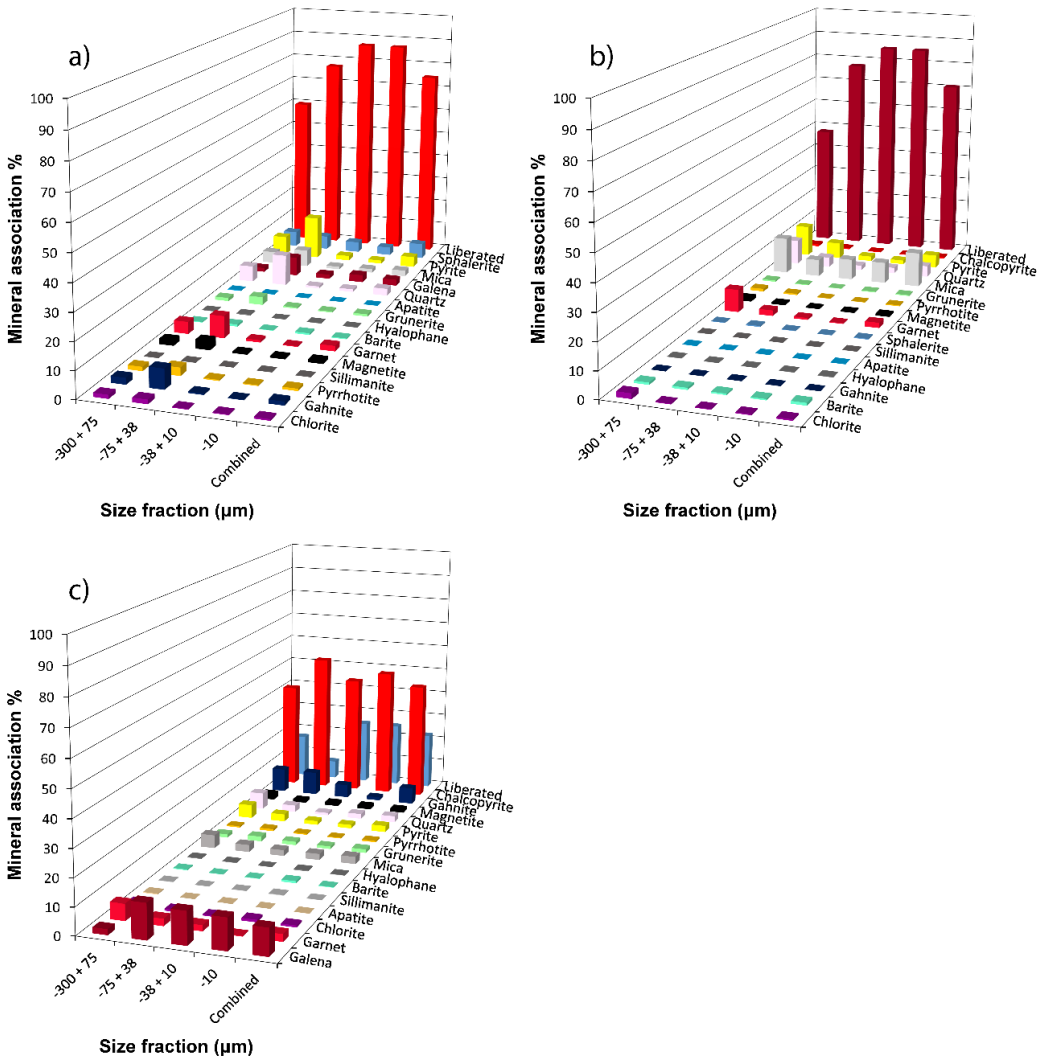

Note: Total (a) chalcopyrite association by size, (b) galena association by size and (c) sphalerite association by size for ore H.

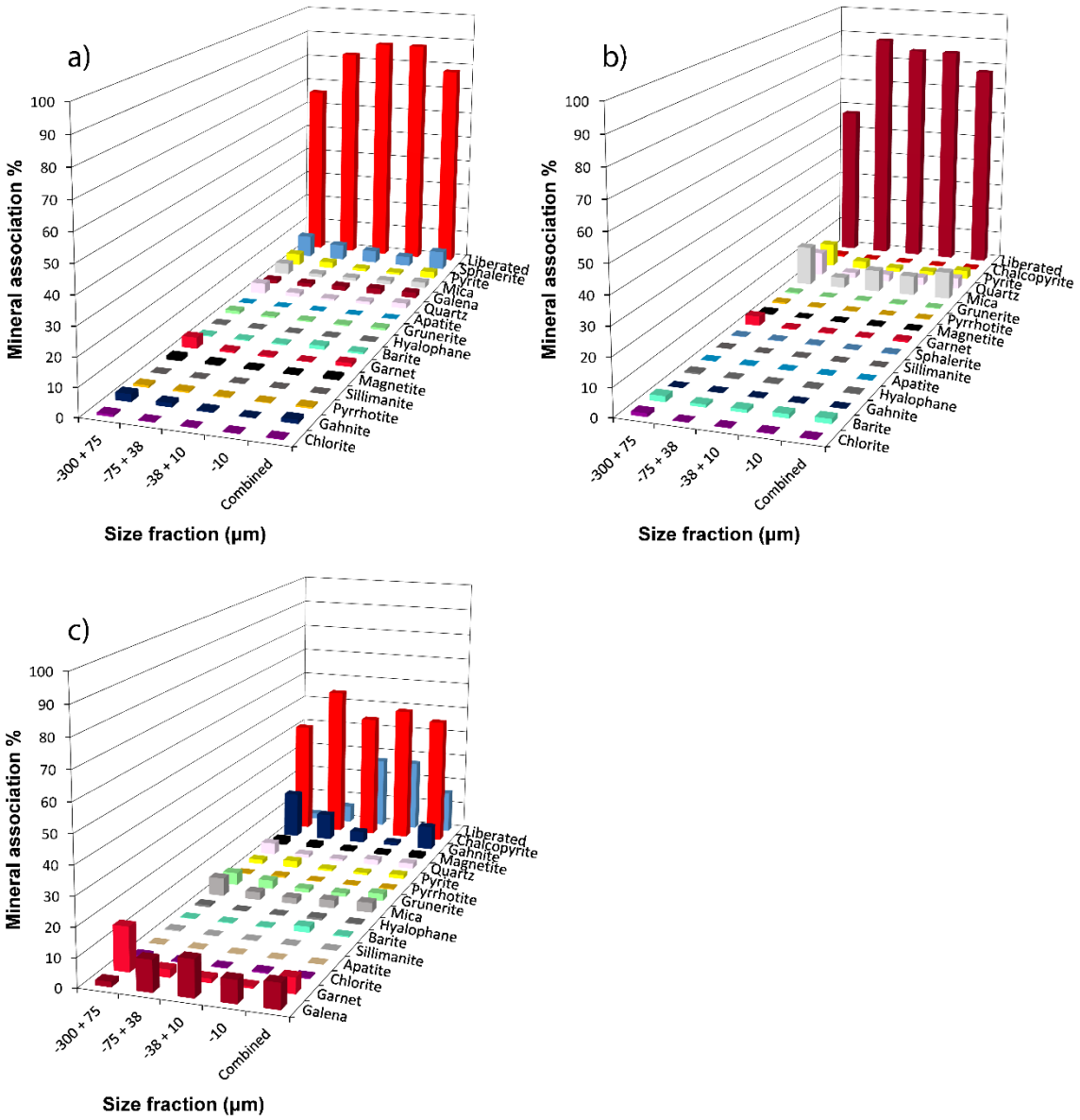

Note: Total (a) chalcopyrite association by size, (b) galena association by size and (c) sphalerite association by size for ore I.

Appendix B: Minerals processing

	C1	C2	C3	C4	FEED	TAILS	TAILS2	TAILS3	C1	131.31	77.93
C + PAPER	135.26	59.08	31.21	13.73	21.66	18.04	18.05	896.68	C2	53.86	62.56
PAPER	3.95	5.22	4.38	5.35	5.23	5.15	5.14	16.96	C3	26.83	140.84
CONC.	131.31	53.86	26.83	8.38	16.43	12.89	12.91	879.72	C4	8.38	183.18
B + H2O	564.04	564.53	604.07	572.64					F	1164.10	
BOTTLE	432.88	333.33	352.00	255.27					T	12.89	
H20	131.16	231.20	252.07	317.37					T2	12.91	
D + C + H20	576.98	597.45	639.32	725.59					T3	879.72	
DISH	236.58	249.83	219.58	216.66							
C + H20	340.40	347.62	419.74	508.93							
					CUM H2O	0	77.93	140.49	281.33	464.51	
H20 REC.	77.93	62.56	140.84	183.18	CUM conc	0	131.31	185.17	212.00	220.38	

	C1	C2	C3	C4	FEED	TAILS	TAILS2	TAILS3	C1	141.36	85.41
C + PAPER	146.64	60.07	23.43	12.36	22.30	17.75	17.50	906.89	C2	54.76	81.59
PAPER	5.28	5.31	4.77	4.66	4.95	4.70	4.77	16.66	C3	18.66	154.63
CONC.	141.36	54.76	18.66	7.70	17.35	13.05	12.73	890.23	C4	7.70	167.09
B + H2O	569.86	573.74	608.23	575.61					F	1175.88	
BOTTLE	381.08	262.74	334.49	236.64					T	13.05	
H20	188.78	311.00	273.74	338.97					T2	12.73	
D + C + H20	652.13	697.18	666.61	730.42					T3	890.23	
DISH	236.58	249.83	219.58	216.66							
C + H20	415.55	447.35	447.03	513.76							
					CUM H2O	0	85.41	167.00	321.63	488.72	
H20 REC.	85.41	81.59	154.63	167.09	CUM conc	0	141.36	196.12	214.78	222.48	

	C1	C2	C3	C4	FEED	TAILS	TAILS2	TAILS3	C1	145.85	87.46
C + PAPER	150.42	55.93	24.22	10.86	20.95	17.30	17.53	910.34	C2	51.38	78.11
PAPER	4.57	4.55	4.53	4.62	4.66	4.64	4.44	16.84	C3	19.69	145.97
CONC.	145.85	51.38	19.69	6.24	16.29	12.66	13.09	893.50	C4	6.24	143.73
B + H2O	573.20	572.90	598.73	573.35					F	1170.48	
BOTTLE	416.22	319.03	368.51	262.98					T	12.66	
H20	156.98	253.87	230.22	310.37					T2	13.09	
D + C + H20	626.87	633.19	615.46	677.00					T3	893.50	
DISH	236.58	249.83	219.58	216.66							
C + H20	390.29	383.36	395.88	460.34							
					CUM H2O	0	87.46	165.57	311.54	455.27	
H20 REC.	87.46	78.11	145.97	143.73	CUM conc	0	145.85	197.23	216.92	223.16	

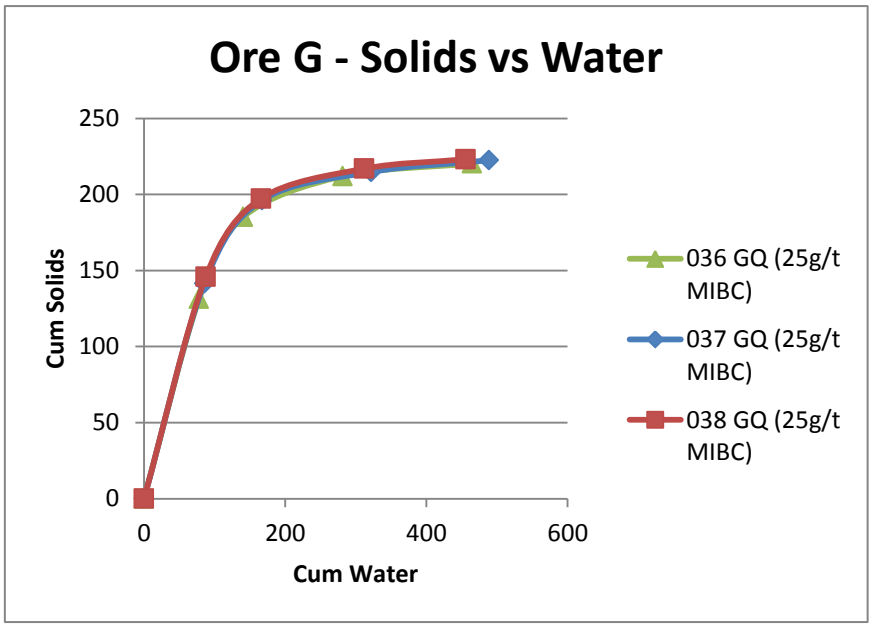

Note: Triplicate floats for ore G, showing repeatability of the flotation experiment.

	C1	C2	C3	C4	FEED	TAILS	TAILS2	TAILS3	C1	126.63	71.30
C + PAPER	131.34	53.28	33.81	20.93	23.10	18.78	19.07	987.85	C2	48.20	78.07
PAPER	4.71	5.08	5.05	4.99	4.88	4.36	4.62	17.08	C3	28.76	102.75
CONC.	126.63	48.20	28.76	15.94	18.22	14.42	14.45	970.77	C4	15.94	144.89
B + H2O	576.81	575.52	611.66	575.43					F	1239.88	
BOTTLE	438.01	298.25	362.98	220.91					T	14.42	
H20	138.80	277.27	248.68	354.52					T2	14.45	
D + C + H20	573.31	653.37	599.77	732.01					T3	970.77	
DISH	236.58	249.83	219.58	216.66							
C + H20	336.73	403.54	380.19	515.35							
					CUM H2O	0	71.30	149.37	252.12	397.01	
H20 REC.	71.30	78.07	102.75	144.89	CUM conc	0	126.63	174.83	203.59	219.53	

	C1	C2	C3	C4	FEED	TAILS	TAILS2	TAILS3	C1	123.62	69.50
C + PAPER	128.27	49.13	39.85	21.47	22.31	18.05	19.38	969.50	C2	44.30	68.69
PAPER	4.65	4.83	4.14	4.17	4.48	4.25	4.95	17.07	C3	35.71	137.83
CONC.	123.62	44.30	35.71	17.30	17.83	13.80	14.43	952.43	C4	17.30	176.02
B + H2O	572.52	575.84	600.61	565.50					F	1230.67	
BOTTLE	413.31	300.36	343.74	203.03					T	13.80	
H20	159.21	275.48	256.87	362.47					T2	14.43	
D + C + H20	588.91	638.30	649.99	772.45					T3	952.43	
DISH	236.58	249.83	219.58	216.66							
C + H20	352.33	388.47	430.41	555.79							
					CUM H2O	0	69.50	138.19	276.02	452.04	
H20 REC.	69.50	68.69	137.83	176.02	CUM conc	0	123.62	167.92	203.63	220.93	

	C1	C2	C3	C4	FEED	TAILS	TAILS2	TAILS3	C1	135.90	80.63
C + PAPER	140.49	43.29	32.96	22.47	23.59	18.84	19.59	965.00	C2	38.89	84.01
PAPER	4.59	4.40	4.50	4.93	4.85	4.94	4.98	17.06	C3	28.46	117.28
CONC.	135.90	38.89	28.46	17.54	18.74	13.90	14.61	947.94	C4	17.54	177.28
B + H2O	576.73	576.36	610.49	576.42					F	1228.23	
BOTTLE	417.90	319.75	379.19	255.50					T	13.90	
H20	158.83	256.61	231.30	320.92					T2	14.61	
D + C + H20	611.94	629.34	596.62	732.40					T3	947.94	
DISH	236.58	249.83	219.58	216.66							
C + H20	375.36	379.51	377.04	515.74							
					CUM H2O	0	80.63	164.64	281.92	459.20	
H20 REC.	80.63	84.01	117.28	177.28	CUM conc	0	135.90	174.79	203.25	220.79	

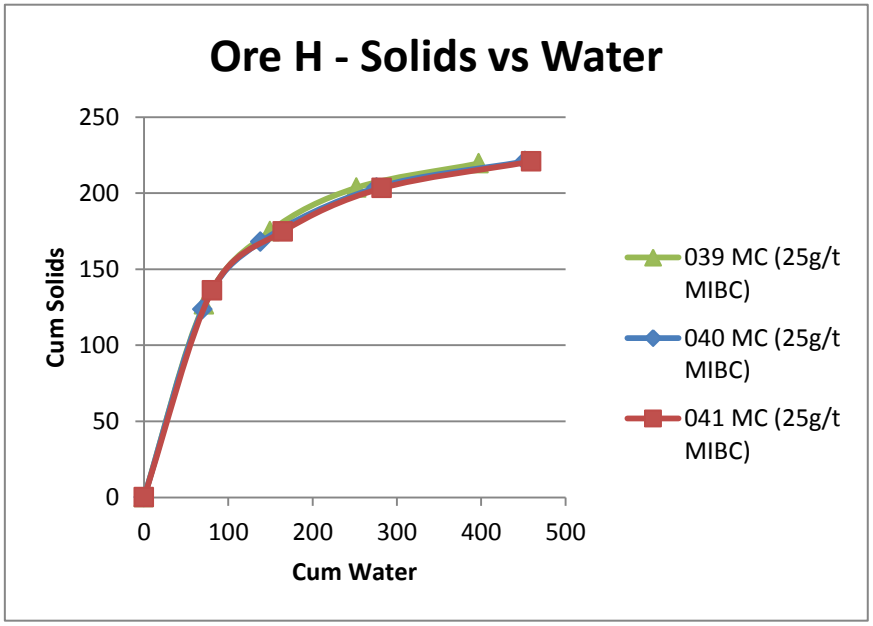

Note: Triplicate floats for ore H, showing repeatability of the flotation experiment.

	C1	C2	C3	C4	FEED	TAILS	TAILS2	TAILS3	C1	117.78	62.59
C + PAPER	122.39	52.28	32.79	19.40	24.46	19.40	18.07	1082.53	C2	47.62	57.80
PAPER	4.61	4.66	4.20	4.35	4.42	4.46	4.47	17.69	C3	28.59	132.88
CONC.	117.78	47.62	28.59	15.05	20.04	14.94	13.60	1064.84	C4	15.05	173.87
B + H2O	561.22	561.50	588.53	561.90					F	1325.61	
BOTTLE	404.91	307.67	356.93	264.72					T	14.94	
H20	156.31	253.83	231.60	297.18					T2	13.60	
D + C + H20	573.26	609.08	612.65	702.76					T3	1064.84	
DISH	236.58	249.83	219.58	216.66							
C + H20	336.68	359.25	393.07	486.10							
					CUM H2O	0	62.59	120.39	253.27	427.14	
H20 REC.	62.59	57.80	132.88	173.87	CUM conc	0	117.78	165.40	193.99	209.04	

	C1	C2	C3	C4	FEED	TAILS	TAILS2	TAILS3	C1	124.97	64.99
C + PAPER	129.12	42.51	29.80	21.33	23.75	19.39	19.79	1071.96	C2	38.21	54.89
PAPER	4.15	4.30	4.38	4.20	4.37	4.05	4.37	17.24	C3	25.42	108.80
CONC.	124.97	38.21	25.42	17.13	19.38	15.34	15.42	1054.72	C4	17.13	190.66
B + H2O	572.91	566.68	592.01	573.49					F	1303.86	
BOTTLE	411.78	274.10	356.93	219.70					T	15.34	
H20	161.13	292.58	235.08	353.79					T2	15.42	
D + C + H20	587.67	635.51	588.88	778.24					T3	1054.72	
DISH	236.58	249.83	219.58	216.66							
C + H20	351.09	385.68	369.30	561.58							
					CUM H2O	0	64.99	119.88	228.68	419.34	
H20 REC.	64.99	54.89	108.80	190.66	CUM conc	0	124.97	163.18	188.60	205.73	

	C1	C2	C3	C4	FEED	TAILS	TAILS2	TAILS3	C1	114.21	60.65
C + PAPER	118.50	48.41	34.72	20.42	23.28	18.76	19.96	1068.33	C2	44.26	59.19
PAPER	4.29	4.15	3.98	4.21	4.18	4.19	4.52	17.89	C3	30.74	136.20
CONC.	114.21	44.26	30.74	16.21	19.10	14.57	15.44	1050.44	C4	16.21	192.10
B + H2O	558.23	568.54	600.78	573.93					F	1295.01	
BOTTLE	406.22	301.30	373.23	252.15					T	14.57	
H20	152.01	267.24	227.55	321.78					T2	15.44	
D + C + H20	563.45	620.52	614.07	746.75					T3	1050.44	
DISH	236.58	249.83	219.58	216.66							
C + H20	326.87	370.69	394.49	530.09							
					CUM H2O	0	60.65	119.84	256.04	448.14	
H20 REC.	60.65	59.19	136.20	192.10	CUM conc	0	114.21	158.47	189.21	205.42	

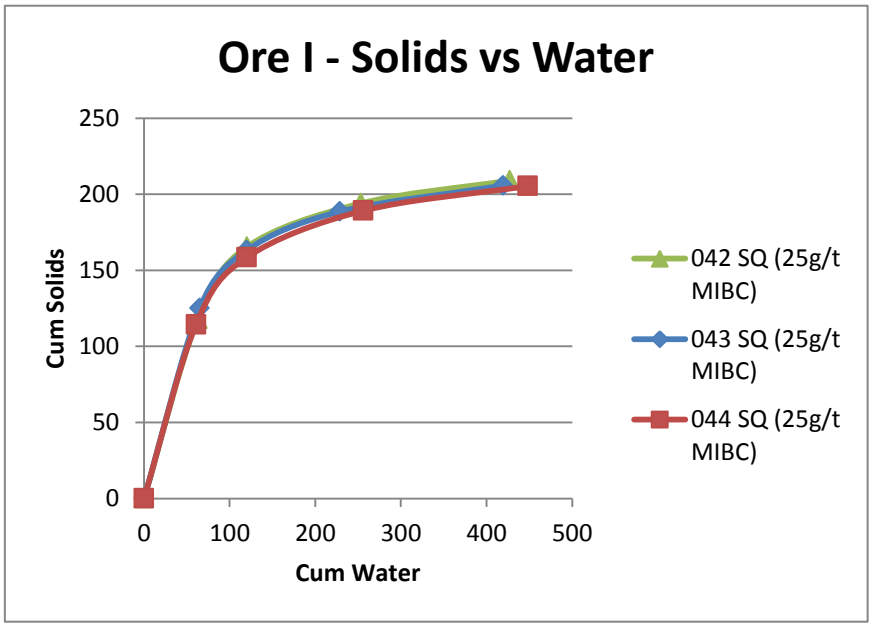

Note: Triplicate floats for ore I, showing repeatability of the flotation experiment.

Note: XRF and ICP-OES assay results of flotation feed (below).

	Ore type						
Ore	G	G	H	H	I	I	BMM Std
Location	CAF	SS	CAF	SS	CAF	SS	SS
Ore	G	G	H	H	I	I	BMM Std
Method	XRF (wt %)	ICP (wt %)	XRF (wt %)	ICP (wt %)	XRF (wt %)	ICP (wt %)	ICP (wt%)
Element							
Si	23.08		28.52		27.82		
Ti	0.07	0.03	0.17	0.02	0.13	0.01	0.08
Al	1.26	0.74	3.21	0.44	2.87	0.21	1.47
Fe	23.50	23.52	10.39	10.62	6.85	7.54	23.14
Mn	0.41	0.25	0.20	0.22	0.12	0.14	1.88
Mg	0.30	0.20	0.84	0.12	0.41	0.06	0.58
Ca	0.74	0.51	0.42	0.22	0.17	0.03	0.47
Na	0.01	0.01	0.04	0.01	0.07	0.01	0.09
K	0.09	0.07	0.55	0.04	0.80	0.06	0.11
P	0.29	0.26	0.02	0.10	0.02	0.00	0.20
S	3.87	5.12	2.21	2.02	2.37	0.33	7.27
Cr	0.05	0.05	0.06	0.02	0.05	0.01	0.01
Ni		0.04		0.02		0.00	0.01
Zn	0.07	0.07	0.20	0.14	0.21	0.13	1.35
Cu	1.46	1.96	0.28	0.32	0.32	0.31	4.73
Ni		0.04		0.02		0.00	0.01
Pb	0.51	0.45	5.83	5.91	6.64	6.52	0.24
Ag ppm		17.65		10.38		12.00	
As ppm		16.83		5.00		5.00	
Ba ppm	149.00	80.39	12703.00	535.06	44146.00	719.93	
Be ppm		1.75		0.72		1.00	
Bi ppm		193.53		71.73		5.00	
Cd ppm		7.30		3.76		2.33	
Co ppm	237.00	262.95	53.00	106.53	33.00	5.00	
Ga ppm	19.00	6.78	127.00	2.40	164.00	2.14	
La ppm	53.00	33.85	18.00	13.70	bdl	5.00	
Mo ppm		59.62		27.16		7.99	
Sb ppm		12.51		6.73		5.00	
Sc ppm		1.76		1.22		1.16	
Sr ppm	15.00	13.56	117.00	6.53	395.00	4.61	
Th ppm		5.00	187.00	5.00	145.00	5.00	
Tl ppm		5.00		5.00		5.00	
U ppm		5.00		5.00		5.00	
V ppm	18.00	8.12	60.00	3.82	115.00	4.44	
W ppm		10.62		5.00		5.00	

Appendix C: Concentrate C_1 mineralogy

Bulk mineralogy - concentrate C1 (wt%)					
Mineral	**Ore G size fraction (µm)**				
	Combined	**-300/+75**	**-75/+38**	**-38/+10**	**-10/+1**
Chalcopyrite	30.7	4.5	9.9	11.1	5.2
Sphalerite	0.4	0.0	0.1	0.2	0.1
Galena	3.8	0.2	1.2	1.7	0.8
Total % Economic Sulphides (ES)	35.0	4.7	11.2	13.0	6.1
Pyrrhotite	2.1	0.3	0.8	0.7	0.3
Pyrite	56.7	10.5	24.7	17.4	4.1
Total % Sulphide Gangue (SG)	58.8	10.9	25.5	18.1	4.4
Magnetite	0.9	0.2	0.2	0.4	0.2
Gahnite	0.1	0.0	0.0	0.0	0.0
Quartz	1.6	0.3	0.5	0.6	0.3
Grunerite	0.7	0.1	0.2	0.3	0.2
Garnet	0.3	0.1	0.1	0.1	0.1
Mica	0.0	0.0	0.0	0.0	0.0
Apatite	0.0	0.0	0.0	0.0	0.0
Sillimanite	0.6	0.1	0.2	0.2	0.1
Hyalophane	0.0	0.0	0.0	0.0	0.0
Barite	0.1	0.0	0.0	0.0	0.0
Chlorite	0.1	0.0	0.0	0.0	0.0
Total % Non-Sulphide Gangue (NSG)	4.4	0.7	1.2	1.7	0.8
ES/SG	0.6	0.4	0.4	0.7	1.4
ES/NSG	8.0	6.7	9.2	7.9	7.8
SG/NSG	13.5	15.5	21.0	10.9	5.6

Note: Bulk mineralogy of concentrate C_1 by size (ore G)

Bulk mineralogy - concentrate C1 (wt%)					
Mineral	**Ore H size fraction (µm)**				
	Combined	**-300/+75**	**-75/+38**	**-38/+10**	**-10/+1**
Chalcopyrite	5.92	1.01	1.47	2.60	0.84
Sphalerite	0.57	0.07	0.10	0.28	0.13
Galena	57.35	3.68	10.63	30.01	13.04
Total % Economic Sulphides (ES)	63.8	4.8	12.2	32.9	14.0
Pyrrhotite	0.6	0.19	0.21	0.18	0.02
Pyrite	29.81	11.32	11.52	6.23	0.74
Total % Sulphide Gangue (SG)	30.4	11.5	11.7	6.4	0.8
Magnetite	0.49	0.10	0.10	0.22	0.06
Gahnite	0.03	0.01	0.01	0.01	0.00
Quartz	1.38	0.38	0.33	0.50	0.17
Grunerite	0.73	0.07	0.09	0.40	0.16
Garnet	0.74	0.24	0.18	0.22	0.10
Mica	0.22	0.04	0.04	0.09	0.05
Apatite	0.05	0.01	0.02	0.01	0.00
Sillimanite	0.12	0.03	0.03	0.04	0.02
Hyalophane	0.03	0.01	0.00	0.02	0.00
Barite	0.58	0.25	0.15	0.15	0.03
Chlorite	0.06	0.03	0.02	0.02	0.00
Total % Non-Sulphide Gangue (NSG)	4.4	1.2	1.0	1.7	0.6
ES/SG	2.1	0.4	1.0	5.1	18.4
ES/NSG	14.4	4.1	12.6	19.6	23.7
SG/NSG	6.9	9.8	12.1	3.8	1.3

Note: Bulk mineralogy of concentrate C_1 by size (ore H)

Bulk mineralogy - concentrate C1 (wt%)					
Mineral	**Ore I size fraction (µm)**				
	Combined	**-300/+75**	**-75/+38**	**-38/+10**	**-10/+1**
Chalcopyrite	5.98	1.1	1.57	2.26	1.06
Sphalerite	0.77	0.05	0.12	0.42	0.18
Galena	67.31	5.27	13.59	30.34	18.11
Total % Economic Sulphides (ES)	74.1	6.4	15.3	33.0	19.4
Pyrrhotite	0.28	0.09	0.09	0.08	0.01
Pyrite	20.72	9.4	7.04	3.77	0.51
Total % Sulphide Gangue (SG)	21.0	9.5	7.1	3.9	0.5
Magnetite	0.36	0.07	0.09	0.15	0.05
Gahnite	0.02	0	0.01	0.01	0
Quartz	1.26	0.33	0.31	0.41	0.21
Grunerite	0.86	0.03	0.07	0.47	0.29
Garnet	0.77	0.24	0.18	0.22	0.14
Mica	0.38	0.04	0.05	0.14	0.15
Apatite	0.04	0.01	0.01	0.02	0
Sillimanite	0.07	0.02	0.02	0.02	0.01
Hyalophane	0.03	0	0	0.02	0.01
Barite	0.23	0.09	0.06	0.05	0.02
Chlorite	0.07	0.01	0	0.05	0
Total % Non-Sulphide Gangue (NSG)	4.1	0.8	0.8	1.6	0.9
ES/SG	3.5	0.7	2.1	8.6	37.2
ES/NSG	18.1	7.6	19.1	21.2	22.0
SG/NSG	5.1	11.3	8.9	2.5	0.6

Note: Bulk mineralogy of concentrate C_1 by size (ore I)

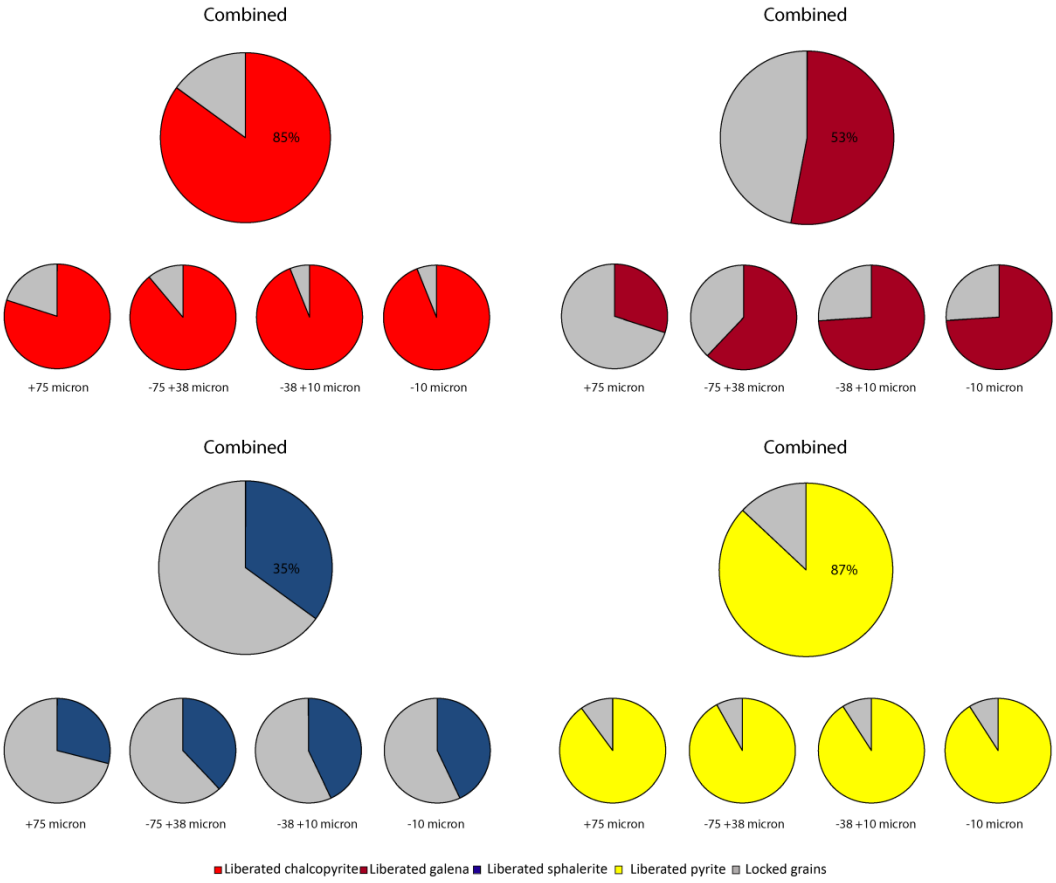

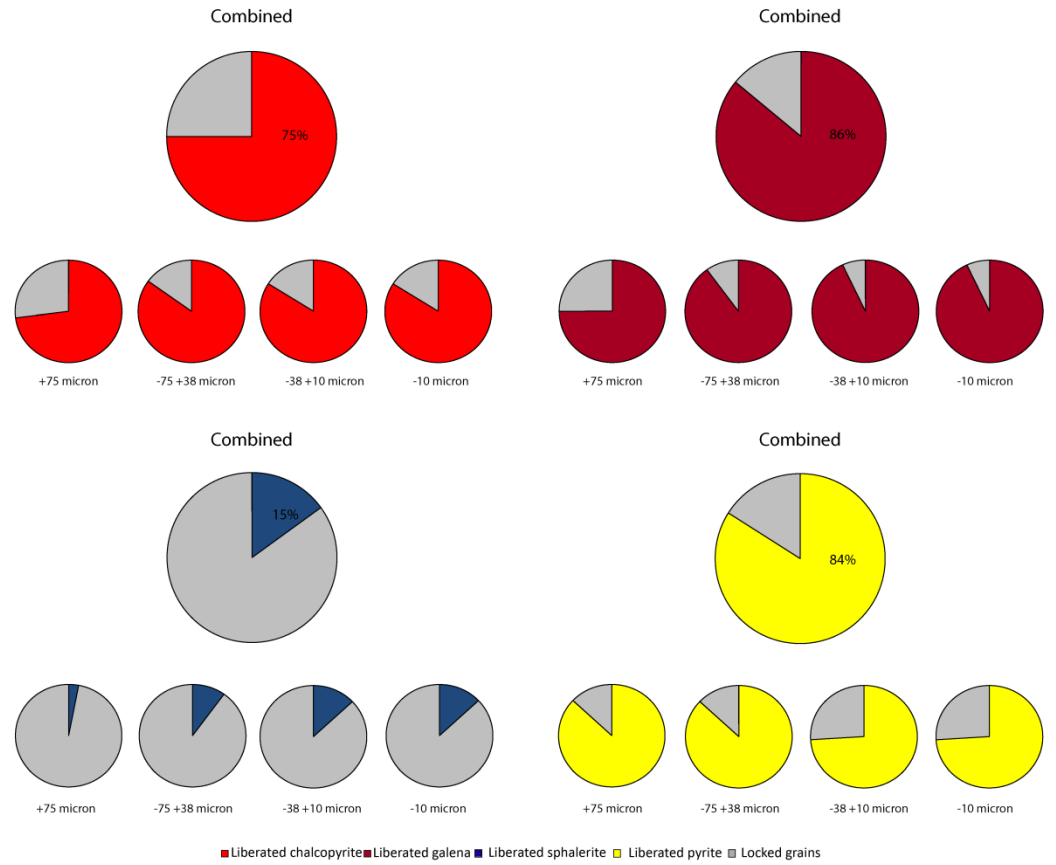

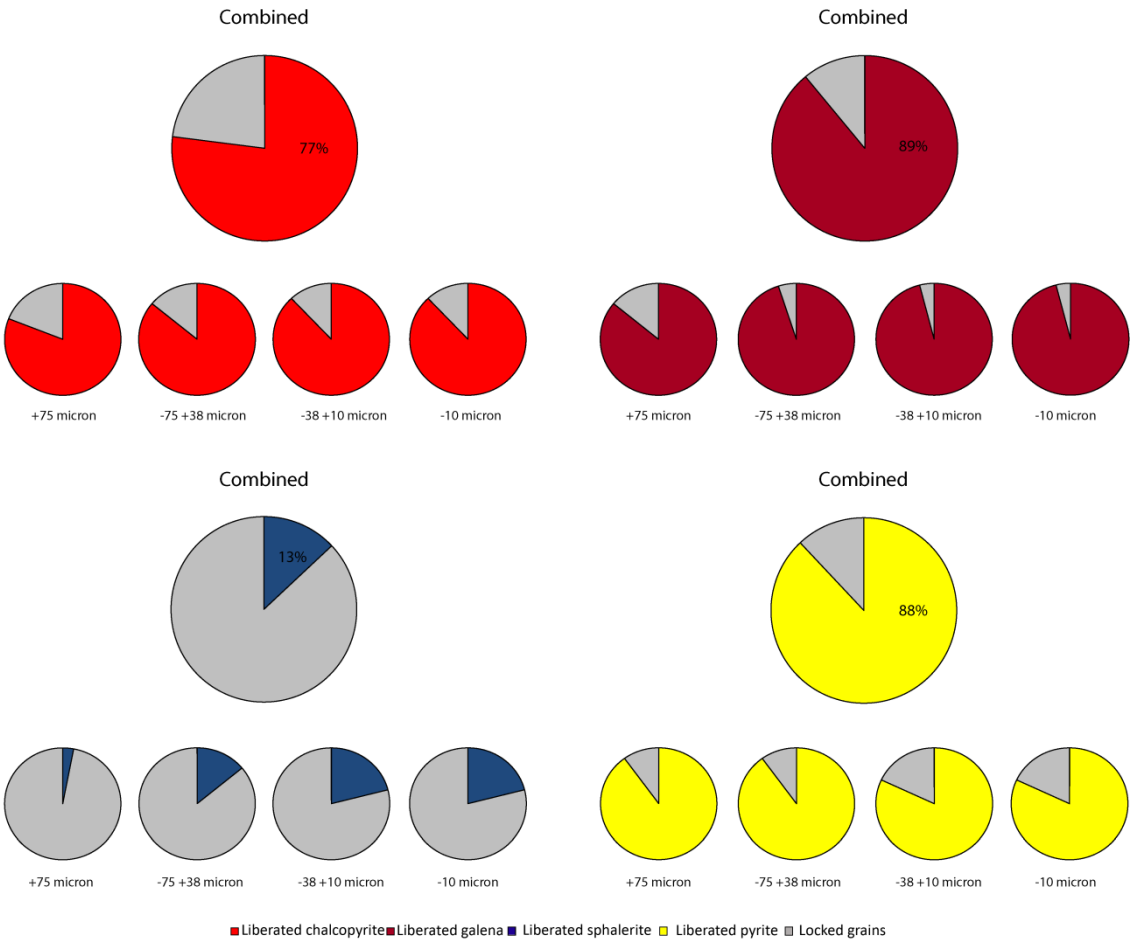

Note: Sulphide liberation by size for the three quartz-dominant ores, ore G (top), ore H (middle) and ore I (bottom). For the values of sulphide liberation by size see Appendix A.